DIRECT MEASUREMENT OF ENERGY LANDSCAPES OF INTERMOLECULAR AND INTERFACIAL INTERACTIONS USING ATOMIC FORCE MICROSCOPY

A Dissertation
Presented to
The Academic Faculty

by

Ahmad M. Haider

In Partial Fulfillment
of the Requirements for the Degree of Philosophy in the
School of Mechanical Engineering

Georgia Institute of Technology
August 2016

DIRECT MEASUREMENT OF ENERGY LANDSCAPES OF INTERMOLECULAR AND INTERFACIAL INTERACTIONS USING ATOMIC FORCE MICROSCOPY

Approved by:

Dr. Todd Sulchek, Advisor
School of Mechanical Engineering
Georgia Institute of Technology

Dr. Oliver Brand
School of Electrical and Computer Engineering
Georgia Institute of Technology

Dr. Peter Hesketh
School of Mechanical Engineering
Georgia Institute of Technology

Dr. Albert Frazier
School of Electrical and Computer Engineering
Georgia Institute of Technology

Dr. Nazanin Bassiri-Gharb
School of Mechanical Engineering
Georgia Institute of Technology

Date Approved: 10 June, 2016

ACKNOWLEDGEMENTS

At the outset, I would like to thank my advisor Dr. Todd Sulchek for his perceptive criticisms, in-depth knowledge of the literature, and endless new ideas. Secondly, I would like to thank my colleague Mr. Daniel Potter, who has been my project partner and an outstanding research collaborator. He has been responsible for performing the AFM experiments that were necessary to complete this dissertation. I would also like to thank my other committee members Dr. Peter Hesketh, Dr. Nazanin Bassiri-Gharb, Dr. Albert Frazier and Dr. Oliver Brand for generously giving their time and expertise to my project. I would like to acknowledge National Science Foundation who has funded a significant portion of my research. I thank Ms. Hima Karri who has so far and hopefully will continue to emotionally support me in times of need, and. also my friends and colleagues with whom I have spent many enjoyable discussions during tea breaks and lunches/dinners. Last but the most important, it has been God's grace and love, my parents' blessings and my siblings' encouragement that has kept me motivated throughout my stay at Georgia Tech, and hopefully beyond.

TABLE OF CONTENTS

LIST OF TABLES

LIST OF FIGURES

LIST OF SYMBOLS

k_B	Boltzmann Constant
T	Temperature
$T_{effective}$	Effective Temperature
β	Inverse Boltzmann Energy
k	Spring Constant of Cantilever
c	Damping Coefficient of Cantilever
m	Mass of Cantilever
r	Load Rate
x_n	Energy Well Width
k_{off}	Off-Rate Constant
h	Planck's Constant
τ	Bond Lifetime
γ	Euler's Constant
k_0	Intrinsic Unbinding Constant
$P(x)$	Position Probability Density along Coordinate x
$G(x)$	Gibbs Free Energy Profile along Coordinate x
ΔG_{ab}	Gibbs Free Energy Difference Between States a and b
$W(t)$	Nonequilibrium Work at Time t
F_i	Arbitrary Free Constant in Boltzmann Equation
N_w	Number of windows in a Force Curve
n_i	Number of Points Sampled in a Window
B	Bandwidth of an AFM Trajectory Simulation
$E(x)$	Lorentzian Energy Landscape Profile used in Brownian Dynamics Simulation

$dE(x)/dx$	Curvature of Energy Barrier used in Brownian Dynamics Simulation
A	Parameter Controlling the Depth of a Lorentzian Energy Well
μ	Parameter Controlling the Location of a Lorentzian Energy Well
σ	Parameter Controlling the Spread of a Lorentzian Energy Well
η	Friction Coefficient used in Brownian Dynamics Simulations
D	Diffusion Coefficient used in Brownian Dynamics Simulations
Δt	Time Step used in Brownian Dynamics Simulations
w	Gaussian Random Number used in Brownian Dynamics Simulations
v	Probe speed used in Brownian Dynamics Simulations

LIST OF ABBREVIATIONS

AFM	Atomic Force Microscopy
BFP	Biomembrane Force Probe
BSA	Bovine Serum Albumin
DFS	Dynamic Force Spectroscopy
DNA	Deoxyribo Nucleic Acid
RC	Reaction Coordinate
RMSE	Root Mean Square Error
Si_3N_4	Silicon Nitride
SFA	Surface Force Apparatus
SMFS	Single Molecule Force Spectroscopy
SPR	Surface Plasmon Resonance
WHAM	Weighted Histogram Analysis Method

SUMMARY

Energy barriers encountered in intermolecular and interfacial interactions determine the kinetics and equilibrium outcome of a multitude of key physical, chemical, and biological processes. The free energy landscape, i.e. the strength and physical extent of interaction energies between molecules, dictates the specificity and affinity of biological interactions, which is an important parameter describing the development of novel molecular therapeutics. Knowledge of the energy landscape is also essential to understand the direction of a chemical reaction, the relative stability of intermediate and final states, and the corresponding reaction mechanisms. Hence determination of free energies has allowed for a number of new insights into chemical processes such as catalysis, phase transformations, and boundary lubrication mechanisms.

Despite advances in measuring interaction forces, determining energy landscapes at nanometer dimensions remains a challenge. Computer simulations do provide a useful approach for estimating free energy landscapes and elucidating corresponding binding pathways, but only to the limit of the accuracy of the model potentials and the integration of the equations of motion. Indirect experimental approaches such as dynamic force spectroscopy measurements, though useful in determination of kinetic constants such as off rates and barrier widths, do not completely determine the shape or curvature of the energy landscape, nor can they detect the presence of intermediate metastable states. Metastable states are important as they are responsible for regulating energy transfer between initial and final states of a reaction. Detecting their presence is important to fully understand and predict complex biological interactions, such as characterizing the

specificity of antibodies in recognition targeting. The steep gradients encountered in energy landscapes of adhesive interactions can also pose measurement difficulties since most conventional probing techniques are unable to sufficiently sample them without encountering snap-in binding instabilities. The emergence of ultrasensitive force detection techniques such as atomic force microscope (AFM) could prove invaluable in direct determination of energy landscapes since they combine excellent force and distance resolution with the ability to probe local interactions at nanoscale levels.

The method we developed applies the Brownian (thermal) fluctuations to vibrate a sensitive cantilever through the energy profile between the tip and surface. By recording subtle deviations from the harmonic cantilever vibrations, and applying Boltzmann transformation techniques, the energy landscape is reconstructed.

In this thesis, we have developed a technique using AFM to directly measure the free energy landscape of biological and interfacial interactions. The specific scientific contributions of this work are as follows:

(i) Applied and validated a new weighted histogram analysis method (WHAM) which minimized errors of combining locally estimated Boltzmann energies to more accurately reconstruct energy landscapes of ligand receptor interactions across the entire reaction coordinate;

(ii) Demonstrated that an enhanced stochastic sampling technique can greatly improve the accuracy of reconstructions of steep adhesive energy landscapes; and

(iii) Simulated the entire parameter space of the factors influencing energy landscape sampling to identify the optimal values that maximize landscape reconstruction accuracy.

These techniques have been applied to measure the binding energy landscapes of ligand-receptor interactions in a biotin-avidin system. We have measured and analyzed the multiple energy wells that are characteristic of biotin-avidin bond formation. Through the use of stochastic excitations, we have also extended the applicability of our methods in measuring energy landscapes of strongly adhesive interfacial interactions with steep energy gradients, such as those encountered in Si_3N_4 and mica interfaces.

CHAPTER 1

INTRODUCTION

The free energy landscape is a central quantity in biological sciences, materials sciences, and physical chemistry sciences. It governs the microscopic behavior of a system in the presence of thermal fluctuations. Free energy landscape of an interaction is defined as a function that describes the variation of the energy of the interaction over a number of collective variables called reaction coordinates, averaged over thermal fluctuations [1]. The progress of any microscopic process occurring in or near equilibrium is controlled by the free energy landscape of appropriately chosen reaction coordinates. For example, in ligand receptor binding, reaction rates can be determined through an Arrhenius transformation of free energy differences between bound and unbound states [2]. In practice, the reaction coordinate represents an experimental quantity that is used to follow the progress of an interaction.

Analysis of the energy landscape also provides the fundamental biophysical framework for understanding the formation of structure in biological macromolecules, including the proper folding of proteins and nucleic acids, and ligand receptor binding [3-6]. The utility of the landscape lies in the fact that one can, in principle, predict the folding/unbinding behavior of a molecule given its energy landscape. Energy landscapes are also dictate the specificity and affinity of biomolecular interactions [7]. The set of conformational changes undertaken by a ligand as it binds to a receptor, and the interaction energy that results, remains an elusive and important target for the identification of novel drugs [8] and understanding protein-mediated processes [9]. Of particular note, the

metastable binding states are responsible for regulating the energy transfer between the bound and unbound states during binding or folding [10], and are formed at local minima in the landscape. Understanding these local minima, both energy depth and extent along the reaction coordinate, will allow us to assess the multiple binding pathways that are available to the molecule to take before it binds to a complementary molecule or a substrate, resulting in better control over the rate of these binding processes [11]. As an example, these metastable states are known to play an important part in determining the specificity of antibodies in antigen recognition [12]. Since antibodies bind their specific antigen target with such high affinity (deep energy well), once locked into position they are effectively irreversible. However, finding this target requires reversible binding with many more non-target sites of binding. Identifying the conformational changes that may occur during induced fit can be a critical step in the molecular proofreading process, which can only be accurately quantified through an energy landscape [13, 14].

Although specific features of an energy landscape, such as heights and widths of barriers, can be characterized by various approaches [15-17], the entire shape of a complex landscape can be quite hard to determine. Computer simulation techniques do provide a useful approach for elucidating the complete binding pathway of proteins, but only to the limit of the accuracy of the model potentials and the integration of the equations of motion [18-20]. Conventional experimental processes fail to fully measure the free energies of dynamic processes such as ligand-receptor binding. Some techniques like surface plasmon resonance can measure the kinetic on and off rates of ensembles of particles. From the kinetic rates, the binding energy can be inferred [21]. Single molecule measurement techniques such as dynamic force spectroscopy (DFS) can partially measure an energy

landscape. In DFS, a force is applied to a ligand-receptor complex to enhance the dissociation of the bond/unfolding rates. Although, DFS can predict kinetic off rates (unbinding rates) and thus the depths of a well in an energy landscape by assuming two state binding models [3, 15, 22-27], it cannot determine entire shape of a complex landscape nor its curvature. Application of DFS is also very time consuming due to the necessity of high statistics and the low number of unbinding events corresponding to single molecule interactions in a single experimental run [28]. To determine off rates (unbinding rates), DFS retracts the force probe at a variety of rates to examine the rate dependent unbinding force and then estimates the off rate built upon Kramers diffusion theory [29] on a two state model. Furthermore, DFS cannot be used to characterize any protein structure or protein-ligand binding reaction that displays irreversibility – for example different folding and unfolding pathways – such as prion proteins and integrin catch bonds, since it looks only at unfolding and unbinding forces, ignoring refolding and rebinding forces [30]. In contrast, energy reconstructions using equilibrium methods demonstrated here use the Boltzmann distribution to measure the statistical distribution of all states and are capable of measuring entire energy landscapes, including metastable states.

In this thesis, we have developed an equilibrium sampling technique using atomic force microscopy to directly map the entire free energy landscape of biological, chemical, and physical interactions. The method utilizes Brownian fluctuations of a microcantilever probe, which is brought into close proximity to the interaction potential of the substrate surface. By recording subtle deviations from the harmonic cantilever vibrations that are caused by proximity to the free energy landscape, the entire energy landscape can be

reconstructed. The reconstructions are performed in a model independent manner based on equilibrium positions of the tip, using Boltzmann distribution statistics.

1.1 Organization of the Thesis

This thesis focuses on thermal fluctuation aided measurement of free energy landscapes of biological and chemical interactions using both experimental and computer simulation approaches, with the goal to gain insight into interaction parameters, including binding energies, barrier widths, and curvatures for one and more energy wells.

Chapter 2 provides the background of the thesis. It covers the tools and techniques that are used to perform direct measurement of energy landscapes. A review is then provided of the current scanning probe techniques, especially atomic force microscopy, that are used to probe the interactions in a quasi-equilibrium manner. This is followed by an extensive overview of the methods that currently exist for computing free energies or their differences, based on various aspects and properties of the free energy landscape. The background ends with description and details of the Brownian fluctuation method used in this thesis to measure free energy landscapes.

Chapter 3 details the measurement of the energy landscape between ligands and receptors interactions, under near-equilibrium conditions. We have used atomic force microscopy to directly map the intermolecular energy landscape curve of biotin-avidin bonds and discriminate multiple energy wells. Our method uses the Brownian fluctuations of a sensitive microcantilever probe decorated with biotin that is in close and lasting proximity to an avidin coated substrate. By recording subtle deviations from the harmonic cantilever vibrations as it translates towards the substrate and then transforming these

fluctuations using a Boltzmann sampling methods, we have reconstructed entire energy landscapes of interactions, including short lived, metastable states. The reconstructed energy landscapes reflect both rare short-lived biotin-avidin interactions and the overall shape of the average energy landscape including the presence of multimodal energy wells. Our analysis reveals a key limitation of the equilibrium method, specifically that it cannot fully measure attractive potential wells with steep gradients.

Chapter 4 addresses a key limitation of the equilibrium method, i.e. the inability to map the complete interaction in the presence of attractive forces with high gradients in comparison to cantilever stiffness, which produce a critical instability [31]. This is particularly a problem at small surface separations in which the attractive forces between tip and sample may exceed this value and cause the tip to snap to the surface prior to contact. This snap-in is a fundamental limitation to accurate energy landscape reconstruction because the tip is no longer moving in response to the energy landscape but rather at the inertial limit of the cantilever mass. A solution is proposed by enhancing the vibrational noise of cantilevers, which increases the range of the reaction coordinate being sampled. In turn, this enables the sampling of regions of large attractive interactions while the restoring force of the cantilever is still sufficient to avoid long-term binding to the surface. The enhanced vibrational noise can be defined in terms of effective temperature of the cantilever tip [32] and is supplied through a voltage signal to an on-chip actuator. The method uses Asylum's iDrive magnetically actuated cantilevers, which uses a small oscillating current loop on the surface which is coupled with the magnetic field created by small magnet attached to the cantilever holder to create forces which cause the cantilever to oscillate. The current is supplied in the form of white noise with amplitude proportional

to the magnitude of current. By modulating the amplitude of white noise, we have enhanced the cantilever's Brownian (thermal) fluctuations to allow it to vibrate through the energy profile between the tip and substrate surface, without getting trapped. By recording subtle deviations from the harmonic cantilever vibrations, the energy landscape was reconstructed. Using these techniques, we have demonstrated the direct mapping of interfacial free-energy potentials of steep potential wells of Si_3N_4-mica interactions in HPLC water at pH 7.

While we demonstrate the enhanced stochastic excitation approach in a simple energy landscape with only well, the approach is also valid for complex energy landscapes with multiple wells. Chapter 5 tests the enhanced stochastic approach via computer simulations of the behavior of a cantilever tip in a two well attractive potential field, using Brownian motion dynamics. We used the simulations to perform a parametric sweep of the different factors influencing measurement of energy landscapes (landscape parameters: barrier height and slope, probe parameters: stiffness and approach speed) and identified trends for optimal effective temperatures required to fully sample the energy landscape for each case.

Chapter 6 serves as an opportunity to summarize the findings reported throughout the thesis and better put these results in context with one another. It also discusses the future directions of the research.

BACKGROUND

This chapter covers the background on both the experimental and theoretical techniques that are combined to reconstruct the binding energy landscapes of ligand-receptor interactions and nonspecific interactions between the tip and substrate using atomic force microscopy techniques. The chapter is divided in six sections. Section 2.1 highlights the importance of energy landscapes for intermolecular interactions. Section 2.2 describes in detail the different measurement techniques that are used to probe energy landscapes. Section 2.3 delves into the AFM and the force-distance mode that is used in this thesis to collect information about intermolecular interactions. Section 2.4 covers the dynamic force spectroscopy methods used to extract the kinetic parameters of the underlying energy landscape of an interaction. Section 2.5 covers the various equilibrium and nonequilibrium methods used to fully reconstruct the free energy landscape of the interaction. Section 2.6 presents the energy landscape reconstruction approach, using cantilever's Brownian fluctuations, that is the basis of this thesis.

2.1 Importance of Energy Landscapes

In the last few decades, a series of experimental and theoretical advances has made it possible to obtain a detailed understanding of the mechanisms underlying many physical and biological binding interactions [33-40]. To explain these mechanisms, chemists, scientists and engineers have spent considerable effort studying the thermodynamics and kinetics of the processes by which these interactions took place. A tremendous amount of experimentation on protein structural stability and protein-ligand binding was aimed at

understanding the driving forces of these reactions, eventually learning that a macromolecule's native structure is the one with the lowest – or nearly lowest – possible Gibbs free energy, and that all the information required for renaturation is contained in the amino acid sequence itself [41-44]. With the increasing power of computer technology and improvements in modeling of force fields, atomistic simulations have become increasingly important because of their ability to generate highly detailed and accurate descriptions of interactions [18, 19, 45-48]. In an attempt to organize these results, scientists conceptualized a pathway for binding/folding of biological molecules, formulating a phenomenological model for the off-rate after observing increased rates of bond dissociation under external force [23, 49-52], and formed the first models of single-molecule kinetics.

In the late 1980s, it was proposed that the most important aspect for understanding an interaction is a global overview of the reactants to product energy surface [5, 33, 53]. The global view would be particularly helpful for those interactions in which the organization of an ensemble of conformations and bonds creates a nuanced energy surface with many barriers and local minima, which is more descriptive than calculating only a few of the most prominent features resulting in an incomplete picture [54]. In such a case, a statistical description of the energy landscape could be used to describe the features of the interaction mechanism[55]. Together, this is the basis of the energy landscape theory.

Energy landscape theory provides the fundamental framework for the modern description of all interactions. It has been experimentally validated primarily for structural self- assembly, or "folding," of biopolymers like proteins and nucleic acids [5, 56]. The landscape encapsulates the critical properties of an interaction or binding/folding event,

including energy changes, barriers, intermediates, roughness or internal friction, alternative pathways or connecting states, and the rates of reaction [54, 57]. Mapping and understanding energy landscapes is thus a key goal in biochemistry, physical chemistry, and biophysics research. To this date, most research has been focused reconstructing protein folding phenomena and less on adhesion phenomena commonly seen in ligand-receptor binding and tip-surface interfacial interactions.

2.2 Experimental Methods to Probe Energy Landscapes

Despite the importance of energy landscapes for understanding reaction mechanisms and the wealth of existing theoretical and computational work in landscape theory, few methods are capable of reconstructing energy landscapes quantitatively from experimental data. Ensemble techniques, including surface plasmon resonance (SPR) [58-60] and calorimetry [61, 62], are commonly employed to extract thermodynamic and kinetic properties of small and macro-molecular structures and their interactions. SPR uses gold-coated glass functionalized with a monolayer of ligand, over which a solution containing its protein conjugate is flowed. Polarized light is reflected off of the glass, and protein-ligand binding causes small changes in the angle and intensity of the reflected light. The sensorgram data is fit with one- or two-state kinetic models to calculate the affinity and dissociation constants. Isothermal titration calorimetry begins with a ligand in solution, and the addition of its protein causes binding and a change in the solution temperature which is brought to equilibrium by a heating element before introducing more protein into the chamber. The thermodynamic properties and the dissociation constant are calculated from the binding isotherm.

Though these ensemble techniques are capable of measuring kinetics and free energy of binding, they are limited to bulk assays. Due to the large numbers of molecules involved in the measurements, they only determine average properties of an interaction. If, as is the case with protein-ligand binding and molecular folding, there exist barriers to reaching a final state, then ensemble techniques capture only the total enthalpy and energy required to transition from starting to final confirmations, and dissociation constants associated with each energy well are averaged to produce a single constant for the entire interaction. For information about interactions at the molecular scale, these techniques prove to be insufficient.

Direct experimental measurement of the interactions between molecules and molecular assemblies has been achieved using techniques such as surface forces apparatus (SFA) [63, 64], biomembrane force probes [3, 65], optical tweezers [17, 66], and atomic force microscopes. The SFA has yielded considerable information about adhesion and friction between molecular assemblies, although these data are averaged over the large numbers of molecules within the 1 mm^2 probing area, thus making it difficult to achieve microscopic levels of information [67]. Biomembrane Force Probes (BFP) were designed for quantification of single molecular bonds and ligand receptor binding on the surfaces of cells. The technique consists of using the deformation of a 10-20 μm vesicle under tension as a force sensor. The tension in the vesicle is controlled by a suction pipette that sets the hydrostatic pressure difference across its membrane. It is a versatile tool that can be used for a wide range of forces (0.1 pN to 1 nN). However, the bandwidth of the optical readout of the probe is limited to 1 kHz, which is insufficient to capture fast transitions in a ligand-receptor binding events [68, 69].Optical tweezers use a focused laser beam to provide an

attractive or repulsive force (typically on the order of picoNewtons) to manipulate and study single molecules conjugated to a bead. Optical tweezers remain a popular choice to study folding landscapes of DNA hairpins attached to DNA handles [70], but they haven't been used for ligand-receptor interactions due to relative large areas of the beads.

In the context of energy landscape determination, atomic force microcopy (AFM) can be very useful for probing interactions between molecules or surfaces by exerting ultra-small forces on sub-nanometer scales with high time resolution. AFM has been used for measurements of single protein-ligand interaction strength [3, 72, 73], chemical-interaction strength [74] and potential-energy profile [75] . Through its ability to position and move a sample in space with angstrom-level precision, high stability, and a wide range of speeds; and microfabricated AFM cantilevers with stiffness low enough for measuring molecular interactions, AFM has become a ubiquitous instrument for probing single molecule or localized interactions.

2.3 Atomic Force Microscopy

Many important biological and chemical processes occur on the length scale of nanometers with a time scale of milliseconds, yet few microscopies can operate in these domains. Scanning electron microscopy can image surfaces and biological structures with unprecedented detail [16]. However, it cannot observe physiological dynamics due to the sample preparation requirements. Atomic force microscopy (AFM) is a scanning probe measurement technique that can image surfaces with complex topographical features with nanometer scale resolution, in air and physiological environments, including DNA, cells, and cellulosic materials [76-78].

AFM was invented in 1986 by Binnig, Quate, and Gerber [79] wherein they demonstrated for the first time nanoscale imaging of insulators via a scanned flexible probe with a sharp tip. By employing a very small and sharp probe tip at the end of a small cantilever, they were able to measure ultrasmall forces caused by close proximity to the surface. The forces between the cantilever tip and the sample surface are composed of both attractive and repulsive components. The main contributions to the attractive forces are the Van der Waals force, electrostatic force, and short-range chemical forces including solvation, hydration and hydrophobic forces [80, 81]. The repulsive forces are very short-range forces which include Pauli-exclusion repulsion and Coulomb interactions [82].

During sample imaging, the deflection direction (towards vs away from the sample) is governed by the tip sample interaction (attractive vs repulsive). A diode laser is reflected off of the cantilever to strike a four-quadrant photodetector, which converts the motions of the cantilever to an electrical signal sent to a computer. The vertical deflections are recorded as the height of each pixel in the image. The sample is raster scanned underneath the tip as the cantilever base is raised and lowered to maintain a setpoint deflection (contact-mode imaging) or amplitude (tapping-mode imaging). The measured height data is plotted versus the x- and y-axis, rendering a three-dimensional image of the surface. A schematic of AFM system is included below in Fig. 2.1.

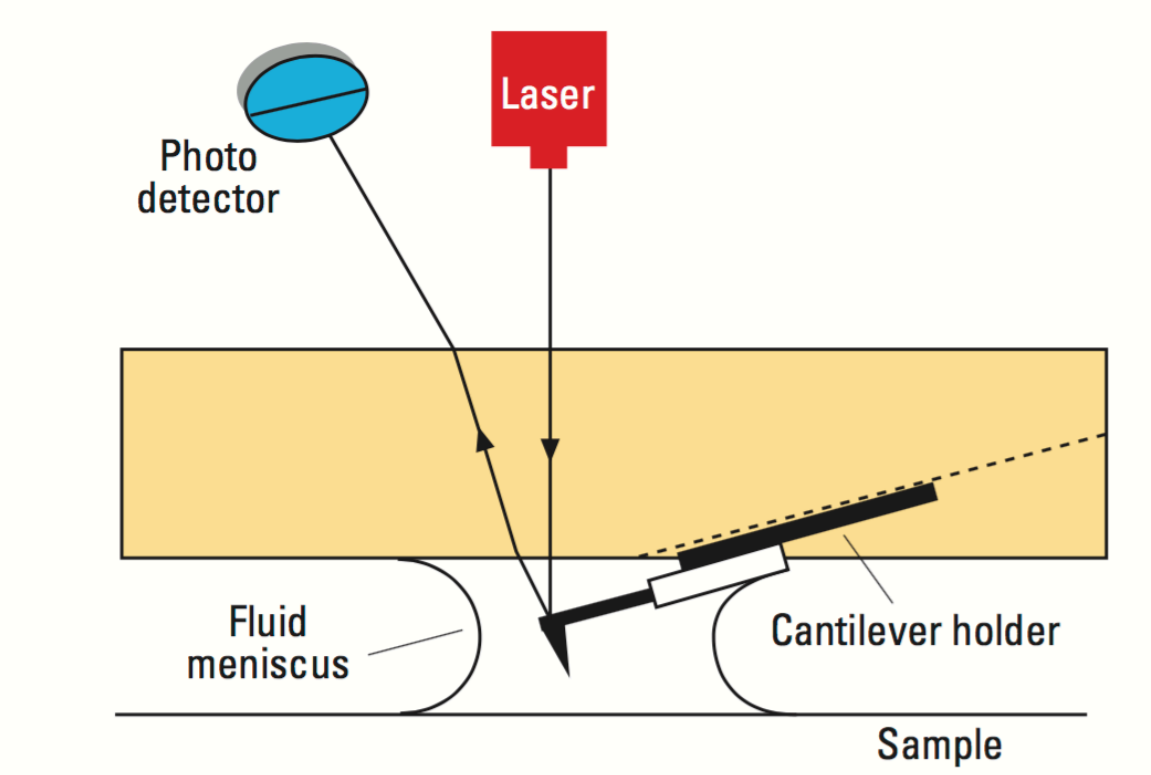

Figure 2.1 Schematic of an atomic force microscopy (AFM) system. Adapted from Sulchek et al. [83]

For imaging, the resolution depends strongly on the size and shape of the tip. The smaller and sharper the tip, the smaller the surface area sampled by the tip and smaller feature sizes can be detected. The most common type of AFM tip is made of silicon nitride (Si_3N_4) and is pyramidal in shape with a tip radii of ~10-60 nm [84]. Si_3N_4 cantilevers have very low force constants (~10 to 1000 pN/nm) relative to silicon cantilevers (~1 N/m), providing excellent force sensitivity while being a low-wear material, minimizing tip wear and distortion of AFM data [85]. Some samples are highly attractive in nature, causing the soft Si_3N_4 cantilevers to readily stick to the surface rather than follow the full attractive and repulsive shape of the energy surface. Stiffer silicon cantilevers can resist the overpowering van der Waals force, but with decreased force sensitivity – potentially missing subtle

shapes along the energy surface. Choosing the right cantilever resonance frequency is also important since high resonance frequencies in the hundreds of kHz require high data collection rates of almost 1 MHz (1 million samples per second) in order to capture all of the deflection information contained in the cantilever's vibration.

The AFM can be operated in either topographic or nontopographic modes [86]. The topographic modes aid in collection of images, whereas nontopographic modes are designed to measure other properties of the sample. In this thesis, the focus is on the nontopographic mode to collect force curves that describe the deflections of the cantilever under the influence of a force field.

2.3.1 Force Spectroscopy Mode of AFM

The AFM is also a powerful tool for sensitive force measurements, on the order of 10 picoNewtons [87]. The softness of the AFM cantilever and the small radius of the AFM tip allow high sensitivity for smaller forces and the capability to probe local interactions at nanoscale levels [88, 89]. In force spectroscopy, the cantilever-tip assembly acts as a sensitive force sensor. The cantilever and the tip are moved towards the sample in the Z-direction. A single movement cycle consists of the tip approaching the sample until it makes contact with the surface and then retracted again. The tip sample interaction force is recorded during the entire cycle. This is then repeated several times at the same spot and different locations to give a better statistical understanding of the interaction. AFM can directly measure the force between the atoms or molecules at the end of the probe and the surface. In ligand-receptor binding, the ligand is often immobilized on the AFM tip and the receptors are immobilized on the surface [90]. The presence of interaction forces causes

the cantilever to deflect and the deflections of the cantilever are recorded which gives rise to force-distance curves.

Force curves provide quantitative information of interaction forces present between the tip and the sample by measuring the amount of force experienced by the cantilever as the tip approaches the sample surface. Fig. 2.2 shows a schematic of a typical force curve generated by the AFM.

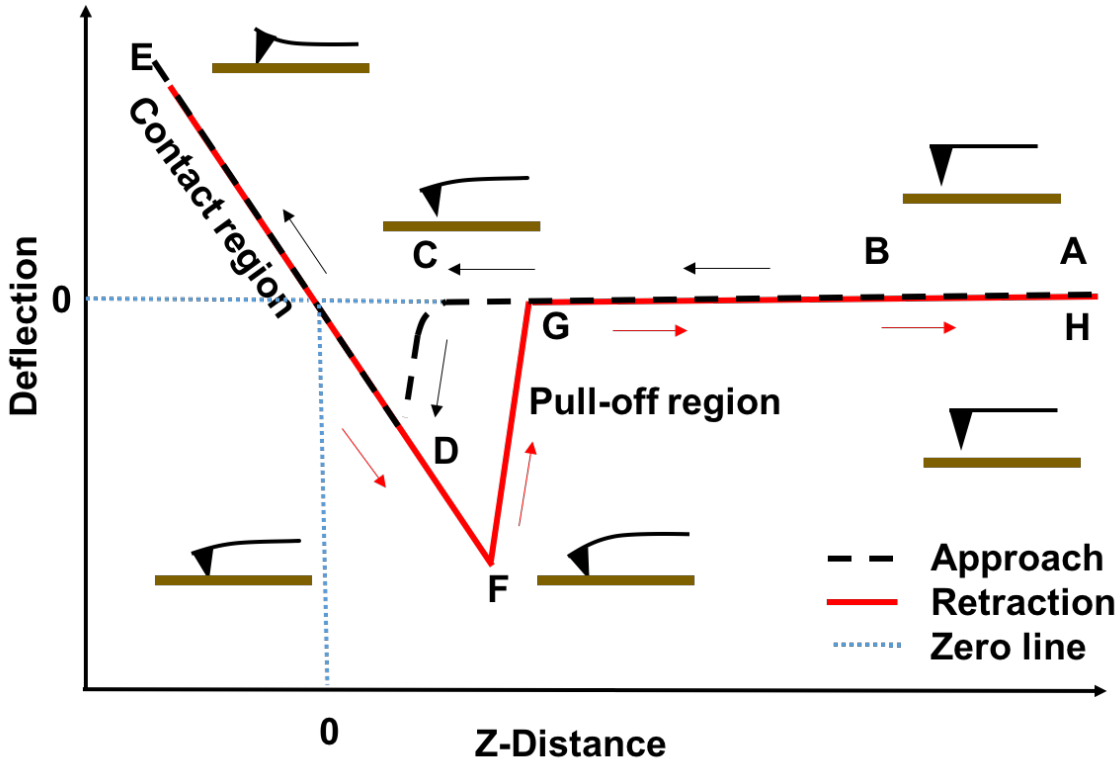

Figure 2.2 Schematic of a typical force-distance curve generated by an AFM system illustrating movement of the cantilever during its approach (black) and subsequent retraction (red) from the surface. The contact region is used to calibrate the deflection signal. Zero point of Z-distance axis is defined as the intersection of straight lines fitted to

section A-B and section D-E (shown by blue dotted lines). Arrows indicate the direction of progress of an AFM experiment

During the approach phase, at position A, which is far away from the sample, there is no tip-sample contact. As the cantilever approaches the sample surfaces from A to B, long-range interactions, such as electrostatic interactions can be felt. At position B and during its movement from B to C, when tip is very close to the sample, short-range forces, such as Van der Waals or capillary forces, play a dominant role. At this distance, when the sum of the forces is attractive (pull-on force), the tip will jump to the surface (position C). This is called a snap-in event (C →D). During the snap-in event, the cantilever is essentially in a free-fall with its acceleration only governed by its dynamics and not by the tip sample interaction force fields. Thus, the approach binding curve cannot be used to accurately determine the adhesive interaction strength. Once the cantilever is in contact with the surface, the cantilever deflects further due to increasing force as the cantilever is pushed towards the sample and this gives rise to the linear part of the force curve (D →E). At this point, the stiffness and elastic response of the sample can be measured. The cantilever then retracts in the Z-direction (E →F) and force felt by the cantilever decreases. Adhesion forces keep the tip in contact with the sample and this leads to a negative deflection of the cantilever and results to a negative peak in the force curve (pull-off force at position F). The cantilever then breaks free from the surface (position G) and returns to its starting deflection (position H). The deflections measured during snap-in (C →D) are typically lower than pull-off (F →G). This is due to several reasons. First, the retraction/pull-offs force curves are recorded at much higher velocities than approach force curves, which translate to correspondingly higher forces due to dynamic effects [65]. Importantly, the

approach curve is not sufficient to sample the strong interactions with deep energy wells [32]. The depth of these energy wells is much higher than the thermal energy of the cantilever; therefore, upon entering the well, cantilever gets trapped at the bottom of the well, losing the opportunity to sample the well or subsequent interaction fully. This is also explained in Chapter 4.

The raw data consists of voltages that are linearly proportional to the deflection of the cantilever. The part of the force-distance curve where the tip is in contact (position 3) is used to calibrate the deflection signal and convert it to nanometers, using deflection sensitivity values. The tip sample force F is then related to the cantilever's deflection through Hooke's law [85, 91]:

$$F = kx \qquad [2.1]$$

where k is the cantilever's spring constant (N/nm), and x is the calibrated cantilever's deflection. The tip sample distance (D) can then be calculated from the cantilever base to surface distance ($Z_{distance}$) and cantilever's deflection (x) using the following relation (Fig. 2.3)

$$D = Z_{distance} - x \qquad [2.2]$$

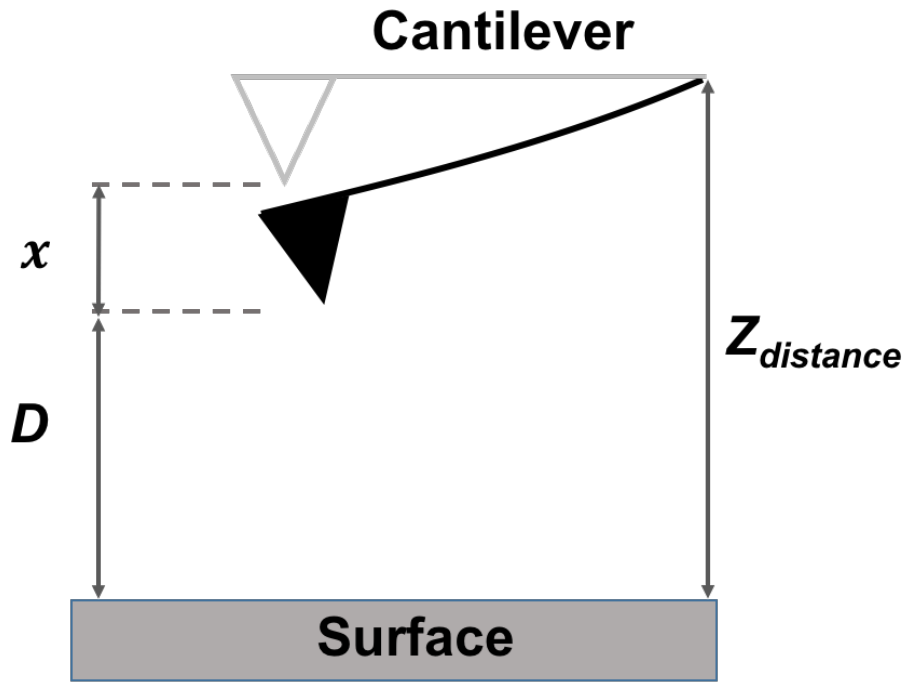

Figure. 2.3 Schematic of an AFM cantilever tip deflecting towards surface from its equilibrium position (gray) under the action of an attractive force. The tip sample distance (D) is calculated by subtracting deflection (δ) from the cantilever base to surface distance ($Z_{distance}$), which is measured by the z-transducer signal

Thus, the tip sample distance can change either from a movement of the Z actuator, or from a stable or dynamic change in cantilever deflection. The force-distance curve is a plot of the force versus the true tip-sample distance calculated from the raw data.

2.3.2 Calibration of Force Curves

The part of the force-distance curve where the tip is in contact with the surface is first used to calibrate the deflection signal in volts and convert it to nanometers. Because a tip in contact with an uncompressible surface follows the movement of the cantilever base, the slope of section D-E in a calibrated curve will be unity (see Fig. 2.2). Taking this into

account, calibration of the force-distance curves is performed by fitting a straight line to section D-E for each approach portion of the force-distance curve of the data set and dividing the scale of the *y*-axis of the curves by the average slope. The calibration of the zero point of cantilever base-surface distance ($Z_{distance}$) is obtained from the intersection of the line fitted from section D-E and the baseline section (shown as zero line in Fig. 2.2). This calibration will eliminate the effect of drift in the Z-direction. The baseline is fitted from sections A-B where there is negligible tip sample interaction.

2.3.3 Determination of Spring Constant

The nominal values of cantilever's spring constant k that are provided by the manufacturer are typically batch averaged values, and more accurate calibration of individual cantilever's spring constants are necessary for sensitive and fluid based applications [92]. The most popular calibration method is the thermal noise method [93]. This method is based on measuring the free fluctuations of the cantilever, and hence it can be performed in liquid and actually in-situ during an experiment. This method involves measuring the cantilever's mechanical response to thermal fluctuations including the diffusion of small particles (Brownian motion). The size of the fluctuations is measured by the AFM system by recording the cantilever's vertical deflections over time and collections of these deflections are then analyzed. These deflections are analyzed by looking at the frequency dependence of the fluctuations. The greatest amplitude is usually seen around the cantilever's resonance frequency. The resonance peak is then fitted with a Lorentz function and the area under the curve is used to estimate the energy in the resonance. Thereafter, the spring constant can be estimated by relating average cantilever deflections ($\langle\delta\rangle$) obtained from Lorentz fit to data, cantilever's spring constant (k) and the energy of

resonance, using the equipartition theorem. The theorem states that the energy in any free mode of system is equal to the thermal energy at the absolute temperature of the system $\left(=\frac{1}{2}k_bT\right)$, where k_b is Boltzmann constant and T is the temperature of the system [94, 95]. Thus the spring constant can be calculated as,

$$\frac{1}{2}k_bT = \frac{1}{2}k\langle x^2\rangle \qquad [2.3]$$

2.3.4 System Noise

The limits of force sensing and force resolution in force spectroscopy are determined by the overall noise in the system, which includes the AFM, the sample, and the environment in which they are [96]. The sources of noise from the AFM include the thermal noise of the cantilever, mechanical vibrations of the components of the AFM, and electrical and optical contributions of the corresponding components in the system [97]. The noise determines the lower limit of force that the AFM can detect. The noise level of our instrument is 2.2 pN in a 1 kHz measurement bandwidth (AFMs are commonly ~ 10 pN [91]).

Thermal noise is directly related to the cantilever' stiffness and its damping coefficient and inversely to its resonance frequency. Since all of the three cantilever properties are related to its dimensions, one way to achieve low noise cantilevers is to shrink all the dimensions sufficiently. [87]. Also smaller cantilevers allow for high signal to noise resolution [97]. Mechanical noise mitigation is achieved by placing the AFM on top of active dampeners and a large granite block that acts as a low- pass filter, then enclosing the entire system in an acoustic chamber that blocks ambient acoustic noise.

Systematic errors that also arise in the calculation of forces can be reduced through accurate estimation of the cantilever spring constant.

2.4 Determination of Kinetic Parameters

AFM pulling measurements can be very useful in determining kinetic properties of interactions. By applying an external mechanical force to a system, it is possible to enhance the dissociation of a bond to understand key properties of the dissociation landscape [3, 18, 27, 98]. Broadly classified, these are called dynamic force spectroscopy techniques and have been used by multiple researchers to predict kinetic/unfolding properties of biological and chemical interactions [15, 24, 26, 27]. In 1978, Bell modeled the exponential increase in the rate of bond dissociation under external force and showed how an increasing force can change the energy landscape and lower the activation energy barrier [23] (Fig. 2.4).

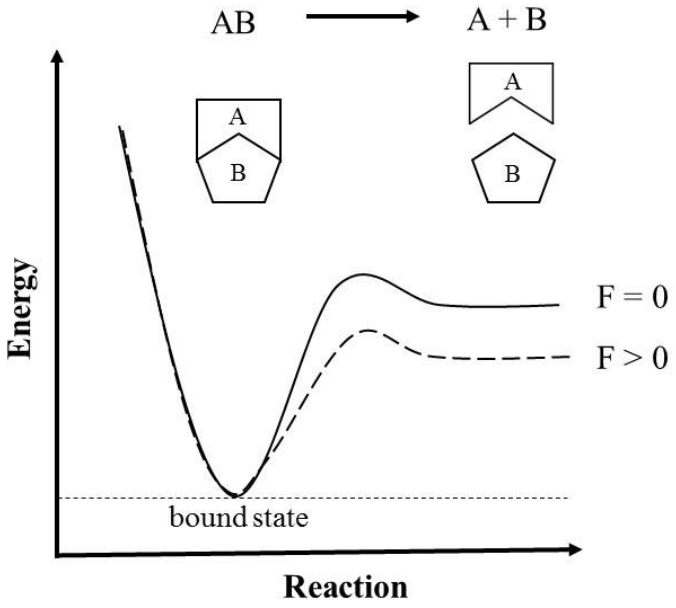

Figure 2.4. A schematic showing the effect of applied force (F) on bond dissociation. Applied forces tilt the energy landscape (dotted lines) and lower the activation energy

barrier thus enhancing bond dissociation, as compared to absence of any external forces (solid lines). Adapted from Lee et al. [99]

When an external force is applied, the path from bound to unbound states can be modeled as a diffusive process along a preferential path over one or several confining energy barriers (Smoluchowsky diffusive model) [100]. The impedance of these energy barriers is described by the time of transit over the barrier and the force applied. In the limit of large statistics, the distributions of rupture times and forces follow a first-order Markov process [101] where time and force are tied together through the loading dynamics of the probe. When pulled by an elastic spring probe, the loading dynamics are set by the pulling speed and the probe stiffness. Keeping this in mind, Evans [22] proposed a 2 state model, where he predicted that the unbinding force of a ligand-receptor bond should depend logarithmically on the loading rate as:

$$F(r) = \left(\frac{k_b T}{x_\beta}\right) ln\left(\frac{r x_\beta}{k_{off} k_b T}\right) \qquad [2.4]$$

$F(r)$ is the most probable rupture force [102] obtained by Gaussian fit to the histogram of the rupture forces data, x_β, the location of the energy barrier, r, the loading rate, k_b the Boltzmann constant, T the temperature and k_{off} the off rate constant at zero force. The loading rate is defined as the product of slope of the rupture event (pN/nm) and the tip's retraction speed (nm/s). A plot of the unbinding force vs. the logarithm of the loading rate usually gives rise to a straight line. The slope of the line is inversely proportional to x_β and the vertical axis intercept of the line can be used to determine k_{off} . Fig. 2.5 shows an

example of Bell-Evans fit of rupture forces data which is used to extract kinetic parameters of dissociation of amyloid β proteins.

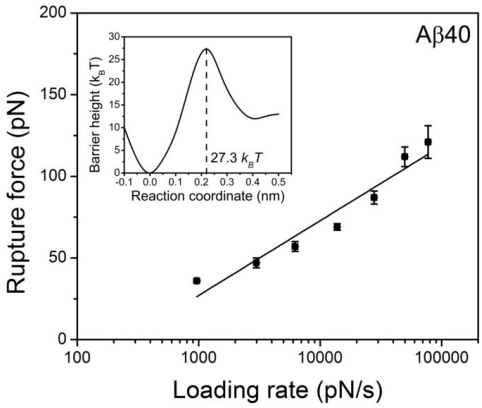

Figure 2.5. The solid line represents the results fit with the Bell−Evans model. The inset shows the reconstructed energy landscapes of misfolded Amyloid β dimers. Adapted from Lyubchenko et al. [103]

For an energy landscape with a single barrier, this would give rise to a simple linear force spectrum on the log scale. For systems involving more than one barrier, this will lead to multiple linear regimes in the force spectrum plot, with each linear regime corresponding to the overcoming of a single energy barrier along the unbinding pathway [3, 99, 104]. By varying the loading rate of the force applied, one can make emphasize different barriers to map the dissociation landscape of the system. This can provide detailed insight on the molecular dynamics of a ligand-receptor system.

The Bell–Evans model, though frequently cited, assumes that k_{off} scales linearly with exp (Fx_β). However, this assumption has been shown to be an oversimplification [105]. The model assumes that the energy barriers are very sharp, and thus cannot determine the curvature of the energy landscape. The Dudko-Hummer–Szabo model [106]

modified the Bell–Evans model and applied Kramer's theory [29] to more rigorously extract kinetic parameters. The effect of molecular linkers can also be included in the Dudko model [106]. Dudko-Hummer-Szabo model is as follows:

$$\tau(F) = \tau_0 \left(1 - \frac{aFx_\beta}{\Delta G}\right)^{1-\frac{1}{a}} exp\left(\beta\Delta G\left[1 - \left(1 - \frac{aFx_\beta}{\Delta G}\right)^{\frac{1}{a}}\right]\right) \qquad [2.5]$$

$$\tau(F) = \frac{\left[\frac{\pi}{2}(\langle F^2\rangle - \langle F\rangle^2)\right]^{1/2}}{r(F)}$$

where τ is the bond lifetime, a is a power scaling factor corresponding to 1/2 for a cusp-like barrier (for harmonic constraining potentials) , 3/2 for a "linear-cubic barrier", and 1 for a recovery of the Bell–Evans model, τ_0 the intrinsic bond lifetime, x_β the barrier width, k_B the Boltzmann constant, T the temperature, $\beta = {}^1/_{k_B T}$ the inverse of Boltzmann energy, and ΔG is the free energy of the landscape, where $\langle F^2\rangle$ is the mean squared rupture force at a given loading rate $r(F)$. Fitting the force spectroscopy data to the model allows us to determine the kinetic parameters. Fig. 2.6 shows a representative Dudko model fit to extract parameters from a protein unfolding experiment.

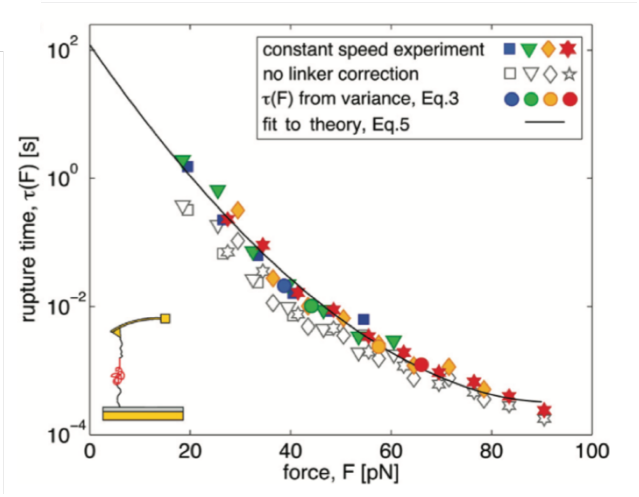

Figure 2.6. A Dudko model fit to extract the kinetic and thermodynamic properties of a protein unfolding experiment. Adapted from Dudko et al. [106]

Recently Friddle, Noy and De Yoreo challenged the assumption made by earlier models that no reversible binding occurs during force experiments [97, 107]. Earlier theoretical modeling of driven bond-rupture processes began by recognizing these two primary states of the system, yet assumed that after the initial bond rupture, reverse transitions back into the bound state were negligible at experimental loading rates. This assumption was not always justified. In contrast, Friddle's analysis which was based on the complete two-state system showed that reversible binding had real effects on the measured force and that the case of irreversible emerged as a limit. They approximated the unbinding force $<F(r)>$ for a N-bond system by the following equation:

$$< F(r) > \cong F_{eq} + F_{\beta} ln\left(1 + e^{-\gamma} R\left(F_{eq}\right)\right), \qquad [2.6]$$

$$F_{\beta} = \frac{N k_b T}{x_{\beta}}, R(F_{eq}/N) = \frac{r}{k_{off}\left(F_{eq}/N\right) F_{\beta}}, F_{eq} = \sqrt{2k\Delta G_{bu}},$$

$$k_{off}\left(F_{eq}\right) = k_0 e^{\left(\beta\left(F_{eq} x_{\beta} - \frac{1}{2} k x_{\beta}^2\right)\right)}$$

where F_{eq} is the equilibrium force for the bond/transducer system, F_{β} the thermal force, γ = 0.577 the Euler's constant, k_0 the intrinsic unbinding constant, x_{β} the barrier width, k_B the Boltzmann constant, T the temperature, $\beta = {}^{1}/_{k_B T}$ the inverse of Boltzmann energy, k the spring constant of cantilever and $\Delta G_{bu} = G_b - G_u$ is the free energy of binding relative to free energy of the cantilever. The above Friddle-Noy-De Yoreo reversible binding equation can be fitted to the either the raw data or most probable force data and free energy landscape parameters k_{off}, x_{β} , F_{eq} and ΔG_{bu} can be estimated. Eq. (2.7) seamlessly describes the two-trends which are often observed in force spectroscopy data as well as the transition between them [108, 109]. In the limit of vanishing loading rate, the spectrum approaches the equilibrium force. Fig 2.7 shows a Friddle-Noy-deYoreo fit of the rupture force data of single ligand-receptor bonds to quantify the binding energy landscape of PAR1.

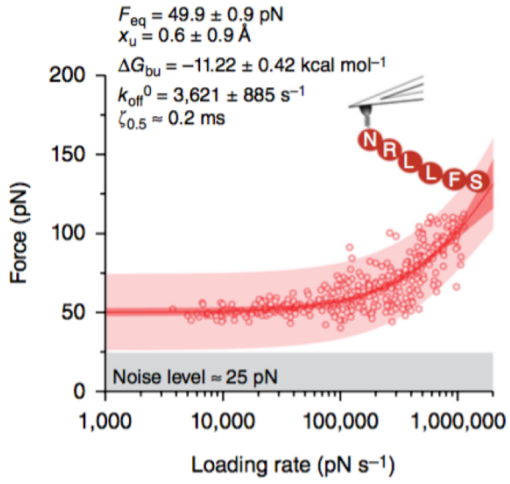

Figure 2.7. Loading rate–dependent interaction forces of single ligand-receptor bonds are utilized to quantify the ligand-binding energy landscape of PAR1 to SFLLAN peptide, using a Friddle-Noy-de Yoreo model fit. Adapted from Alsteens et al. [110]

2.5 Reconstruction of Free Energy Landscapes

In single-molecule force spectroscopy (SMFS) experiments, mechanical tension is applied across a single molecule so as to perturb its structure, and the extension of the molecule is measured as its structure changes under the applied load [111-113]. Various types of force probes have been used for SMFS, most commonly atomic force microscopes (AFMs), optical tweezers, and magnetic tweezers [111, 114]. The molecule is attached at one point to a force probe and at another point to a fixed surface (in AFM) or a second force probe (optical traps). The response of the molecule to applied force is subsequently measured in one of the four ways:

(*a*) constant force, where fluctuations in extension are recorded as the load is held constant with a force clamp (Fig. 2.8A)

(*b*) constant position, where fluctuations in both molecular extension and force are recorded as the probe is held at an unchanging position (Fig. 2.8B)

(*c*) force ramp, where the molecular extension is recorded as the force is ramped up or down by moving the probe at a constant speed (Fig. 2.8C), and,

(*d*) force jump, where the molecular extension is recorded after the force is changed abruptly to a different value (Fig. 2.8D).

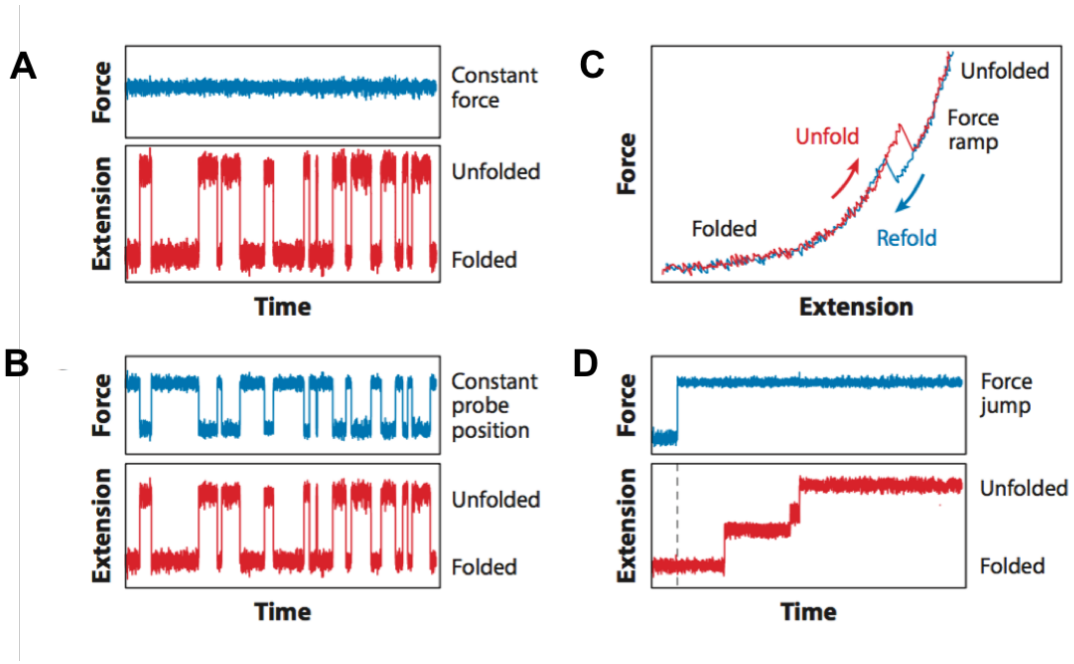

Figure 2.8. (**A**) Constant-force mode measurement to record the fluctuating extension as a molecule unfolds and refolds while the force is clamped. (**B**) Constant-position mode measurement where both the extension and the force fluctuate as biomolecules bind/unbind. (**C**) Force-ramp mode measurement where molecules are made to unfold and refold at accelerated rates leading to a nonequilibrium process. (**D**) Force-jump mode where the force is abruptly jumped and then clamped at the new value. The extension then increases in steps as the molecule changes unfolds and refolds. Adapted from Woodside et al. [1]

The first two methods record equilibrium fluctuations whereas the last two are nonequilibrium based, owing to the rapid force changes that cause state change in one direction only. Landscape profiles can be reconstructed, with varying degrees of success, using each of the measurement techniques, as will be elaborated upon in the following sections.

2.5.1 Reconstruction using Equilibrium Measurements

2.5.1.1 Constant Force Measurements: Free energy is defined as the logarithm of the marginal probability density of the system in equilibrium corresponding to the chosen thermodynamic ensemble. Hence, to calculate a free energy we need to estimate the probability density $\rho(x)$ (e.g. by constructing histograms) from constant force ($F_{1/2}$) probe deflection data. The free energy landscape profile $G(x)$ is found directly from $P(x)$ by inverting the Boltzmann relation, up to a constant (C).

$$G(x) = -k_b T ln\big(P(x)\big) + C \qquad [2.7]$$

where k_bT is the thermal energy. Eq. 2.7 is also known as inverse Boltzmann equation or transform. Note that $G(x)$ is the total free energy of the system and includes the contribution of the force probes (AFM cantilever or the optical traps etc.). An essential requirement of this type of reconstruction is that the applied load be held constant over the full temporal bandwidth of the protein folding or molecular binding process.

Cleveland and co-workers first harnessed the Boltzmann relation to observe perturbations to the spring harmonic well by water ordering near calcite and barite surfaces [115]. Woodside et al. [116] later extended this approach using high resolution optical trapping measurements of the folding of DNA hairpins as a model system.

Reconstructing energy landscapes using the inverse Boltzmann transform (Eq. 2.11) for the constant force method poses many challenges. Firstly, the probe must have very low stiffness in order to register a deflection in response to changes in interaction force gradients. At constant forces, achieved through passive force clamps [117],

transitions between bound and unbound states become rarer as the energy barrier between the two states become higher. Hence, one needs to wait impractically long amounts of time in order to record sufficient bound-unbound equilibrium transitions of high energy states to have enough statistics to fully reconstruct the energy surfaces [118]. Since the effect of noise, particularly instrumental drift, also becomes more pronounced as the data collection time increases, the instrument must have extraordinary stability. Finally, the dynamics of the interaction are still convolved with the dynamics of the force probe. In order to recover the underlying free energy surface of the interaction, one needs to deconvolve the effect of the probe. Using a nonlinear iterative Fourier deconvolution procedure, the underlying intrinsic landscape of the interaction can be obtained [116, 119]. But the Fourier deconvolution procedure has its own set of limitations. Any experimental noise added to the deflection signal by the system after the convolution by probe will be greatly amplified when the Fourier transform of the signal is divided by the Fourier transform of the probe. Since the high frequency components of the probe are typically very small, the operation will result in a great amplification of high frequency noise in the resulting deconvoluted signal. Hence, only a limited range of frequency information can be correctly recovered by Fourier deconvolution, which restricts the resolution of the reconstructed landscape [116].

2.5.1.2 Constant Position Measurements: A similar approach to landscape reconstruction can be applied to measurements where the position of the force probe is held constant, rather than the force. The system is again in equilibrium and inverse Boltzmann equation determines the total energy at any specified position. However, in constant position measurements, force varies linearly with the molecular extension owing to the finite probe stiffness. Measurements based on a constant probe position provide an advantage over

constant-force measurements with a zero stiffness probe. For sufficiently stiff probes, the motion of the probe tip over the energy landscape is constrained by the harmonic potential imposed, such that only a portion of the range of the reaction coordinate is explored in a given measurement. This constraint allows the probe to sample the states near the energy barrier more frequently than would otherwise occur. These are precisely the states that are the most influential for the energy landscape reconstructions, but also normally the least occupied. By sampling close to the energy barrier, it is possible to reconstruct the barrier accurately with lesser number of statistics. It has been shown that harmonically constraining the folding trajectories on DNA hairpins can lead to faster landscape reconstructions than constant force measurements [118]. Harmonically constrained trajectories can allow reconstruction techniques to be extended to landscapes with higher energy barriers and hence more infrequent cantilever tip transitions, than might be possible otherwise.

2.5.2 Reconstruction using Nonequilibrium Measurements

2.5.2.1 Force-Ramp Techniques: A key limitation of equilibrium-based approaches is that the necessary equilibrium to sample enough bound-unbound transitions is difficult to attain in experiments. For example, when the energy barrier is high, the equilibrium transition frequency may be so slow that the only practical approach is to observe transitions well away from equilibrium, by ramping or jumping the force [120-122]. To address such cases, alternative methods for reconstructing landscapes have been developed on the basis of nonequilibrium statistical mechanics.

These methods move a given molecular system between two terminal states by means of an external potential in force-ramp experiments, which perturbs the system far away from its equilibrium. The average mechanical work done to move the system is generally greater than the free energy of the system, due to work being dissipated in a nonequilibrium process. This is in accordance with the second law of thermodynamics. In 1973 and in 1981, Kawasaki et al. [123] and Kuzovlev et al., [124] developed nonequilibrium partition identities and generalized fluctuation dissipation theorems, respectively to obtain equilibrium energies from nonequilibrium work. However, their statements were limited in application since they considered near equilibrium regimes, and were not applicable to truly irreversible systems. Then in 1997, C. Jarzynski presented a theoretical framework able to directly connect the exponential average of the external work performed during the molecular perturbation (W) and the corresponding free energy difference (ΔG).

$$< e^{-\beta W} >= e^{-\beta \Delta G} \qquad [2.8]$$

Using Jarzynski equality, one can average the work calculated during multiple nonequilibrium experiments with a Boltzmann weighting, in order to obtain free energy differences between the states. The Jarzynski equality (Eq. 2.8) cannot be directly used to calculate free energy landscape because it only gives the free-energy difference between two states, whereas energy landscape represents the evolution of free energy along a suitably chosen reaction coordinate. Hummer and Szabo [14] adapted the Jarzynski equality to energy landscape profile calculation using the weighted histogram method [21].

$$e^{-\beta G_0(x)} = \frac{\sum_i \frac{< \delta[x - x(t)] e^{-}(\beta W(t)) >}{< e^{-}(\beta W(t)) >}}{\sum_i \frac{e^{-(\beta V(x,t))}}{< e(^{-}\beta W(t)) >}} \quad [2.9]$$

The term $G_0(x)$ in this formula is the value of the Gibbs free-energy at a specific point *x* along the reaction path, *W(t)* is the work sample at time t and *V(x,t)* is the external potential (instantaneous deflection potential). This approach was tested experimentally by measuring DNA hairpins with optical tweezers [70]. This reconstruction agreed well with the constant-force reconstruction obtained before force probe deconvolution. However, the spatial resolution of the reconstruction was somewhat lower, owing to the coarse binning needed to produce well-defined work distributions, particularly near the barrier position. As a general rule, nonequilibrium methods typically require ever more data to recover equilibrium energies as the amount of dissipated work increases [125]. In particularly difficult cases, when the transition is far from equilibrium corresponding to high ramp speeds or soft probes, the reconstruction may become unreliable or incomplete for some values of the reaction coordinate.

2.5.2.2 Force-Jump Techniques: In cases when it is difficult to obtain a reaction coordinate which can continuously describe the reaction progress [126], fluctuation theorems, which are based on continuous changes in control parameters, such as Jarzynski's equality are not applicable. Zhang et al. [127] developed an alternative approach applicable to such discontinuous measurements, under the assumption of overdamped Langevin dynamics, which was based on inverting the nonequilibrium stationary probability density. Folding trajectories, starting in the unfolded state at x_U and ending at x_F, sample the probability

density P, obtained from integrating the Fokker–Planck equation associated with the Langevin dynamics, according to

$$P(x) = \alpha e^{[-\beta G(x)]} \int_{x_F}^{x} \frac{e^{[\beta G(y)]}}{D(y)} dy \qquad [2.10]$$

for $x_F < x < x_U$, and $P(x) = P(x_U)$ for $x \geq x_U$. Here, α is a normalization constant, and $D(x)$ is the coefficient for diffusion along the landscape profile. The landscape is then given by

$$G(x) = -k_b T ln\big(P(x)\big) - k_b T D(x_F) P(\acute{x}_F) \int_{x}^{x_U} \frac{dy}{D(y)P(y)} \qquad [2.11]$$

for $x_F < x < x_U$. Comparing to the inverse Boltzmann equation (Eq. 2.8), the second term in Equation 2.11 corrects the free energy for the bias in the probability density arising from being out of equilibrium. Usage of the force-jump equations requires knowledge of $D(x)$, which is difficult to obtain experimentally. However, the equation becomes independent of D whenever this diffusion coefficient is independent of x, an assumption often made in the literature for simplicity [128]. Moreover, the effect of the probe needs to be removed, which can be done through deconvolution process. Another potential complication is that qualitatively different binding pathways may be probed during rapid force quenches, when compared to measurements performed closer to equilibrium [129], and therefore the reconstructed landscapes may not be directly comparable.

2.6 Reconstruction of Free Energy Landscapes using Brownian Fluctuations

The concept of using the cantilever's Brownian noise to sample adhesive interactions with stiffnesses close to the probe stiffness was initially proposed by Cleveland et al. [115] who used the technique to show the presence of potential wells near calcite and

barite surfaces. They used the inverse Boltzmann equation (Eq. 2.7) for this purpose, which determines energies up to a constant value. The measurement was done at constant cantilever tip position and yielded limited information about the entire interaction profile. To obtain information about the entire profile, researchers obtained similar measurements at different tip sample distances and obtained corresponding energies at each tip position [130]. However, three problems still existed in obtaining the interaction energy landscape: (1) The harmonic energy contribution of the probe was included in the measured potential values, (2) Only relative energy values could be computed at each tip positon since the inverse Boltzmann equation calculates energy up to a constant value, and (3) Boltzmann based methods at fixed tip positions only allowed for sampling energy barriers up to 3-4 k_BT, i.e. sampling was limited by thermal energy of the probe itself.

Computation of harmonic potential at any tip position required accurate knowledge of the position of the cantilever, and small errors in position could manifest in large errors of computed harmonic potential [131]. Willemsen et al. [132] addressed this problem by collecting multiple approach force curves to cover the entire range of tip positions, and averaging them to simulate a slow approach curve, through which they could accurately determine the position of the cantilever at any point in the measurement. However, this force curve averaging approach also averages out the transient states experienced in individual force curves, thereby leading to a loss of information. On the other hand, there was no clear method of objectively computing the constant in inverse Boltzmann equation, and subjective estimations of the constant led to errors as large as 25 k_BT [133]. Some researchers entirely circumvented the issue of constant determination by computing forces instead of energies and developed a Brownian force profile technique to measure solvent

forces [80]. The solution to the third problem came from unexpected quarters, i.e., the computational simulation community who were trying to address a similar issue. Torrie and Valleu during their Monte-Carlo simulations had realized the inefficiency of a Boltzmann weighted sampling distribution for sampling complex energy landscapes in limited computational time [134, 135]. Hence they came up with an arbitrary sampling potential superimposed on Boltzmann sampling, which could provide enhanced sampling. They demonstrated the effectiveness of their approach, called Umbrella Sampling, via simulations on a Lennard-Jones system under wide range of temperature and density conditions.

However, their method was limited to only a small window of the energy landscape, and no ideas were provided about combining the results of multiple window. Hence, their technique had limited applicability until Kumar et al. [136] proposed a weighted histogram technique which allowed molecular dynamics researchers to combine the potential energy results of multiple windows into an accurate combined estimate for the entire reaction coordinate, by minimizing errors of computed energies at the end of any two adjacent windows. Both Umbrella Sampling and Weighted histogram methods have been extensively applied in molecular dynamics simulations [48, 137], and, very recently, in experimental protein folding studies using optical traps [118], but not to measurement of adhesive energy landscapes using AFM.

This section combines the experimental and simulation based approaches previously discussed to extract the free energy landscape of ligand-receptor interactions and that of bare tip-sample adhesive interactions. We employ an AFM cantilever to probe the interactions at very slow rates (v~200-300 pm/s), thereby achieving quasi-equilibrium

conditions. By moving the cantilever slowly and capturing high rate deflection information at each tip-sample position of the cantilever, we acquire sufficient statistics to reconstruct the entire energy profile. The reconstruction procedure uses the Boltzmann equation along with umbrella sampling techniques to reconstruct the total free energy landscape followed by the weighted histogram method to retrieve the underlying free energy landscape of the interaction.

We employ the following approach to reconstruct free energies surfaces. The tip of the cantilever is brought into close proximity to the interaction potential of a substrate surface. As the cantilever fluctuates close to the surface, changes in cantilever's deflection from its average position are caused by interaction between the probe tip and substrate surface. Adhesive energy landscapes contain large energy barriers along the reaction coordinate, which prevents an accurate sampling of the interaction. When the cantilever tip encountered such large barriers, the cantilever spring's restoring force is unable to compensate for the high attractive force gradients of these barriers and it undergoes a free fall movement unconstrained by the underlying energy landscape. As a result, the actual barrier itself is poorly sampled. To solve this issue, a biasing potential is superimposed on the interaction potential, which serves to confine the movement of the cantilever tip within the funnel of the umbrella. This helps to achieve a more efficient sampling at the bottom of the funnel, leading to accurate reconstructions. In the AFM, the biasing is naturally provided by the cantilever in the form of a harmonic potential. Because the sampling is confined to a small region within a single umbrella funnel, only a small piece of the free energy is accurately estimated. The z-piezo movement of the cantilever creates many such equally spaced umbrellas across the entire reaction coordinate, through which multiple

small pieces of free energy of the landscape can be computed accurately. These small pieces of accurately estimated free energies are combined using weighted histogram techniques to obtain the entire free energy landscape.

To combine the free energies of all sections together, the cantilever's deflection signal is linearly transformed to the tip sample distance using the Z-Position data. The tip sample distance data is parsed into N_w small windows and tip positions (x) from each window is binned into histograms in order to calculate the tip position probability density $P(x)$ [138]. These biased histograms include the contribution of the cantilever harmonic potential in addition to the tip-sample interaction at each tip sample position. The biased probability distributions for each window were converted to corresponding unbiased distributions using weighted histogram analysis techniques (WHAM) as follows:

$$[P(x)]_i^{biased} = \sum_{i=1}^{N_w} [P(x)]_i^{unbiased} \left[\frac{n_i e^{\left[-(w_i(x)-F_i)/k_bT\right]}}{\sum_{j=1}^{N_w} n_j \, e^{\left[-(w_j(x)-F_j)/k_bT\right]}} \right] \quad [2.12]$$

$$e^{-F_i/k_bT} = \int [P(x)]_i^{biased} e^{-w_i(x)/k_bT} \, dx \quad [2.13]$$

where i is the window number, n_i is the number of points sampled in window i, F_i is an arbitrary free energy constant involved in all energy calculations, $w_i(x)$ is the biasing potential and k_bT is a unit of thermal fluctuation energy. In the case of AFM, $w_i(x)$ is the harmonic potential of the cantilever probe.

$$w_i(x) = \frac{1}{2}k(x - x_{0,i})^2. \qquad [2.14]$$

where k is the stiffness of the probe and $x_{0,i}$ is the equilibrium position of the probe for the ith window. The equilibrium positions of the probe is equal to mean values of reaction coordinate for corresponding windows.

Because the distribution function itself depends on the set of constants F_i, the Eq. 2.12 and 2.13 must be solved self-consistently. In practice this is achieved through an iteration procedure. Starting from an initial guess for the N_w and free energy constants F_i, an estimate for the unbiased distribution is obtained from Eq. (2.12). This estimate for $P(x)$ is used in Eq. (2.14) to generate new estimates for the free energies constants F_i and a new unbiased distribution is generated with Eq. (2.12). The iteration cycle is repeated until both equations are satisfied. Finally, the underlying free energy landscape is calculated from the unbiased distributions using inverse Boltzmann distribution (Eq. 2.7).

The entire process of energy landscape reconstruction using umbrella sampling and WHAM methods is shown in Fig. 2.9A, where an interaction energy landscape (blue) is sampled using harmonic biasing potential (umbrellas) at each tip position (shown in red). To illustrate the reconstruction procedure, a small section of the energy landscape is selected (gray zone) along with its associated harmonic biasing potential. The section size is chosen to be large enough that sufficient statistics exist for each tip position, yet not so large that interaction energy varies significantly between adjacent sections. Fig. 2.9B, which shows the selected region, illustrates the fact the biasing potential limits the motion of the tip (red circle) to within the bottom of the potential funnel. This helps to achieve greater sampling at the bottom of the funnel close to the cantilever's equilibrium position,

thereby reducing the probability of stochastic sampling errors. The funnel also protects the cantilever tip from jumping onto the surface even when it is close to a region of steep energy gradient, by restricting the natural unconstrained movement of the tip. This allows for very accurate sampling of regions very close to jump-ins, which would otherwise not have been possible. The sampled positions are binned into probability histograms, $P(x)$, which is then transformed into energies, $G_{total}(x)$, using Boltzmann distribution. The harmonic biasing contribution is then removed to obtain the interaction energy, $G_{interaction}(x)$, for the given section. Fig. 2.9C shows the interaction energy contribution for all the sections of the energy landscape. Since the Boltzmann distribution only computes energy up to a constant, the interaction energies of each section are typically offset from their true values; leading to multiple interaction energies at a single tip sample distance. This unphysical effect is corrected by WHAM techniques which iteratively computes the correct constant for each energy section and stitches them together to obtain the overall energy landscape (blue curve in Fig. 2.9C).

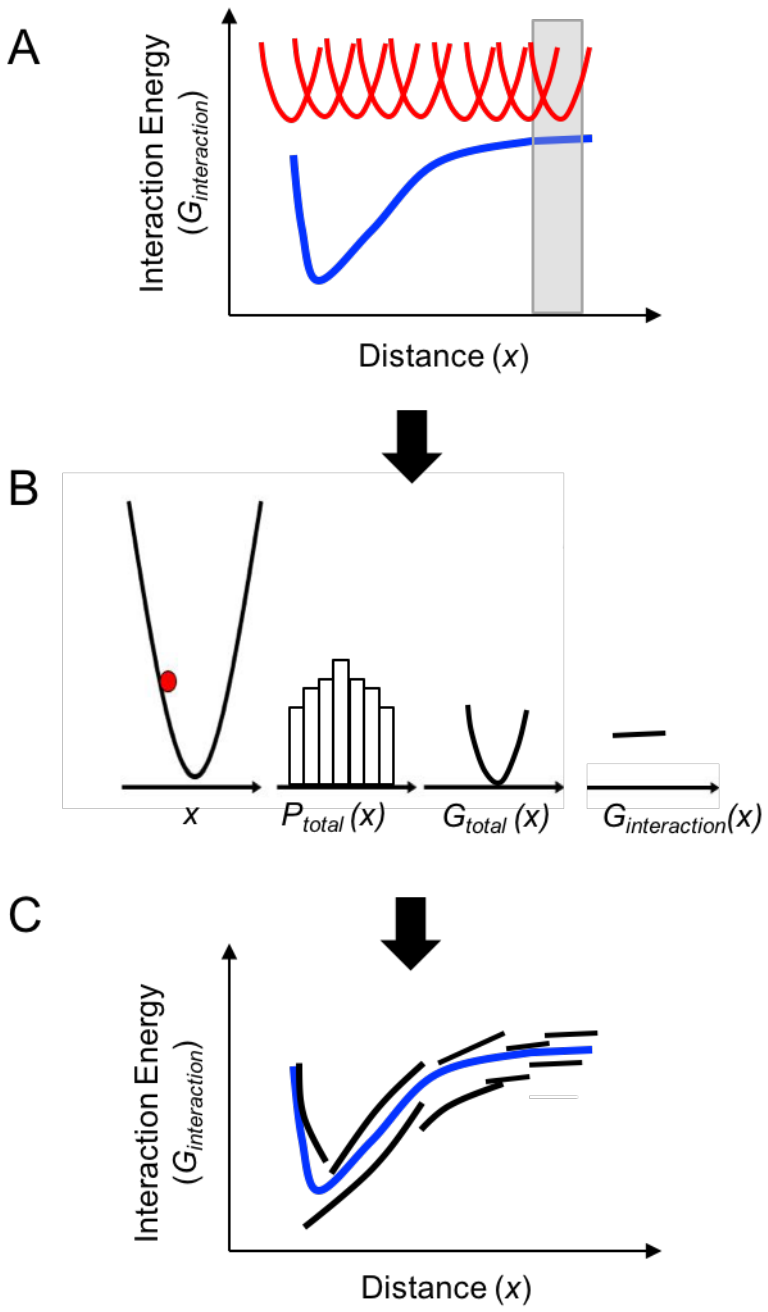

Figure 2.9. A. Sampling of an interaction energy landscape (blue) using harmonic biasing potential (umbrellas) at each tip position (shown in red). A small section of the landscape is selected for further analysis (gray box). **B.** Constrained motion of the tip (red circle) within the harmonic potential funnel (furthermost left) is transformed into probability histograms (second from left) and total energy (third from left) using Boltzmann

distribution. Harmonic contribution is removed to obtain interaction energy (right most) for the given section. **C.** Multiple energy sections are stitched together using WHAM techniques to accurately reconstruct the underlying energy landscape (blue).

2.6.1. Choice of Reconstruction Parameters

Reconstruction parameters, i.e. window size and the histogram bin width plays an important role in determining the shape of reconstruction. Both the harmonic potential of the cantilever probe as well as the thermal energy of the tip limits the sampling range of the tip. Therefore, the window size should be large enough to ensure that the entire sampling range of the tip is covered at a fixed probe position. At the same time, the window size needs to be small enough to keep the tip-sample interaction constant within its range yet so not small to affect the precision of the probabilities calculated from the histograms. The histogram bin width also needs to be small so as not to average out small deflection changes within a window, and yet not so small as to add to the sampling noise.

2.6.2. Assumptions of Brownian Reconstruction Method

The method of reconstructing energy landscapes from Boltzmann distribution of cantilever's thermal fluctuations depends on a few assumptions:

(i) Point-mass model of cantilever dynamics: It has been assumed that the cantilever bends as if a static point load is being applied at the cantilever's free-end and the corresponding static stiffness is used to derive a single degree of freedom point-mass model. Hence, while higher harmonics of excitation frequency may be present in the cantilever vibration, using a point-mass model allows us to choose only one dominant eigenmode to describe the cantilever's dynamic motion.

(ii) Extension of linkers connecting ligands to AFM tips: Brownian reconstruction procedure assumes that the interaction forces be tightly coupled to the cantilever. For biological experiments, we typically use long linkers and non-specific interactions to attach the molecules of interest to the tip. If these linkers are not sufficiently stiff, they can stretch significantly when pulled, thereby isolating the cantilever's potential from the tip-surface interaction, hence removing the information content from the cantilever motion. In this thesis, we used short glutaraldehyde linker molecules (0.75 nm long) which are sufficiently stiff, such that the cantilever tip is able to accurately follow the underlying energy landscape.

(iii) Sampling of thermal noise: In Brownian reconstruction, the span of the thermal noise causes the tip to sense both the strongly attractive regions along with the weakly attractive regions within a very short interval of time. To ensure that the entire span of the thermal noise is captured, the deflections are assumed be sampled at frequencies greater than or equal to twice the Nyquist frequency ($2f_0$), where f_0 is the resonance frequency of the cantilever. In this thesis, the deflection signals are recorded at frequencies greater than or equal to $4f_0$, which allowed us to sample the entire thermal noise bandwidth thereby ensuring high reconstruction accuracy.

CHAPTER 3

DIRECT MEASUREMENT OF ENERGY LANDSCAPES OF LIGAND-RECEPTOR INTERACTIONS

3.1 Introduction

In this chapter, we will utilize the Brownian fluctuations method, developed in the previous chapter, to measure the energy landscapes of strongly adhesive interactions seen in ligand-receptor interactions. The energy landscape between ligands and receptor interactions are very important since they determine the kinetic and equilibrium properties of binding in biological systems. Even though their energy landscapes have been computationally simulated, the direct mapping of biomolecular energies between the two molecules under near-equilibrium conditions has been a challenge because of strong binding affinities. In this chapter, we combine the atomic force microscopy measurements with the Brownian fluctuation method to directly map the intermolecular energy landscape curve of ligand-receptor system (biotin-avidin in our case) and discriminate multiple energy wells. The procedure involves vibrating a sensitive microcantilever probe decorated with biotin that is in close and lasting proximity to an avidin coated substrate. By recording subtle deviations from the harmonic cantilever vibrations as it translates towards the substrate and then transforming these Brownian fluctuations using Boltzmann sampling methods, we can reconstruct entire energy landscapes of interactions, including short lived, metastable states. The reconstructed energy landscapes reflect both rare short-lived biotin-avidin interactions and the overall shape of the average energy landscape including the presence of multimodal energy wells. Even though the quantitative values do not agree

with some previous published experimental work, these results are qualitatively consistent with computational simulations that show a rearrangement of peptide loops that border the binding pocket of avidin, causing metastable energy states. We close the chapter by explaining the reasons for quantitative discrepancy in the energy reconstruction method, which are addressed by the technique in Chapter 4.

3.2 Background

The reversible binding of ligands to receptors underpins specificity of nearly all biological interactions, including adhesion, catalysis, and structural maintenance [139-142]. The energy landscape, that is the energetic depth and physical extent of interaction potentials between biological molecules, dictates the kinetics and affinity of biological interactions. While of such fundamental importance, the understanding of dynamic conformational changes undertaken by a ligand as it binds to a receptor, and the interaction energy that results, remains an elusive and important focus for the development of novel drugs through identification of therapeutically relevant antibodies, and understanding protein-mediated processes [143-145].

Despite the importance of the energy landscape, conventional experimental approaches cannot fully measure subtle variations within the interaction wells of biomolecular bonds [59, 146-154]. While these techniques can measure binding affinities and thermodynamic properties of ensemble of molecules, the subtleties of the energy landscape only be inferred or computed. In contrast, computer simulation has shown that energy landscapes can exhibit subtle topographic features, but its accuracy is limited by

uncertainty in the underlying model potentials and the integration of the equations of motion [18-20].

Atomic force microscopy (AFM) offers an unprecedented ability to resolve interaction forces between biological molecules. Since bond strength is typically characterized by recording the force at which bond dissociation occurs [155], the approach measures the deepest portions of energy wells. Alternatively interaction lifetimes can be measured [156] [157], but bond lifetimes are primarily defined by the most stable binding state and very short metastable binding are not observed due to an inability to sufficiently sample the interaction.

Complementing adhesion measurements, dynamic force spectroscopy (DFS) applies a force at a variety of bond loading rates and applies models of two state binding [22, 23], to derive a kinetic off rate from which the depth of an energy well can be inferred [3, 22, 24-26]. For this approach to be accurate, hundreds of force-retraction cycles must be conducted over multiple retraction rates to acquire the data to derive kinetic off-rates. However, due to assumptions of two state transition and irreversible transitions [27], many DFS models do not work well for complicated energy landscapes and misses intermediate states [158]. DFS models can only determine energy barriers and lacks the ability to fully measure the shape of the energy landscape along the reaction coordinate.

The recent use of non-equilibrium measurements applying Jarzynski's equality have been successful at reconstructing equilibrium free energy landscapes of single molecule unfolding of biopolymers [70, 159, 160]. However, deconvolution of the energy has only been demonstrated for quickly folding proteins and has not been successfully

applied to interactions with very short reaction coordinates that are found in ligand receptor interactions [116]. Particularly, when the transition is far from equilibrium or when the extension change for unfolding is large, the reconstruction for regions immediately past the transition may yield large amounts of error due to limited sampling times [1, 160].

We have used atomic force microscopy to directly map the intermolecular energy landscape of a ligand-receptor interaction. The method utilizes Brownian fluctuations of a microcantilever probe decorated with a ligand, which is then brought into close proximity to the interaction potential of complementary molecules that are attached to a substrate surface. By recording the variations in fluctuations of the cantilever as it passes close to the substrate surface, the free energy landscape can be reconstructed through a transformation of Boltzmann's equation. Using this technique, we have determined the interaction potential between biotin and avidin interactions. The method was able to discriminate two attractive energy wells with average energies of ~6.5k_bT and ~3k_bT before undergoing repulsive contact. The energy landscape depends only on the kinetic rates of the interaction [29], and once its shape is known, can be used to deduce the binding rate constants and the affinity of the interaction.

3.3 Materials and Methods

3.3.1. Molecular Functionalization of Probe and Surface: Avidin and biotin-BSA were functionalized to mica and AFM cantilever tips, respectively as seen in Fig. 3.1.

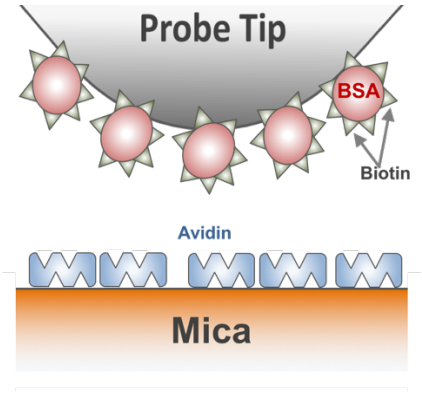

Figure 3.1. Schematic of an AFM probe tip with attached BSA-biotin in close proximity of an avidin coated mica substrate

Following the methods of Gruber [161], silicon nitride cantilevers (Bruker) were derivatized with amino groups and crosslinked with biotin ligand. Cantilevers were washed in chloroform and then in ethanolamine. Hydrochloric acid (HCl) is dissolved in dimethyl sulfoxide (DMSO) and heated to 70°C until complete dissolution. After cooling, the cantilevers were immersed in the solution overnight. After washing with DMSO followed by ethanol and drying with nitrogen gas, the cantilevers were incubated with a 0.75 nm glutaraldehyde linker solution and rinsed in Phosphate buffered saline (PBS). A 0.75 nm glutaraldehyde linker was used, which was sufficiently stiff and resistant to stretching, thus resulting in more repeatable measurements. For each cantilever, a 1 mg/mL aliquot of biotin-BSA were prepared and diluted 5X with PBS. The cantilevers were incubated for 10 min, then washed and immediately used for experiments. To attach avidin to a muscovite mica substrate, we utilized 20 μL of 1mg/mL avidin diluted 10X with 1 mM NaCl and lightly mixed. 50 μL was pipetted onto the freshly cleaved mica and incubated for 15 minutes, rinsed with NaCl ten times and then with PBS twenty times.

3.3.2. AFM Approach Force Measurements: The mica sample remained hydrated and was placed in the AFM (MFP-3D Bio, Asylum Research). A flexible cantilever with a resonance frequency of 13 kHz was used to obtain force curves. The cantilever was transferred to the holder and placed in the head, maintaining a hydrated cantilever. To minimize drift, the cantilever was equilibrated within a closed chamber for two hours until the thermal drift was below 200 pm/s. Typical experiments are performed at 100 +/- 10 pm/s. The cantilever was brought to within ~40 nm of the surface, and a custom Igor Pro script was used to record the raw deflection signal of the cantilever at 50 kHz data rate (~4x the cantilever resonance frequency and therefore satisfying the Nyquist sampling theorem and thereby ensuring all resonance vibrations are measured in the deflection signal). Calibration of zero point of cantilever base position is obtained from intersection of the lines fitted from the unbound and bound regions of these approach force curves. After the force curves were collected, the cantilever spring constant and deflection sensitivity was calibrated using the thermal method [94].

3.3.3. Energy Landscape Reconstruction Approach: The process of probing molecular interactions using Brownian fluctuations is based upon umbrella sampling and weighted histogram averaging methods (WHAM) [134, 135, 138, 162]. Deflection signals are processed as described in Fig. 3.2. To validate the procedure, we reconstruct a simulated force profile, using a damped simple harmonic oscillator cantilever model approaching a surface (Fig. 3.2(a)), using the following equation (y is cantilever's deflection):

$$ky + c\dot{y} + m\ddot{y} = F_{ts} + F_{BR} \qquad [3.1]$$

where k, c, m are the stiffness, damping and mass of the cantilever, respectively. F_{ts} and F_{BR} are the tip sample interaction and the thermal/brownian noise forces, respectively. The tip sample interaction force is modeled using a 6-3 chemical force profile $F_{ts}(x)=100\left({}^{0.1}/_{x}\right)^{6}-0.006\left({}^{0.1}/_{x}\right)^{3}$ where x is the tip sample distance in angstroms [80]. The thermal fluctuations are modeled using the Brownian force noise F_{BR}, which is computed by using a pseudo-random number generator that produces Gaussian noise with a variance of $4k_BTcB$ where k_B, T, c, B are the Boltzmann constant, temperature, damping constant, and frequency bandwidth for the simulation, respectively [80]. The cantilever base position and corresponding deflections are recorded at twice (or higher) the resonance frequency of the cantilever, during the approach of the cantilever tip towards the substrate (Fig. 3.2(b)). The deflections are then transformed into tip sample distances by a linear transformation, to plot tip position versus cantilever base position. The entire tip sample distance data are parsed into multiple small windows chosen such that the corresponding data histograms of each section do not differ appreciably from the adjacent ones (Fig. 3.2(c)). The tip sample distance data from each window is then binned into histogram in order to calculate the tip position probability density (Fig. 3.2(d)). These histograms are biased since the contribution of the tip-sample interaction is convolved with the contribution of the cantilever's spring ($P_{biased} = P_{interaction} \otimes P_{probe}$). Fortunately, the Boltzmann distribution can be used to relate the cantilever probe's energy, which is a second order quadratic, ($G_{probe} = \frac{1}{2}k(x - x_0)^2$), to its probability distribution ($P_{probe} = Ce^{-G_{probe}/k_BT}$). Here x_0 is the average position of the cantilever probe base and C is the partition coefficient for the Boltzmann distribution which is an arbitrary constant. Thus, the cantilever's histograms belong to a Gaussian distribution (blue curve) with its mean

given by the average position of the cantilever base and the standard deviation computed from the stiffness of the cantilever spring. Fig. 3.2(e) shows the biased probability distributions (red) along with the contribution of the cantilever spring (blue) for windows A and C. Thus, the probability distribution of the tip position for each window is a relative value whose magnitude depends on the values of the partition coefficient for that window. Since every window in the force curve overlaps with adjacent windows, the tails of the probability distributions of each window essentially overlaps with that of adjacent windows. Therefore, incorrect estimation of the partition coefficients leads the overlapping tails of the probability distribution of each window being offset from those of adjacent windows. Because it is physically obvious that the tip cannot be in two places at the same time, these offsets need to be minimized. Since the Boltzmann distribution heavily weights the contribution of the energy of rarely sampled states, which naturally occur at the tails of these probability distributions, the resulting error in energy computation can be massive if the offsets effects are not minimized. To correctly estimate the partition coefficients for each window, thereby deconvolving the contribution of the cantilever probe from that of the tip-sample interaction, we use an iterative WHAM approach. WHAM solves for the values of partition coefficient for each window such that the offset in probability distribution between any two adjacent windows is below a certain predefined threshold. This threshold is set to be 10^{-20}. The threshold value should be carefully chosen. The threshold value should be lower than the tip probability distribution which is to be solved for, while not so low that it results in unacceptably high computer run-times. Fig 3.2(f) shows the corresponding unbiased distributions after removing the cantilever's contribution. The inset of the left figure is used to show a zoomed in view of the shape of

the unbiased distribution of section C, which is not easily visible in a standard view due to its low histogram counts. The inverse of Boltzmann's distribution is then used to calculate the total potential energy at each tip position value in each section (Fig. 3.2(g)). The overall tip-sample energy landscape is obtained by adding the unbiased contributions of all the windows (Fig. 3.2(h)). The method is able to accurately reconstruct the analytical input energy profile, derived by simply integrating the input chemical force profile. Comparison of the reconstructed tip sample interaction energies with that of analytical profile at each tip position yields an error distribution characterized by mean of -0.2850 k_BT and a standard deviation of 2.050 k_BT. The error in detection of the tip position at the deepest point of the energy well is 0.02 nm, which is significantly smaller than the width of the biotin-avidin binding pocket (~ 2 nm). Data processing and reconstruction was performed by custom routines written in MATLAB (MathWorks Inc., Natick, MA).

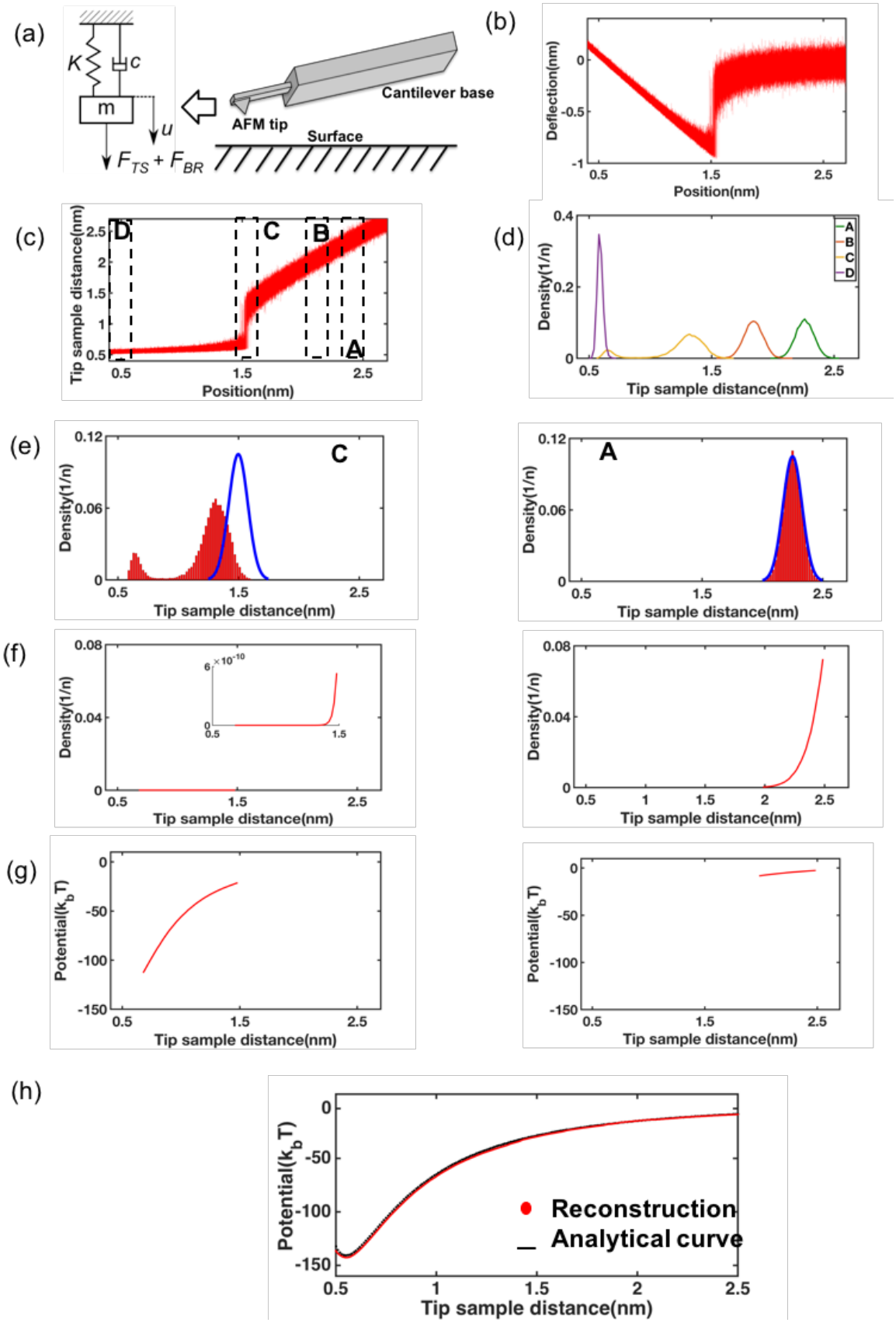
(a)
K
c
m
u
F_{TS} + F_{BR}
AFM tip
Cantilever base
Surface
(b)
Deflection(nm)
Position(nm)
(c)
D
C
B
A
Tip sample distance(nm)
Position(nm)
(d)
A
B
C
D
Density(1/n)
Tip sample distance(nm)
(e)
C
Density(1/n)
Tip sample distance(nm)
A
Density(1/n)
Tip sample distance(nm)
(f)
Density(1/n)
Tip sample distance(nm)
Density(1/n)
Tip sample distance(nm)
(g)
Potential(k_bT)
Tip sample distance(nm)
Potential(k_bT)
Tip sample distance(nm)
(h)
Potential(k_bT)
Reconstruction
Analytical curve
Tip sample distance(nm)

Figure 3.2. (a) Schematic of an AFM cantilever tip approaching a surface modeled using a damped simple harmonic oscillator in a chemical force field (b) Overall approach curve, including thermal fluctuations (c) Transformation of the deflection to tip sample distances to generate histograms of tip positions at different window locations indicated by the boxes (d) Four representative probability density histograms of the tip positions during fluctuations at different window locations (e) Biased probability density histogram of tip positions at window locations indicated by A and C on right and left, respectively. The contribution of the cantilever is indicated by its Gaussian probability distribution shown as the blue curve. The position of the Gaussian is dictated by the average cantilever base position for each window (f) Unbiased probability distribution for window A and C obtained by deconvolving the cantilever's contribution from the biased distributions. Inset in the left figure allows to visualize the low counts of unbiased distribution for section C by zooming in. (g) Energy of each window computed using inverse Boltzmann's distribution. (h) Total tip sample interaction energy from many windows stitched together

3.3.4 Single Molecule Binding: Probing the energy landscape of biotin-avidin systems can result in either non-specific (bare tip-surface interaction) or specific interactions (formation of single or multiple bonds). The specificity of the bonds formed can be inferred from the jump-in distance of the probe during binding. For example, when the jump-in distance is averaged over all cases where the bond displayed adhesion during rupture (specific binding) versus those where no adhesion was observed (non-specific binding), it was clear that higher adhesion forces correspond to higher jump-in distances (Fig. 3.3 (a)). This allows to separate the non-specific from specific interactions. The AFM tip, due to its large radius as compared to that of BSA-biotin molecules, contains many closely spaced biotin

molecules. These are exposed to the multiple binding pockets created by the avidin coated surface, resulting in the possibility of multiple bond formation. For measuring metastable binding in which the probe is slowly brought into contact with the sample before retraction, longer contact times typically allowed more molecular binding events to occur, increasing the probability of multiple bonds forming, thereby overestimating the energy well depth from reconstructions. In such cases, retracting the AFM tip also resulted in multiple jumps in force curves corresponding to multiple bond dissociations. Fig. 3.3 (b) shows a typical biotin-avidin approach force curve (red) containing multiple binding events indicated by the downward pointing arrows. Fig. 3.4 (c) shows the corresponding unbinding events observed during retraction (blue) indicated by the upward pointing arrows. For illustration purposes, the data is smoothed (black line) to highlight the binding and unbinding observed in the force curves. To ensure that we only reconstruct single molecule binding events, firstly we used the retraction data to calculate the equilibrium dissociation force (F_{eq}) required to break a single biotin-avidin bond. This was done by conducting a dynamic force spectroscopy (DFS) study of biotin-avidin dissociation and fitting a Friddle-Noy-deYoreo model to the measurements to obtain F_{eq} = 25.2 pN. (Fig. 3.3 (d)). The DFS measurements were done by perfusing the fluid cell with 1 mM avidin blocker to cause no more than one in five force curves to demonstrate biotin-avidin binding, characterized by linearly increasing pull-off force before full bond separation. Thereafter, we selected only those approach curves for reconstruction whose jump-in forces were within one standard deviation of F_{eq} measured by DFS. This allowed us to sample only single-molecule binding events, while discarding both non-specific and multiple binding events. Fig. 3.3 (e) shows an approach force curve which shows jump-in forces of ~15 pN upon approach, which are

much smaller than F_{eq}. Thus, these are labeled as non-specific bonds and their corresponding retraction curves do not show a sudden sharp increase in rupture force upon retraction (Fig. 3.3 (f)); a feature which is characteristic of a specific bond dissociation. Furthermore, we also observed that when jump-in forces are in excess of a standard deviation of F_{eq}, as in seen in Fig 3.3 (b), they display two or more unbinding events in close succession, indicating multiple-bond formation.

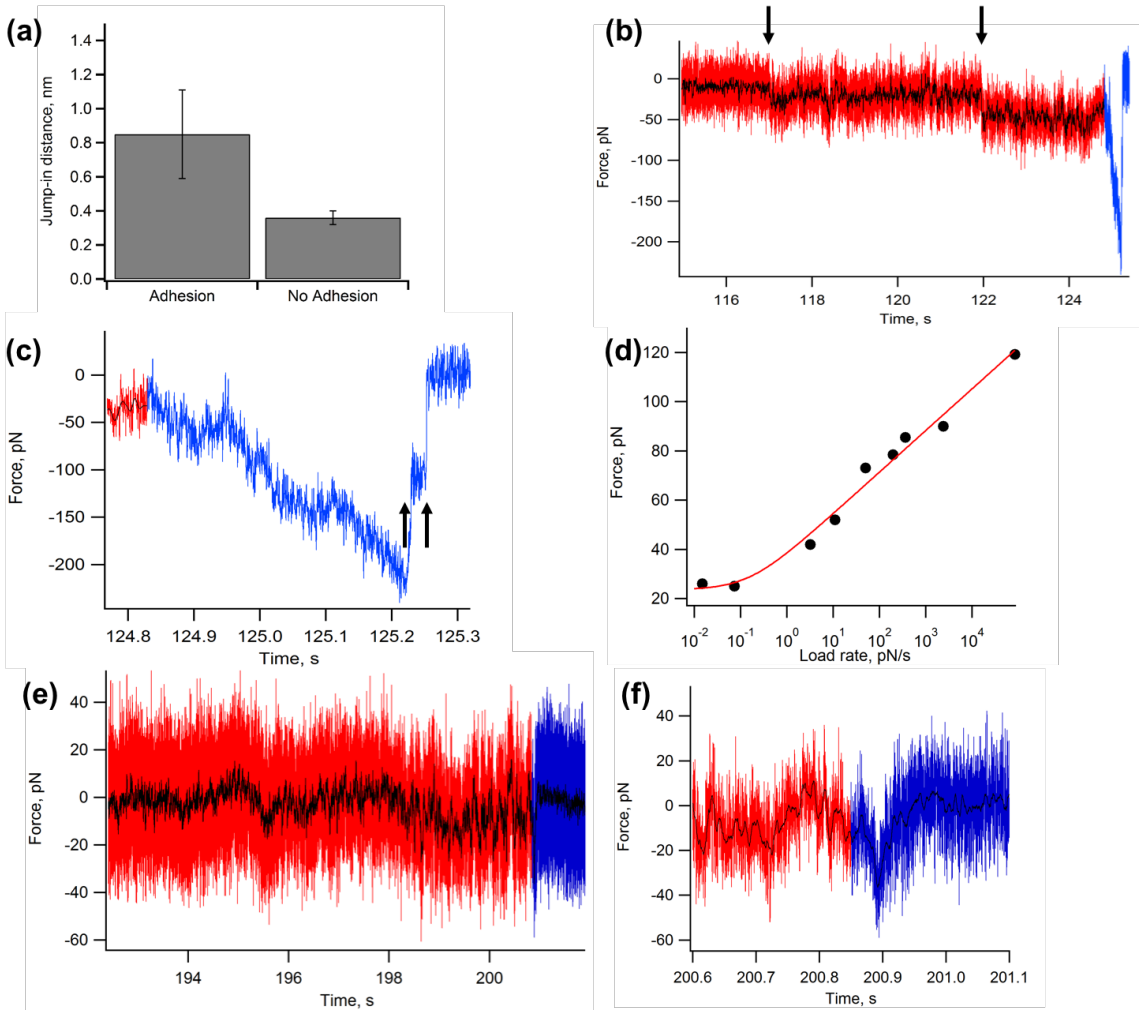

Figure 3.3. (a) Comparison of the average jump-in distances during biotin approach to the surface for the cases when adhesion was observed upon retraction versus those when

adhesion was not observed upon retraction (b) Approach force curve (red) showing two binding events in succession indicated by the downward pointing arrows. The black line is the smoothed force profile used to highlight the average movement of the tip as it approaches the surface (c) Retraction force curve (blue) showing corresponding dissociation events indicated by the upward pointing arrows (d) Friddle-Noy-deYoreo DFS model fit to the dissociation data to extract the equilibrium forces required to break a single biotin-avidin bond (e) Approach force curve (red) for a non-specific binding event when the jump in forces (~15 pN) are much lesser than equilibrium binding force (25.2 pN) (f) Zoomed in section of the force curve showing that the retraction curve of a non-specific binding event does not show a sudden sharp increase in rupture force that is associated with a specific binding event

3.3.5. Comparison with Conventional AFM Measurements: Thermal (Brownian) noise of a cantilever, with a standard deviation of $\sqrt{4k_BTcB}$, can surpass 1 nm (RMS) of tip sample distance, and thus sample a substantial portion of the interaction potential (Fig. 3.4(a)). Conventional force profile measurement techniques employ smoothing techniques to determine the average force at a fixed position, and therefore ignore information contained in the instantaneous forces at each instantaneous tip position (Fig. 3.4(b)). For cases of small gradient of the potential, or during retraction and de-adhesion measurements, this simplification results in little loss in essential information of the bond. However, when approaching a steep potential curve, the thermal noise necessarily averages the strongly attractive and weakly attractive regions of the curve. The insight of the Brownian fluctuation method is that thermal fluctuations are inherently accounted for and leveraged to sample steep wells without snap-to-contact through stable sampling of rare downward

fluctuations in which significant restoring force exists. To illustrate, the simulated 6-3 chemical force profile was smoothened using standard techniques (moving average filters with a half window sizes of 30 points and 1000 points). A zoomed in section of the force curve is shown in Fig. 3.4(c). When using a 30-point filter (blue curve), it can be seen that the smoothed profile tends to miss sharp transition states which can correspond to rare binding events. As smoothing increases to a 1000-point filter (green curve), smoothed profile manages to just about capture the overall trend without recording any instantaneous deflection data. From the corresponding histograms, we see that while the raw data is bimodally distributed, smoothing leads to blurring of the peaks in case of 30-point filter and eventually a unimodal distribution in case of 1000-point filter. We compared the potential energy profiles obtained by integrating the smoothed force curves and those obtained by reconstructions obtained using Brownian fluctuations, with the input energy profile obtained from integration of tip sample interaction forces (labeled as analytical curve) (Fig. 3.4(d)). As can be seen from the residual measurements in Fig. 3.4(e), the potential well is more faithfully sampled using the reconstruction method of its ability to utilize the rare fluctuations into the well which helps in improved probing of the well depth and curvature. In contrast, without the help of these Brownian fluctuations which allowed the tip to sample steeper potential gradients without the cantilever base actually entering the well, the cantilever ends up snapping on to the surface in a free fall without being constrained by the underlying energy surface. This is what happens in the integrated energy profile when the double gradient of energy surface increases beyond cantilever stiffness. Although stiffer levers can also enable the conventional force curve to sample deeper into a potential well, the cost is a loss of sensitivity to subtle variations in the well, for example

due to semi-stable states. However, the reconstruction method requires a substantial sampling in proximity to the potential well. Therefore, methods to hover the cantilever at a fixed distance will substantially improve the recording of subtle variations of rare binding states.

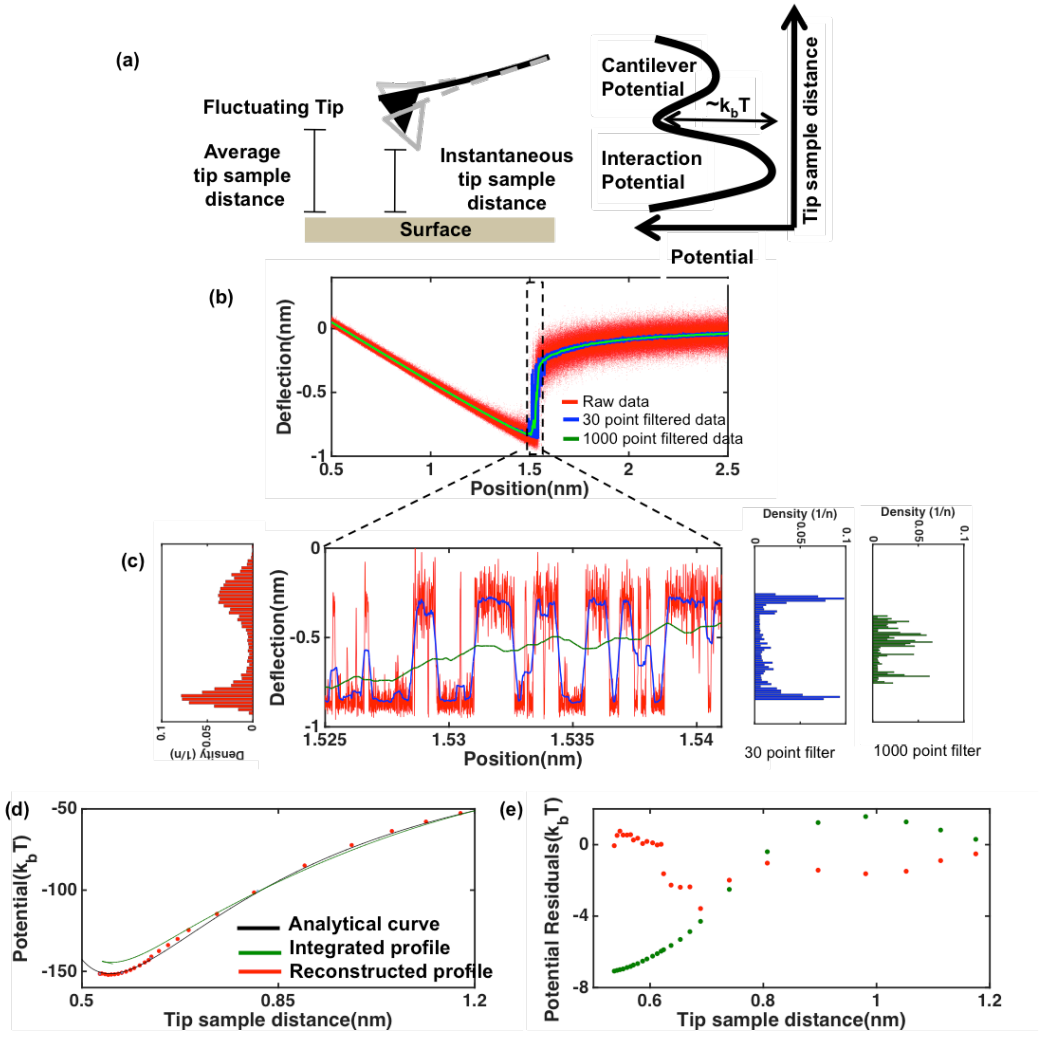

Figure 3.4 (a) Left: Fluctuating AFM tip hovering over a surface illustrating the difference between average and instantaneous tip positions. Right: Schematic of energy landscape of an AFM tip sample interaction, showing the ability of the tip to oscillate between the

reference cantilever's potential well and the tip sample interaction potential well, due to tip's inherent thermal fluctuations (b) Typical force curve (red) of an AFM tip approaching a surface generated by simulating a simple harmonic oscillator model. Raw data includes thermal fluctuations. Moving average filters applied for smoothing to generate average deflections (c) Zoomed in section for the force curve. Deflection histograms of raw (left) and smoothed data (blue and green) for a small section of the force curve with filter sizes of 30 and 1000 points, respectively, indicates missed transition states due to averaging (d) Comparison of the potential measurements obtained by analytical, integration and reconstruction methods (b) Residuals of the integrated and reconstructed potential energy profiles obtained by subtracting them from analytical curves. Lower potential residual signifies a better method

3.4 Results and Discussion

3.4.1 Probing the Energy Landscape of Biotin-Avidin Interactions

To probe the biotin-avidin energy landscape, a biotin-BSA AFM tip was slowly brought in close proximity of an avidin coated mica substrate (Fig. 3.5(a)). The fluctuations of the cantilever tip as it vibrates under the influence of the biotin-avidin interaction force are recorded while the cantilever is approaching the surface (Fig 3.5(b)). The biotin-avidin approach curve shows multiple snap-ins to the surface before binding. A zoomed in section of the curve shows metastable behavior of the tip as it oscillates between the unbound and bound states. Smoothing reveals three states; 1 unbound and 2 bound states (Fig. 3.5(c)). Linear translation of the position data to tip sample distance (Fig. 3.5(d)) is followed by histogram binning of the tip positions of the cantilever (Fig. 3.5(e)). Finally, application of

inverse Boltzmann theorem and WHAM based allows us to reconstruct the average potential energy of biotin-avidin interaction (Fig. 3.5(f)). Reconstructed energy landscape reveals two wells with average depths of 6.5 k_bT and 3 k_bT and well widths of 1.8 nm and 0.75 nm respectively. These wells correspond quite nicely to the cantilever's snap ins towards the substrate. `

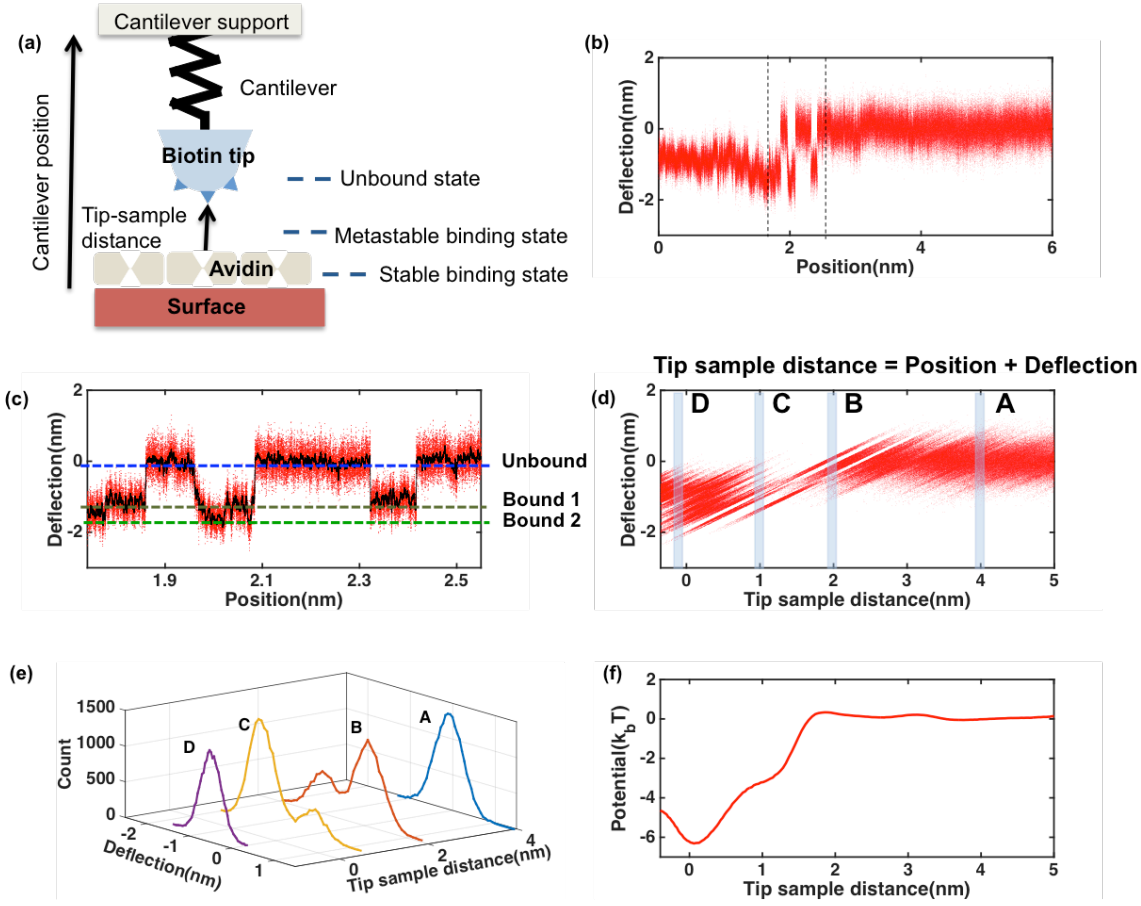

Figure 3.5 (a) Schematic of the experimental setup depicting the biotin decorated AFM tip attached to a flexible cantilever approaching an avidin coated substrate. (b) Deflection of the cantilever as a function of its position as it moves closer to the surface. (c) Zoomed in section of the deflection data. As the as the tip moves close to the surface, it starts oscillating between the unbound and bound states in a metastable manner. Smoothing

(black profile) highlights the presence of multiple binding states. (d) Linear transformation of position to obtain deflection as a function of tip sample distance. The entire data is divided into multiple windows, with 4 representative windows shown. (e) Histograms depict shift in cantilever's deflection from unimodal to bimodal states as the biotin molecules come within the range of avidin attraction potential (f) Application of inverse Boltzmann distribution and WHAM averaging to obtain average potential energy reconstruction, thereby capturing the presence of metastable binding states in the form of multiple wells

3.4.2 Energy Landscape Statistics

Multiple force curves were collected and postprocessed to obtain the energy profiles and retraction forces. Force curves that exhibited non-uniform drift while still far away from the surface were discarded, due to their unsuitability for reconstruction. Approximately 50 data sets were used to reconstruct the energy landscapes and then compute the average values of well depths (binding energies) and well widths (binding ranges) of biotin-avidin interactions. Fig. 3.6(a) shows 10 such energy curves that are reconstructed from the slow approach force curves. Inspection shows approximately 70% of the energy profiles featured two energy wells. A typical two well energy landscape as shown in Fig. 3.6(b) is used to illustrate the definitions of well widths and depths. Using these definitions, average well depths and average well widths for all the reconstructions are compiled together in the form of a scatter plot and corresponding box plots (Fig. 3.6(c)). The unimodal data corresponds to cases where only a single energy well was observed. Table 3.1 shows the average energy well depth of the inner and outer wells to be 2.85 k_bT and 5.5 k_bT and widths to 0.70 nm and 1.60 nm, respectively, for the bimodal cases. These

values are lower than published values of biotin-avidin bond strengths measured during unbinding experiments [3, 163-165]. The reason for the discrepancy is explained in the next section. To examine whether the measured energy well corresponds to more stable bonds, the retraction rupture forces were also measured for each approach curve (Fig. 3.6(d)). The energy well measurement is positively correlated to the corresponding retraction bond rupture force with a Pearson's Coefficient of 0.87. The average adhesion force of 120 pN corresponded to an average well depth of 5.5 k_bT, indicating specific biotin-avidin interactions.

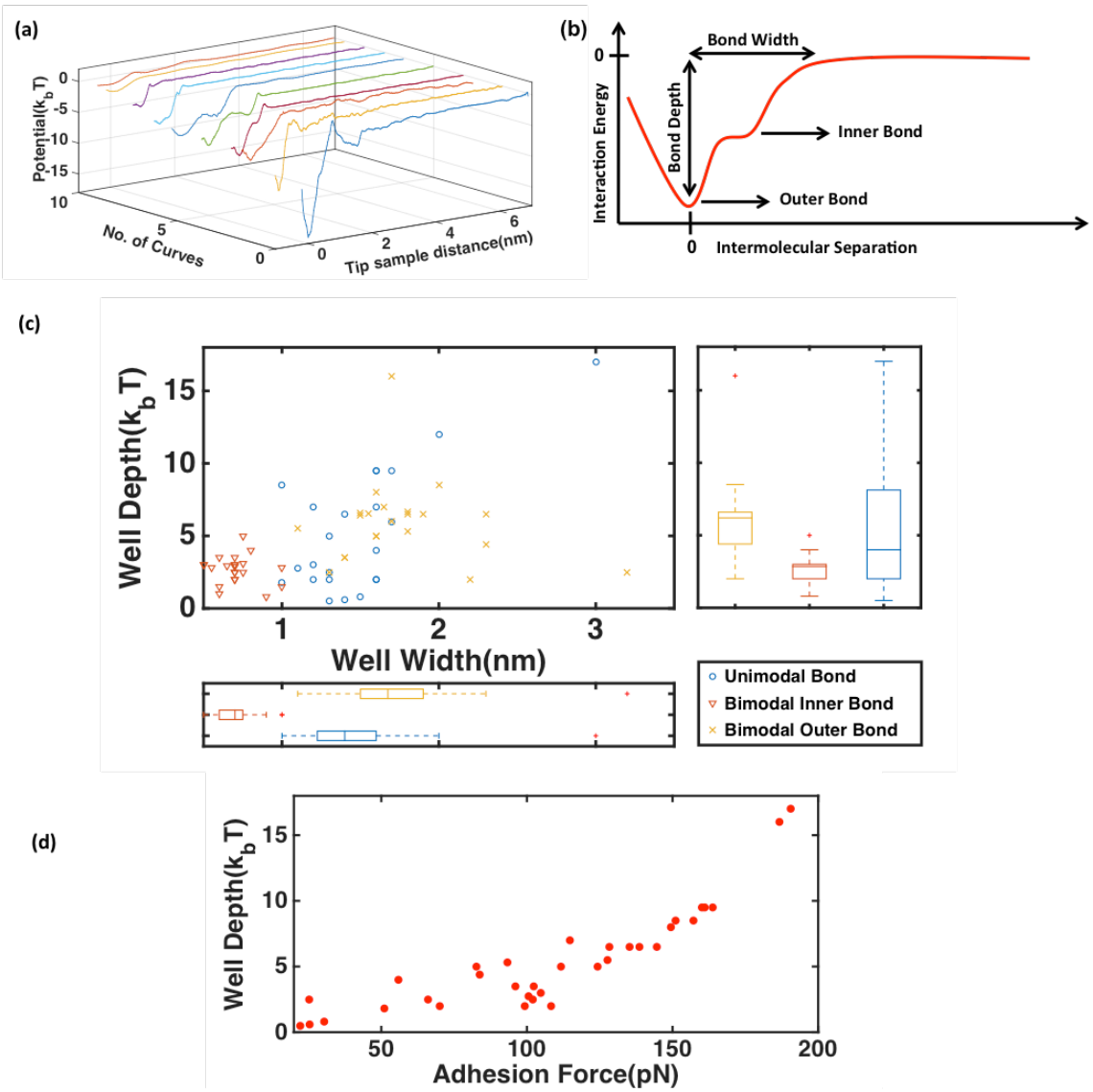

Figure 3.6. (a) Ten representative potential energy reconstructions of avidin and biotin interactions plotted to show the range of measured attractive potentials (b) Schematic of an attractive energy landscape with two wells (c) Scatter plot and box plots of well depth vs. well width for each of the two bonds in the bimodal biotin-avidin interaction. Unimodal bond corresponds to cases when only one energy well was observed (d) The energy well depth measured during approach versus the adhesion force measured upon retraction shows a positive correlation, indicating a stable bond is apparent upon formation

	BIMODAL WELL DEPTH (k_bT)		BIMODAL WELL WIDTH (nm)		UNIMODAL WELL DEPTH (k_bT)	UNIMODAL WELL WIDTH (nm)
	Inner	Outer	Inner	Outer	--	--
MEDIAN	2.85	5.50	0.70	1.60	5.85	1.40
STANDARD DEVIATION	0.96	3.60	0.13	0.45	4.01	0.41

Table 3.1. Statistics of energy landscapes of biotin-avidin interactions

3.4.3. Energies of Rare Binding States

The binding energy landscape which depicts the interaction pathways between biotin-avidin interactions is determined by the probability of the cantilever position at each tip-sample distance. The average trace, which is computed by a weighted average cantilever residence time at each position [166], determines overall landscape trends such as presence of multiple wells corresponding to alterations in molecular positioning or multiple binding events. In contrast, metastable binding events which correspond to rare binding pathways, typically with a lifetime of less than 5 ms, are not properly determined due to infrequent sampling at the current translation speed. To better examine metastable interactions, small sections of the approach curve were analyzed for binding energies and cantilever residence times in each of the energy states (Fig. 3.7). Fig. 3.7(a) shows the cantilever moving from an unbound state (D) to bound state (A) via two metastable binding events (B and C), while approaching the surface. Please note that although state B is denoted as a metastable state, it corresponds to the same binding pocket as that of state A. The cantilever tip jumps in the same binding pocket twice resulting in the two states A and B, the difference between them being the amount of time spent the cantilever tip in the pockets. Since the tip spends very less time in state B as compared to A, state B is denoted

as a metastable state. To compute binding energies and cantilever residence times at each tip sample distance, the cantilever positions are first transformed to tip sample distances to obtain deflections as a function of tip sample distance (Fig. 3.7(b)). The instantaneous binding energies of each of the four states (A, B, C, D) are separately computed via the reconstruction method and shown in box plots of Fig. 3.7(c). Since time spent by cantilever in each state is proportional to the number of points recorded for that state, the residence times at each of the four states are calculated by a count of the number of points in each state (Fig. 3.7(d)). For illustration purposes, coarse tip sample distance increments of 0.25 nm are used and residence times are plotted as a percentage of the total interaction time. The overall average binding energy can be calculated by an average of binding energies weighted by cantilever residence times at each state (Fig. 3.7(e)). It shows both the average and the range of binding energies for each state during approach. Fig 3.7(f) shows the same instantaneous binding energy landscape along with the average trace, but reconstructed at much smaller tip sample distance increments. Fig. 3.7(f) is very useful since it shows the binding energy pathways for those rarely sampled binding events that would not be otherwise visible in an average potential trace. We see that while our method can detect rare biotin-avidin interactions with maximum instantaneous binding energies of ~18.5 k_bT, it estimates the average energy landscape of biotin avidin interactions as having two binding pockets with average energies of 6.5 k_bT and 3 k_bT. Finally, similar analysis is performed for our entire dataset at fine tip sample distance increments and the results plotted in Fig. 3.7(g). As can be seen, the biotin-avidin energy values calculated by our methods are lower than published values. Our methods compute binding energies of biotin-avidin during approach as opposed to unbinding energies computed during retraction [3].

Since unbinding energies include an additional non-equilibrium work that is dissipated during retraction, binding energy values tend to be lower than corresponding unbinding energies. Also, reconstructed binding potentials relies on good sampling of the potential well in order to record all subtle variations in binding states. Ability to improve sampling, such as slower approach rates or enhanced stochastic excitations, will aid in probing rarer binding pathways corresponding to deeper potential wells of biotin-avidin interactions.

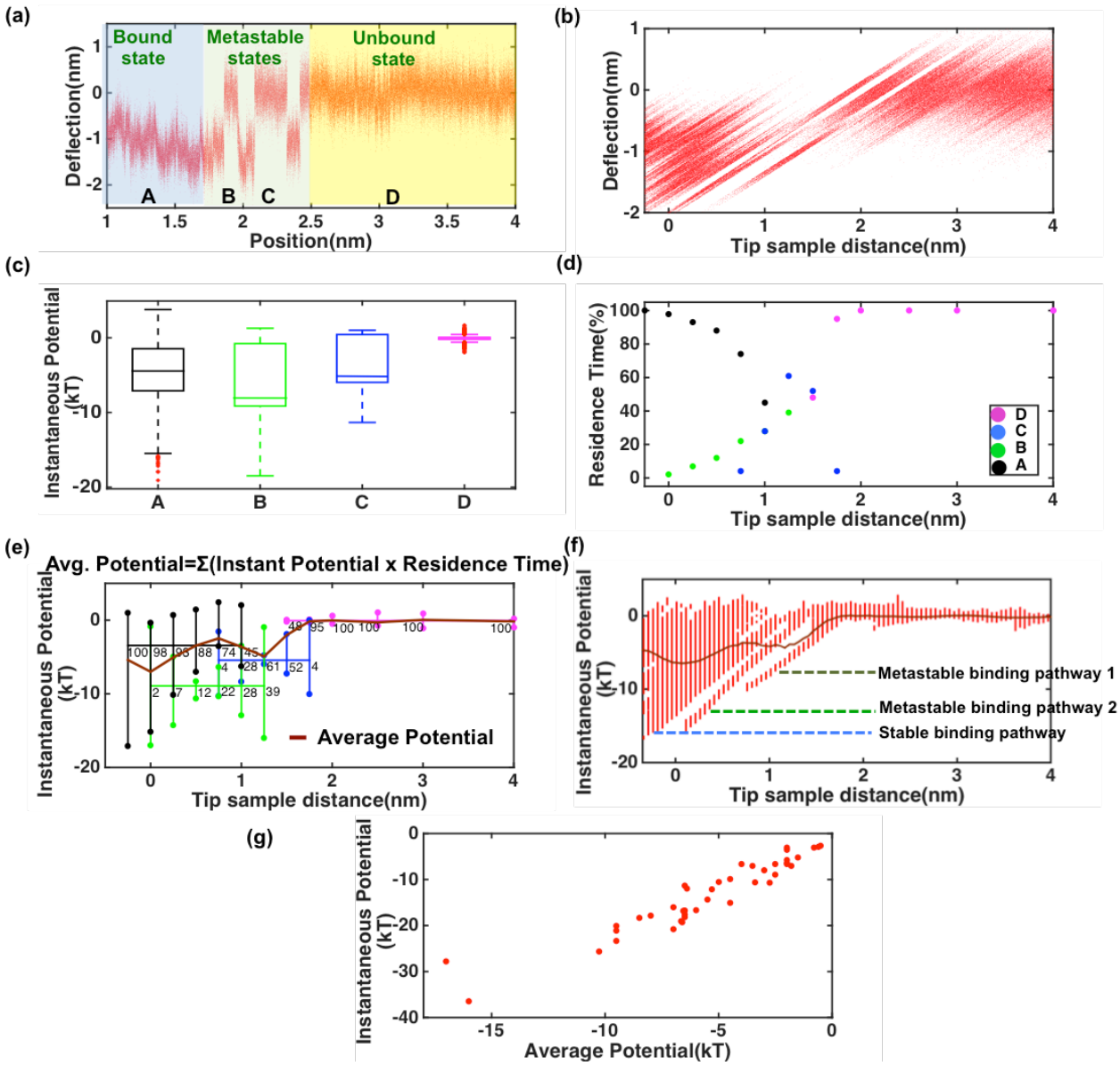

Figure 3.7. (a) Approach force curve for a biotin-avidin system, indicating the different binding states (b) Transformation of position to tip sample distance to calculate cantilever residence times (c) Box plot of binding energies for each state (A, B, C, D) (d) Residence times computed by an estimate of point count in each state, at tip sample distance increments of 0.25 nm (e) Range of binding potentials of each state and average potential computed by weighted average of instantaneous potentials and residence times at each tip

sample distance (f) Binding energy landscape reconstructed using a fine resolution of tip sample distance increments, indicating binding pathways including those of rare events (f) Instantaneous binding energies for the entire dataset plotted versus corresponding average potentials

3.5. Conclusions

We have used atomic force microscopy to directly map the intermolecular energy landscape of biotin-avidin interaction. By utilizing the variations in fluctuations of the biotin bound AFM tip as it passes close to an avidin coated surface, the free energy landscape is reconstructed through inverse Boltzmann equation. Using this technique, we have reconstructed and analyzed the multiple energy wells that are characteristic of biotin-avidin bond formation. The energy landscape qualitatively resembles those obtained through computational simulation as biotin initially binds to an avidin loop followed by binding to beta-barrel residues. However, the landscape is not quantitatively accurate since the cantilever is not able to sufficiently sample the rare binding states that contribute significantly to energies of biotin-avidin bonds. The biotin-avidin bonds are strongly adhesive with steep energy landscapes whose force gradients quickly exceed cantilever's stiffness during bond formation process, thereby forcing the cantilever tip to quickly jump from unbound to bound states without recording many rare transition states. This is a common problem seen in sampling strongly adhesive energy landscapes and is addressed in the following chapter.

CHAPTER 4

ENHANCED STOCHASTIC EXCITATIONS TO MEASURE STEEP ADHESIVE ENERGY LANDSCAPES

4.1 Introduction

The free energy landscape governs the behavior of all interactions in the presence of thermal fluctuations in physical chemistry, materials sciences, and the biological sciences. From the energy landscape follow all critical information about an interaction, such as the reaction kinetic rates, bond lifetime, and the presence of intermediate states. Despite its importance to understanding reaction mechanisms, most experimental methods do not directly measure energy landscapes, particularly for realistic interactions with steep force gradients. As seen in the previous chapter, we were unable to reconstruct the strongly biotin-avidin interaction landscape, due to premature jump to contact of the probe resulting in insufficient sampling of transition regions.

In this chapter, we present an atomic force microscopy (AFM) method to increase sampling times of these strongly adhesive interactions by enhancing the cantilever's thermal fluctuations using white noise excitation. By combining enhanced fluctuation method while recording subtle deviations from harmonic potential with Boltzmann sampling discussed in chapter 2 (Eq. 2.7), we show increased accuracy of the reconstructed interfacial energy landscapes. Analysis of the energy landscape reveals that there exists an optimum excitation voltage that corresponds to a maximum accuracy of landscape determination accuracy. The chapter concludes with stressing on the importance of identifying the optimum excitation level, which is the subject of the next chapter.

4.2 Background

Conventional AFM interaction force profiles are measured using a force-distance curve, in which a soft spring deflects due to interfacial forces such that the average spring position corresponds to the force for each separation distance [167]. While force interactions are important, they are insufficient to directly compare to bulk assays [168] and simulations [169]. It may be tempting to obtain energy profiles indirectly by integrating the measured forces, but to do so is problematic due to inaccuracies in the measured force and separation at small distances where force gradients are large and the cantilever position does not accurately reflect tip-sample force due to dynamic effects. This problem appears in force curves as snap-in behavior resulting from large gradient attractive forces that exceed the probe spring constant [132, 170]. Using stiffer cantilevers to prevent snap-in also reduces sensitivity to forces at all length scales [80], especially subtle, near-surface force-field variations that extend over sub-nanometer distances. Actively modifying the cantilever stiffness using magnetic forces [171] and capacitance [133] can prevent snap-to-contact, however, low-bandwidth stiffening does not precisely control the cantilever motion [117]. Hence there exists a need for direct measurement of interfacial energy landscapes for strongly adhesive interactions.

Several non-equilibrium and equilibrium techniques [111, 112, 116] have been developed to measure energy landscape profiles. Among the non-equilibrium methods, Jarzynski's equality has been used to reconstruct unfolding free energy landscapes of nucleic acids and individual biopolymers [159]. However, this method fails to reconstruct the energy surface immediately past the transition states due to a very sharp increase in dissipated work, which cannot be estimated accurately in the short time span of the

transition [160, 168]. Meanwhile, equilibrium methods model the thermal vibrations of the probe by a thermal particle in a well which is performing a Boltzmann-like sampling of the potential well imposed by both the cantilever and the sample [80, 115]. This approach was successfully used to probe potential wells created by the ordering of water near a calcite surface and electrical double-layer forces in aqueous solutions [130, 131]. Force and energy profiles generated by the transformation of probabilities using Boltzmann's equation have been used to characterize electrostatic, van der Waals and solvation forces [80, 132].

Reconstructing the entire interaction energy profile can be challenging due to the presence of large barriers that are difficult to sample on the time scale of a measurement [115]. To acquire sufficient data around high barriers, it is advantageous to constrain the cantilever's position near these features, or to traverse them at nanometer-per-second velocities [118]. Precise movement of the probe harmonic potential tilts the interaction profile such that the probe jumps between energy wells along the energy landscape. In this way the entire energy landscape is mapped by stitching together energy measurements made at different positions along the reaction coordinate [118]. However, a limitation of this technique is the inability to map the complete interaction in the presence of attractive forces with gradients greater than the cantilever stiffness, due to a critical instability that limits sampling [31].

As a solution to this problem, Hoh and colleagues showed that approach forces can closely approximate retraction forces by adding a white noise signal to gather sufficient statistics around barriers and steep energy gradients [32]. In all conventional approaches to measuring forces, cantilever noise negatively impacts the accuracy of the interaction

measurement. However, enhancing the vibrational noise of the cantilever increases the cantilever's restoring force, allowing it to avoid getting trapped in energy wells for long periods of time, transition repeatedly over barriers and transiently sample regions of large attractive interactions. Yet this approach has not been applied to the reconstruction of energy landscapes.

In this chapter, we demonstrate the direct mapping of interfacial free-energy potentials using enhanced thermal fluctuations combined with a Boltzmann sampling method to oversample the probability distribution and improve mapping of the energy landscape. The enhanced Brownian (thermal) fluctuations vibrate the cantilever through the energy profile of the surface and surrounding medium while the cantilever restoring force prohibits binding, enhancing the profile sampling. As a cantilever fluctuates close to a surface, the close proximity to the free energy landscape causes deviations from the harmonic potential. By recording the variations in fluctuations of the cantilever as it approaches and interacts with the substrate, and combining it with inverse Boltzmann equation (Eq. 2.7), the free energy landscape is reconstructed.

4.3 Materials and Methods

4.3.1. Preparation of AFM Tip and Sample Surface: Silicon nitride, iDrive compatible BL-TR400PB cantilevers (Asylum Research, Santa Barbara, CA) were cleaned in chloroform (3 × 5 minutes), dried in nitrogen, and then cleaned for one minute on medium power in a PDC-32G plasma cleaner (Harrick Plasma, Ithaca, NY) before being placed in the cantilever holder. Freshly cleaved grade V-1 mica discs (SPF Supplies, West Chester, PA) were glued to glass slides. In the AFM, 40 μL of HPLC water (Sigma Aldrich, St.

Louis, MO) was placed on the mica, the cantilever (f_0 = 30 kHz, k = 90 pN/nm nominal in liquid) was immersed in the fluid and equilibrated for several hours at room temperature.

4.3.2. AFM Setup for Enhanced Stochastic Fluctuation Measurements: All AFM measurements were performed with an Asylum Research MFP-3D Bio-AFM. Data was collected at 50,000 samples per second to capture all deflection information through the cantilever's first eigenmode. The inverse optical lever sensitivity was measured in liquid just prior to collecting approach-retract traces. Spring constants were calibrated in air after the experiment using the thermal method [94, 172]. A DS 345 function generator (Stanford Research Systems, Sunnyvale, CA) was used to generate a white noise signal (bandpass filtered from 95 Hz to 112 kHz), which was then sent to the iDrive cantilever at voltages varying from 1 V to 7 V via controller input. All deflection data was sampled at a frequency of 50 kHz. Given that the cantilever's primary resonance mode in water is ~9 kHz, the sample rate is sufficient to satisfy the Nyquist criterion and capture all of the primary resonance mode deflections [80]. The current travels along a wire micro-machined into the cantilever, generating a magnetic field that acts on a magnet embedded in the cantilever holder. The field may either attract or oppose the magnet's field, vibrating the cantilever. The applied voltage causes a linear increase in the RMS vibration of the cantilever. The cantilever was equilibrated until drift was below 60 pm/s. Z-Piezo drift was measured directly using a sensor, and was less than 200 pm/s. Total drift, calculated as the difference between the approach velocity (the contact region slope of the deflection vs time trace) and Z-Piezo velocity command sent to the AFM, was always less than 20% of the approach velocity. The z-piezo displayed hysteresis when moving quickly over hundreds of microns. Once the motion was complete, the hysteresis was allowed to dissipate prior to collecting

a deflection trace. Both cantilever and Z-Piezo drift effects were negated by subtracting their velocity from the velocity command sent to the Z-Piezo. Approach-retract cycles were conducted prior to every set of measurements to calibrate the approach velocity from the contact region of deflection vs time traces. For each deflection trace, the zero point of the cantilever base-surface distance (Z-Position) was obtained from the intersection of the contact and far-from surface regions of the deflection trace. This calibration eliminated the effect of drift in the Z-direction [132].

4.3.3. Free Energy Landscape Reconstructions: Adhesive energy landscapes between silicon nitride and mica were obtained by operating the AFM in force-distance mode and collecting approach force curves at a variety of velocities. As the cantilever fluctuates close to a surface, the proximity to the interfacial free energy landscape causes deviations from the harmonic potential. By recording the variations in fluctuations of the cantilever as it approaches and interacts with the substrate, the free energy landscape can be reconstructed. Energy landscape reconstruction is as follows. The deflection signal was linearly transformed to the tip sample distance by subtracting the Z-position data from the cantilever deflection signal. The tip sample interaction potential was obtained from the overall tip sample distance data using a technique analogous to umbrella-sampling [173] in which the cantilever's harmonic potential was used to constrain the tip movement within a small region to maximize local sampling. The tip position data was parsed into multiple small windows and the tip positions from each window were binned into probability histograms, $P(x)$, in order to calculate the tip position probability density. Directly measured histogram distributions are biased since they are dependent on both the cantilever harmonic potential as well as the interfacial potential. To remove the contribution of the

probe spring, weighted histogram analysis methods (WHAM) [136, 138, 162] were employed to iteratively solve for the interfacial potential distributions, $P_{interaction}(x)$. Finally, the inverse Boltzmann relation was used to convert the interfacial potential probability distributions into the overall energy landscape, $G(x) = -k_B T ln\left(P_{interaction}(x)\right)$. The reconstructed binding energy well depths are defined as the depth of the energy well relative to zero energy far from the surface. The barrier width is the distance from the energy minimum to the barrier, where the position of the barrier is defined by the reaction coordinate where the tip sample interaction appreciably deviates from the harmonic potential. The reconstructions were carried out with 5000 point windows and 0.05 nm bin widths using custom routines written in MATLAB (MathWorks Inc., Natick, MA). In general, slow approach rates were desired (v < 2 nm/s) to increase sampling throughout the energy landscape but particularly the barrier region.

4.3.4. Dynamic Force Spectroscopy and Extraction of Kinetic Parameters: To compare the energy landscape reconstruction results to conventional retraction adhesion methods, we conducted dynamic force spectroscopy (DFS) to establish retraction energy-well parameters [97]. After contact between the tip and sample was established with a 3 nm trigger deflection, the cantilever was retracted. Retraction velocity was varied from 1 to 500 nm/s, corresponding to force loading rates of 10 to 10^5 pN/s, which was measured using the slope of the force vs. time retraction plot prior to unbinding. Hundreds of approach-retract cycles were carried out to provide sufficient data to fit to the dissociation model. The force spectrum and corresponding load rates were plotted in a force vs logarithm of loading rate plot. The Friddle-Noy-de Yoreo model [107], which considers rebinding of molecular bonds that can occur at slow retraction rates, was fit to this dynamic

force spectrum to obtain the equilibrium rupture force, barrier distance, and kinetic off-rate. Custom scripts written in Igor Pro (Wavemetrics, Lake Oswego, OR) were used for all model fitting to calculate rupture forces and load rates from force vs time plots. We fit the aggregate raw retraction unbinding force ($\langle F \rangle$) vs. loading rate (r) data to the analytical approximation of the Friddle-Noy-de Yoreo model for single bonds in order to extract free energy landscape parameters:

$$< F > \cong F_{eq} + F_{\beta} ln\left(1 + e^{-\gamma} R\left(F_{eq}\right)\right) \quad [4.1]$$

with,

$$F_{\beta} = \frac{k_B T}{x_{\beta}}, F_{eq} = \sqrt{2 k_{cant} \Delta G_{bu}}\,, R\left(F_{eq} = \frac{r}{k_{off}\left(F_{eq}\right) F_{\beta}}\right) \text{ and } k_{off}\left(F_{eq}\right)$$

$$= k_0 e^{\left(\beta\left(F_{eq} x_{\beta} - \frac{1}{2} k_{cant} x_{\beta}^2\right)\right)}$$

where γ is Euler's constant, k_B is Boltzmann constant, T is temperature, k_{cant} is spring constant of cantilever, r is loading rate, x_{β} is barrier distance, $\Delta G_{bu} = G_b - G_u$ is the free energy of binding (G_b) relative to free energy of unbinding (G_u), F_{β} is the thermal force, F_{eq} is the equilibrium force, which is the minimal force required to break the bond for the bond/transducer system, and k_0 the intrinsic unbinding constant. Fit convergence criteria were evaluated with a nonlinear iterative Levenberg-Marquardt algorithm set to allow a maximum fitting error of 10^{-10} and implemented using custom MATLAB scripts.

4.3.5. DLVO energy landscape calculation. DLVO theory [174-176] describes surface-surface interactions as comprising repulsive electrostatic and attractive van der Waals forces. The forces of the tip-sample interaction were fit to the DLVO model,

$$F(z) = -\frac{HR}{3z^2} + F_0 e^{-z/\lambda} \quad [4.2]$$

where H is the Hamaker constant, R the tip radius, F_0 the electrostatic interaction strength, λ the Debye screening length, and z the tip-sample distance. Integration of this force-distance relation was used to calculate a theoretical energy surface and compared to Boltzmann reconstructed energy landscapes.

4.4. Results and Discussion

White noise driven iDrive Si_3N_4 cantilevers were slowly translated towards mica in HPLC water (Fig. 4.1A). The vibration response of the cantilever probe is shown in Fig. 4.1B in both passive and active states. The reconstructed potential energies of the cantilever are also shown, indicating the added noise did not alter the harmonic properties of the cantilever, but do increase the physical extent of vibration. Both harmonic reconstructions overlapped and fit to the same quadratic curve, demonstrating that while added excitation increased the range of potentials being sampled, the cantilever's stiffness remained unchanged. Three representative approach curves are shown in Fig. 4.1C for added noise voltages of 0 V, 4 V and 7 V. A 0.5 nm region for each is shown indicating a static binding event (0 V), discrete, thermally-driven toggling events between unbound and bound states (4 V), and large vibrations with no obvious tendency to remain bound or unbound (7 V). With increasing excitations, higher tip sample forces were recorded corresponding to earlier jump to surface. While a broader tip-sample distance is explored with increasing voltage, this comes at the cost of the supplied noise overpowering the energy well. To examine the binding states, the deflection data is binned into probability density histograms for each voltage (Fig. 4.1D). Both 0 V and 4 V show bimodal distributions indicating bound and unbound states. Unlike 0 V, excitation at 4 V allowed

us to sample transition states between the two bound states, accumulating more information during the transition of the interaction (Fig. 4.1D inset). Increasing the excitation voltage to 7 V results in a unimodal Gaussian distribution signal with no ability to distinguish between bound and unbound states.

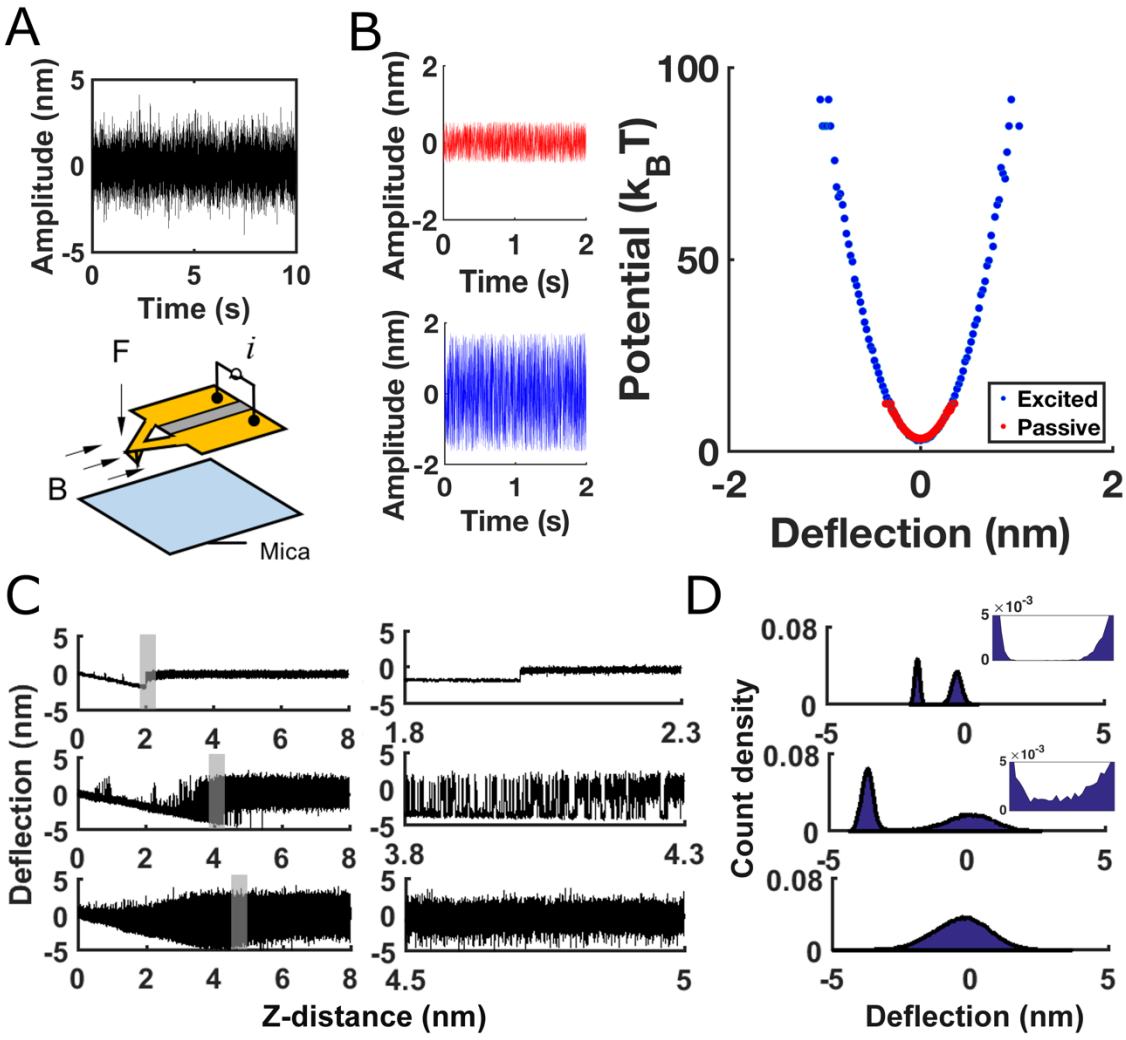

Figure 4.1. A. Schematic of the Asylum iDrive Si_3N_4 cantilevers used to sample adhesive energy landscapes of mica surfaces with enhanced stochastic fluctuations provided by white noise signals of varying amplitudes. **B.** Fluctuations of the undriven (red) and white noise driven cantilever at 3 V (blue) along with their potential energy reconstructions far away from the mica surface. **C.** Full deflection traces of the cantilever at 0 V, 4 V and 7 V,

along with their zoomed in counterparts. From the deflection traces, it can be seen that higher applied voltages increase both the range of sampling and the frequency of cantilever transitions between bound and unbound states. **D.** Count density histograms of the deflection signal at 0 V, 4 V and 7 V

We explored a range of excitation voltages to compare the approach force curves and the reconstructed free energy landscapes of Si_3N_4 and mica surfaces. The excitation noise amplitude was varied with RMS voltages ranging from 0 V (no excitation) up to 7 V in 1 V increments and the recorded deflection traces are shown in Fig. 4.2A from top (0 V) to bottom (7 V). As the voltage increased, RMS amplitude of cantilever's Brownian fluctuations increased proportionately from 0.31 nm to 0.97 nm. The larger amplitude resulted in bond formation while the equilibrium position of the cantilever was further out, allowing deeper and more frequent sampling of the underlying energy landscape. This was evident by increased Z-Position distance over which metastable binding occurred during the transition region (Fig. 4.2B). The underlying adhesive energy landscape for all voltages is shown in Fig. 4.2C.

Reconstruction of the 0 V approach curve showed a potential well depth of 34.6±3.9 k_BT, significantly less than the equilibrium force determined by retraction measurements using the Friddle-Noy-de Yoreo model of 188.20±20.48 k_BT. As excitation voltage increased from 0 V (which showed no transitions between bound and unbound states), the reconstructed energy well depth increased to a maximum 206±46.7 k_BT with 4 V excitation. Greater excitations above 4 V produced a smaller well depth. The measured energy well width also increased from 1.37 nm to 2.5 nm with 0 V to 4 V before declining. We observed a similar maximal value of the measured slope of the energy landscape, dG/dx,

experienced by the tip at 4 V sampling. These results are summarized in Table 4.1. The effective temperature of the tip corresponding to each excitation level was calculated using the equipartition theorem

$$T_{eff,2} = T_1 \left(\frac{x_2}{x_1}\right)^2 \quad [4.3]$$

where $T_{eff,2}$ is the tip effective temperature at enhanced cantilever deflection x_2, and x_1 is the cantilever deflection at no excitation at room temperature, T_1=300 K. Effective temperature can be interpreted as the temperature of a thermal bath that is coupled primarily to the cantilever probe.

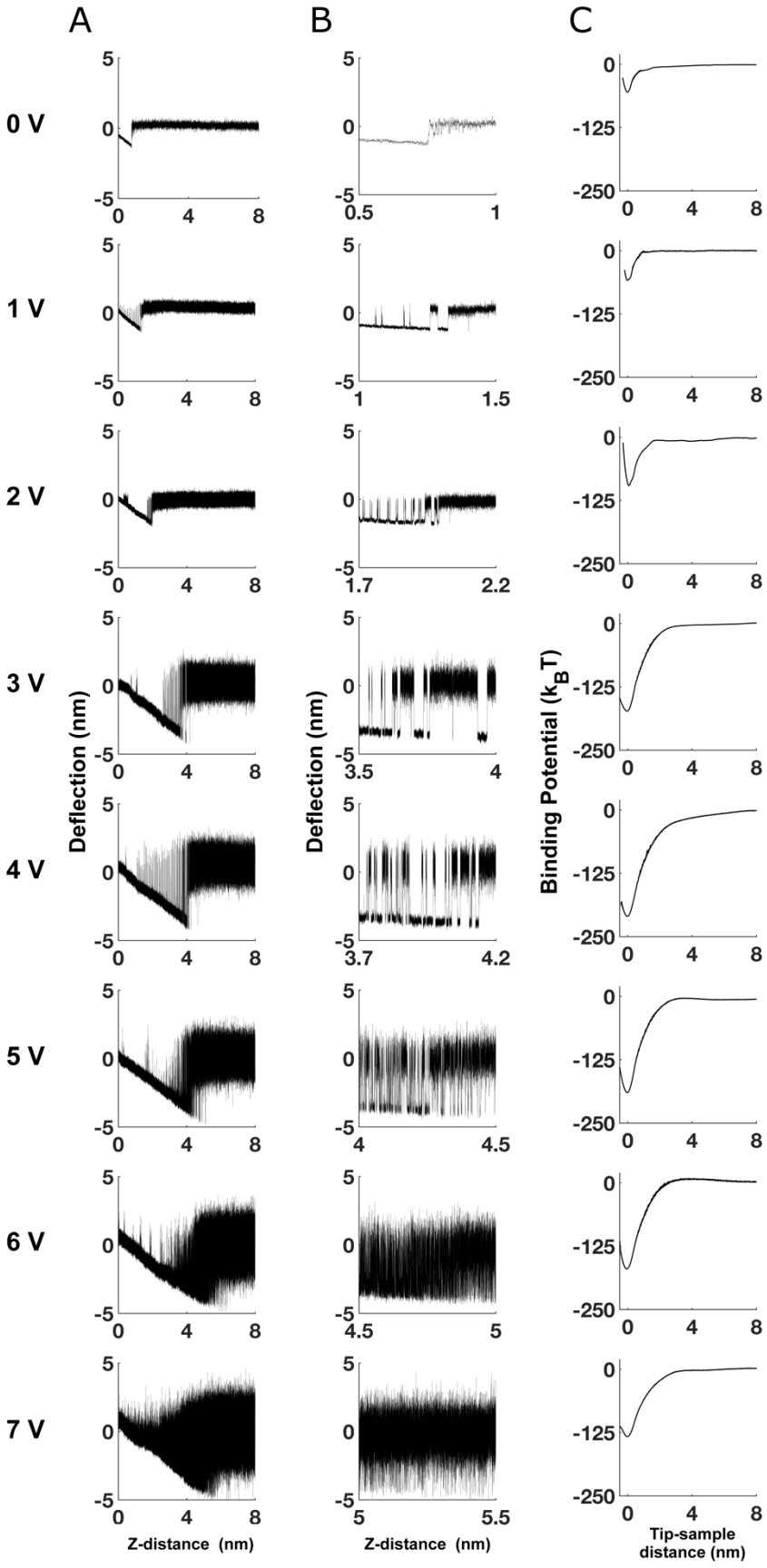
A
B
C
0 V
1 V
2 V
3 V
4 V
5 V
6 V
7 V
Deflection (nm)
Deflection (nm)
Binding Potential (k_BT)
Z-distance (nm)
Z-distance (nm)
Tip-sample distance (nm)

Figure 4.2. A. Approach deflection traces as a function of Z-distance for the Si_3N_4 cantilever approaching the mica surface in HPLC water at pH 7. The cantilever was plasma cleaned prior to experiment to remove tip contamination. The cantilever was driven from 0 V to 7 V and at least six curves were collected for each voltage. **B.** Zoomed in sections of the approach curves showing the transition regions when the cantilever moves from unbound to bound state. **C.** Reconstructions of the potential energy landscapes of the interactions for each voltage. Reconstructions show that binding energies and barrier widths are maximized at 4 V

Excitation (V)	T_{eff} (K)	ΔG (k_BT)	x_β (nm)	$\langle dG/dx \rangle$ (pN)	t_{tp}(μs)
0	300	34.6 ± 3.9	1.37 ± 0.32	106.7 ± 18.4	240 ± 34.5
1	344.1	65.2 ± 26.7	1.83 ± 0.87	150.7 ± 26.6	220 ± 41.2
2	494.4	93.8 ± 40.1	2.04 ± 0.76	188.5 ± 45.4	120 ± 49
3	785.8	182.6 ± 35.1	2.31 ± 0.41	324.7 ± 15	117.5 ± 35.7
4	1147.3	206 ± 46.7	2.50 ± 0.38	353.7 ± 71.1	115 ± 41.6
5	1154.5	173.3 ± 46.8	2.39 ± 0.43	296.8 ± 55.6	112.5 ± 25.2
6	2174.3	162 ± 25.9	2.35 ± 0.17	285.4 ± 57.5	85 ± 22.5
7	2881.4	118 ± 49.1	2.18 ± 0.44	213.9 ± 51.2	72.5 ± 20.5

Table 4.1. Energy landscape parameters for Si_3N_4 - mica interactions obtained from the reconstructions of approach force curves. The values represent the average of at least six measurements. Error bars are standard deviations for all data at each voltage

In cases where the energy well is too deep or too wide to be representatively sampled by the cantilever's ambient thermal vibration alone, enhanced cantilever fluctuations result in improved sampling of an interaction. Fig 4.3A illustrates a model of this effect in which a cantilever tip approaches an energy landscape with a moderate curvature (left) versus a steep curvature (right). The direction of cantilever movement is

indicated by the arrow, and the positions of the tip along the interaction landscape are indicated by red dots. When the cantilever stiffness is greater than or equal to the curvature of the energy landscape, the cantilever's restoring force is able to match the attractive force of the interaction, thereby allowing the tip to accurately follow the energy profile. However, when the probe is not sufficiently stiff to match the interaction forces, it tends to snap onto the surface in a free fall manner, with its trajectory being governed by its own dynamics (blue dashed lines), instead of by the constraining interaction energy profile. In such cases, the probe is only able to partially sample the landscape. With the help of enhanced excitation, the cantilever tip is now able to sample larger regions of the energy landscape from a given cantilever position than is possible with thermal vibrations alone. With sufficient excitation, it is possible for the tip to sample steep regions of landscape, enabling full reconstruction of the landscapes of these steep profiles.

To validate our reconstructions of the free-energy profile, we compared the results to kinetic and energetic parameters extracted from dynamic force spectroscopy (DFS) retraction measurements. The reconstructions were performed when the cantilever was approaching the surface (data in black) at low velocities (v < 2 nm/s), and the DFS was performed on subsequent retraction (data in blue) at faster velocities (Fig. 3B). The inset (Fig. 4.3B) shows that slower approach speeds allowed the detection of multiple transitions between bound and unbound states, which would not have been possible at higher speeds. Fitting the Friddle-Noy-de Yoreo model yielded F_{eq} = 373.14±19.62 pN, ΔG_{bu}= 188.20±20.48 $k_B T$ and x_β= 0.097±0.031 nm (Fig. 4.3C). We also reconstructed free energy landscapes of the interaction from the approach deflection traces using the inverse Boltzmann sampling technique. Fig 4.3D shows a representative binding potential vs. tip-

sample distance reconstruction performed at 4 V excitation level. We compared the reconstructions of the landscape free energy at different voltages with that of the estimated retraction binding energy (Fig 4.3E). The binding energy sampled at 4 V (206±46.7 k_BT) was similar to the Friddle-Noy-de Yoreo binding energy predictions (188.20±20.48 k_BT), providing a validation of our method. Plots of barrier widths obtained from reconstructions for each voltage (Fig. 4.3F) show that at 4 V excitation, the cantilever sampled a maximum barrier width of 2.50±0.38 nm. We also divided the binding energy by the barrier width to obtain the mean slope of the energy landscape, $\langle dG/dx \rangle$, that the cantilever experienced while descending into the well (Fig. 4.3G). We expect the mean slope to correspond to the average equilibrium force that the cantilever experiences during its transition from the unbound to the bound state. This is validated by reconstructions where we see the 4 V excitation results in a maximum mean force of 353.7±71.1 pN, similar to the equilibrium force predicted by the Friddle-Noy-de Yoreo model. Finally, we plotted the transition times for jumps between bound and unbound times as a function of excitation voltage (Fig. 4.3H). As expected, transition path times, t_{tp}, decreased as the jumping frequencies increased with increasing voltage.

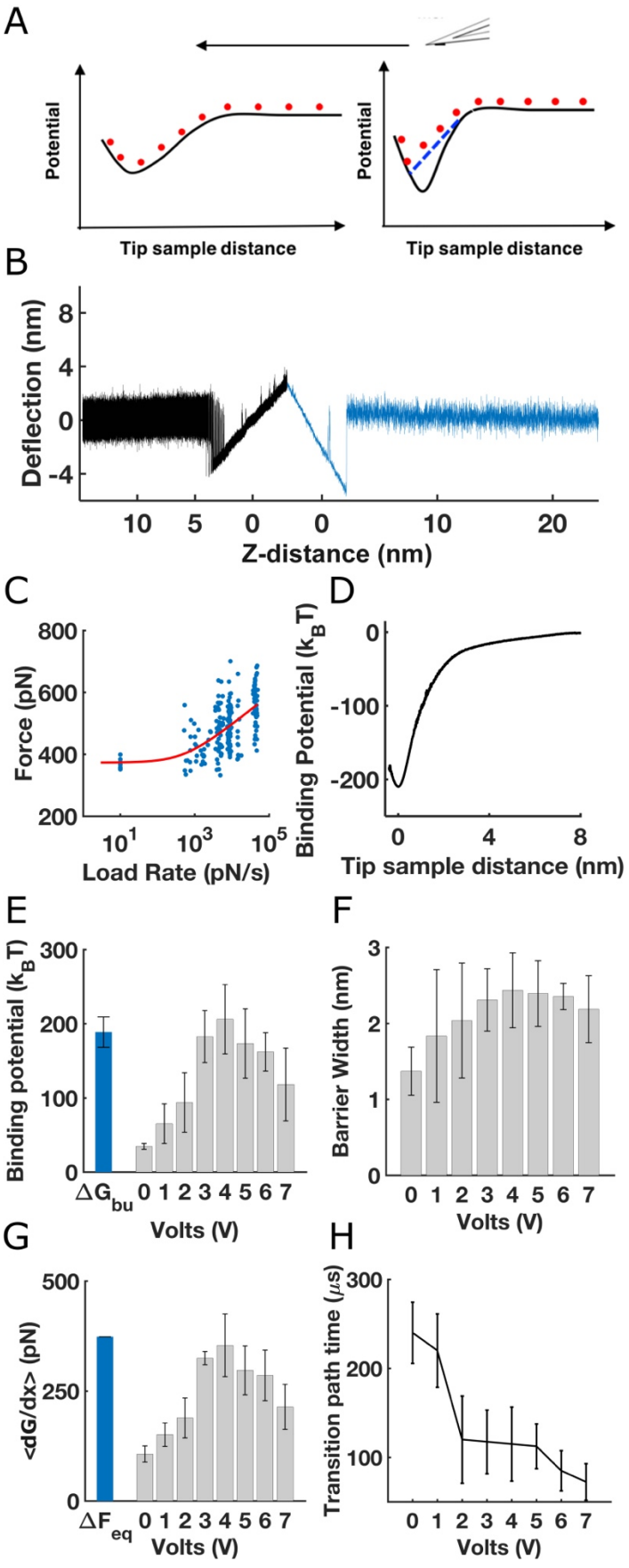
A
Potential
Tip sample distance
Potential
Tip sample distance
B
Deflection (nm)
8
4
0
-4
10 5 0 0 10 20
Z-distance (nm)
C
Force (pN)
800
600
400
200
10^1 10^3 10^5
Load Rate (pN/s)
D
Binding Potential (k_BT)
0
-100
-200
0 4 8
Tip sample distance (nm)
E
Binding potential (k_BT)
300
200
100
0
ΔG_{bu} 0 1 2 3 4 5 6 7
Volts (V)
F
Barrier Width (nm)
3
2
1
0
0 1 2 3 4 5 6 7
Volts (V)
G
<dG/dx> (pN)
500
250
0
ΔF_{eq} 0 1 2 3 4 5 6 7
Volts (V)
H
Transition path time (μs)
300
200
100
0 1 2 3 4 5 6 7
Volts (V)

Figure 4.3A. Schematic of an AFM cantilever approaching a moderate (left) vs a steep (right) potential well (shown in black) from right to left. The positions of the tip on the energy landscape is indicated by the red dots. Dashed blue lines indicate the trajectory of the cantilever when it snaps on to the surface. **B.** A typical force-distance curve recorded, with the approach section is colored in black while subsequent retraction is colored in blue. Inset shows expanded section of the approach curve where the tip behaves in an oscillating manner with multiple jumps over the barrier. **C.** Dynamic force spectrum with raw data (blue) is fit to the Friddle-Noy-de Yoreo model (red), and the underlying free energy landscape parameters are calculated. **D.** A free energy reconstruction of the approach data collected at 4 V shows the reconstructed binding energy and barrier width. **E.** Histograms of mean binding energies at different approach voltages compared to the binding energy estimation from the model, with error bars as standard deviations over at least six measurements for each voltage. **F.** Bar plots showing mean and standard deviations of barrier widths at each voltage **G.** Comparison of the energy profile slopes at all applied voltages with that of the equilibrium forces estimated from the model. **H.** Measured transition path times as a function of applied voltage, with error bars as the standard deviations of the path times at each voltage

One discrepancy we observed was that the energy barrier distances measured by Boltzmann reconstruction were greater than that of the Friddle-Noy-de Yoreo method by an order of magnitude. This difference could be explained by the multiple molecular bonds formed between the tip and the surface, where the true barrier distance, x_β, is reduced to [177] according to $x_\beta^{app} = x_\beta / N$ [107]. The ratio of the barrier distances for the 4 V

reconstructed surface and DFS of 25 Å and 1.28 Å, respectively, results in $N = 25$. We tested this estimate with predictions from Hertzian contact mechanics model. Applying Hertzian contact mechanics [178] to a silicon nitride tip (E = 230 GPa, ν = 0.23) of DLVO-estimated radius of 56 nm compressing a muscovite mica (E = 34 GPa, ν = 0.21) surface with experimentally relevant loading forces of 300 to 900 pN obtained from the force curve contact regions, the contact area ranges from 1.7 to 3.6 nm^2. Approximating functional group areas of exposed cantilever nitrogen and substrate oxygen atoms as ~0.2 nm^2 [177], and dividing the contact area by the area per bond, the number of formed bonds ranges from 8 to 17, slightly underestimating the 25 bonds predicted by DFS (Fig. 4.4) . This discrepancy may be due to the Hertz model assumption of a perfectly spherical tip, ignoring tip wear during repeated experimentation, and deformation caused by adhesion between the tip and surface [179, 180] which would increase bond formation. In experiments, the adhesion force during retraction was not affected by contact time or contact force, indicating the same contact area formed no matter the force, contrary to the Hertz model which predicts greater contact surface area with greater load force. Thus, it is plausible that during measurements ~25 bonds are formed.

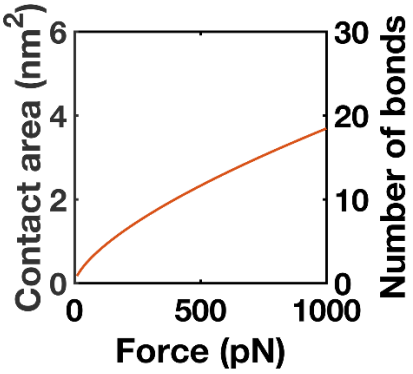

Fig. 4.4. Hertzian contact area as a function of load force (modeling the cantilever tip as a sphere (red) of radius 54 nm)

To compare the reconstructed energy surfaces to those predicted by DLVO theory, the tip-sample forces were fit to a simple DLVO model (Eq. 4.2) in Fig. 4.5. The Hamaker constant was fixed to 30 pN-nm [181] for a silicon nitride-mica interaction and the fit results in a Debye screening length of 18.6 nm and tip radius of 54 nm, consistent with the manufacturer's specifications. The ionic strength of the HPLC water is nearly zero, and as expected resulted in a longer Debye length than the ~6 nm found for Si_3N_4-water-mica systems in which the water contains millimolar salts [182, 183]. At greater distances, the cantilever experienced a slight repulsion from the surface, which is also seen in the reconstructions. The repulsive portion of the curve arises from the negative zeta potentials of both surfaces, where silicon nitride has an isoelectric point (pI) of 6-7 in water at pH 7 [81, 184], and mica presents a negative zeta potential at every pH [185]. At smaller tip-sample distances, van der Waals attraction causes snap-to-contact at 3.2 nm. The force fit parameters were used to calculate the individual energy contributions in Fig. 4.5B. The energy contributions of each force field, as well as corresponding curvatures are also indicated in Fig. 4.5C for small tip sample distances. DLVO predicts a peak-to-trough energy depth of 379 k_BT and barrier distance of 3.2 nm, significantly larger than those found for the 4 V reconstruction. It should be noted that the depth of the DLVO calculated energy surface is extremely sensitive to the forces at separations of just a few nanometers, but the fact that the AFM cantilever snaps to contact just prior to this distance may cause the DLVO model to overestimate the adhesive force and barrier location at these short distances.

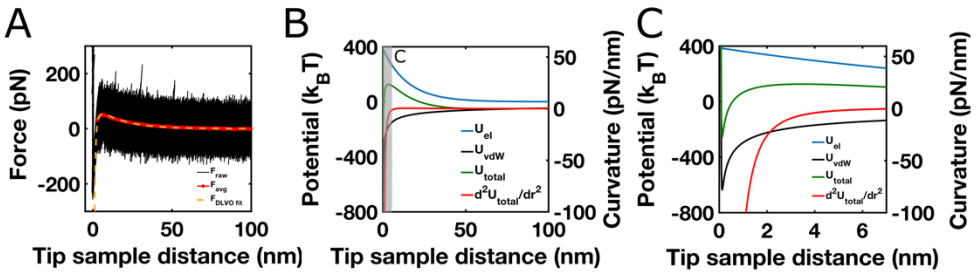

Fig. 4.5A. A total of 98 overlaid force curves (black dots) acquired on mica using a silicon nitride in HPLC water at pH 7 at 100 nm/s velocity. The force data average for every 0.2 nm tip-sample distance (red line) was fit with a DLVO force model (yellow dotted line) prior to snap-in. **B.** Electrostatic (blue line), van der Waals (black line), total energy (green line), and total energy curvature (red line) calculated from the DLVO parameters. **C.** Zoomed in total energy and curvature plot for short tip sample distances

4.5 Tuning the Chemical Environment

Interfacial energy landscapes between surfaces, such as the Si_3N_4-mica system, is a function of the environmental conditions such as pH, salt concentration, hydration forces etc. [85, 186]. Variation of these conditions can allow us to tune the liquid environment in order to minimize adhesive tip-sample forces that can damage a sample in AFM imaging applications [115]. Here, we experimentally verify, through the help of energy measurements, that changing the pH of the liquid from 3 to 7 does change the interaction from an attractive to a repulsive one, which is also reflected in corresponding energy landscape reconstructions. We recorded slow approach force-distance approach curves for silicon nitride-mica surfaces in HPLC water at pH 3 and pH 7. Fig. 4.6A shows these force curves and Fig. 4.6B shows the corresponding reconstructed energy surfaces for pH 3 (left) and pH 7 (right). The energy landscapes were reconstructed using the Brownian

fluctuation method described in the previous sections. The energy surface reconstructions gave a ΔG of 70 ± 5 k_bT and 34.6 ± 3.9 k_bT at pH 3 and 7, respectively. For pH 3, the energy surface lacks the repulsive hump seen in the energy surface at pH 7, as expected from the deflection traces.

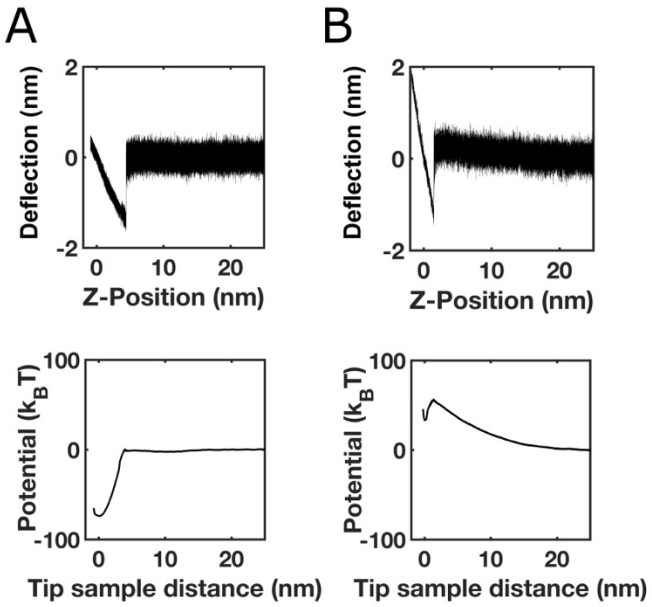

Figure 4.6A. Force-distance curve of silicon nitride-mica interface in HPLC water at pH 3 (left) and pH 7 (right). **B.** Corresponding energy landscape reconstructions for pH 3 (left) and pH 7 (right). Both the force curves and energy landscapes exhibit that increasing the pH changes the interaction from adhesive to repulsive

4.6 Comparison with Reconstruction of Biological Interactions: To our knowledge, this work represents the first mapping of energy landscapes with steep curvatures of ~315 pN/nm, approximately 15 times higher than other reconstructed landscapes, such as ~20 pN/nm found for DNA-aptamer, prion (64) (Fig. 4.7) and leucine zipper folding (65, 66). The energy landscape curvature is calculated for both prion protein folding and Si_3N_4-mica interaction by computing the double derivative of the potential energy vs. extension (or tip

sample distance) plots. The energy and corresponding extension values for prion folding were estimated from its energy landscape plot in Woodside *et al*. paper (64). Since derivative computations adds noise to the data, the curvature values were further smoothed using a robust form of local regression using linear least squares method (rloess), which assigns lower weights to outliers. Fig. 4.7(a) shows the energy landscape and its curvature for prion folding and Fig. 4.7(b) shows the same for Si_3N_4-mica interactions studied in this paper. As can be seen, the maximum energy landscape curvature for Si_3N_4-mica interactions (~ 315 pN/nm) is significantly higher than those for prion folding events (~20 pN/nm), thus illustrating the ability of the enhanced stochastic excitation method to sample steep energy landscapes.

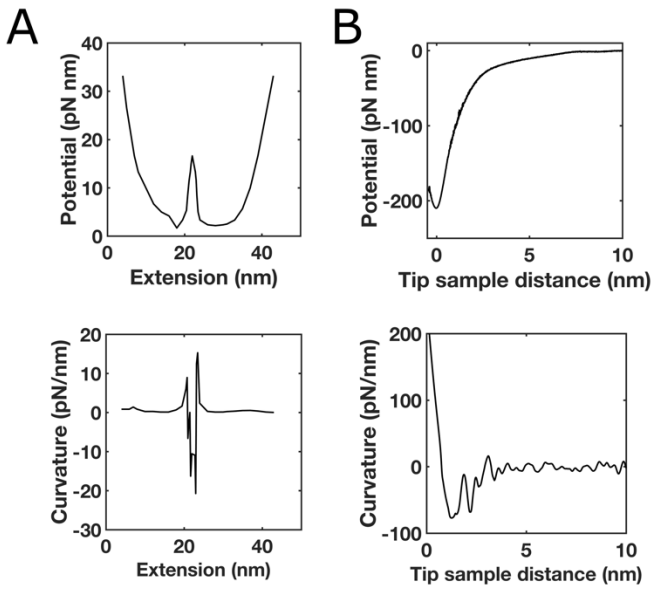

Fig. 4.7 (a) Potential energy versus extension plot for prion folding landscape (top) and its corresponding curvature (bottom). **(b)** Potential energy versus tip sample distance plot for Si_3N_4-mica landscape (top) and its corresponding curvature (bottom)

4.7 Conclusions

We have described and validated a novel method to accurately measure adhesive energy landscapes of nanoscale interfacial interactions. An important advantage of our approach is the accurate determination of energy wells even for steep gradients that greatly exceed the probe's stiffness, allowing for the use of highly force-sensitive probes. Through both deflection histograms and free energy reconstructions, we have shown that driving a cantilever with a white noise signal increases its capability to fully sample an interaction. We have shown that there is an optimal driving voltage magnitude, beyond which the cantilever's vibrational noise reduces the measurement accuracy.

Brownian reconstruction methods can be very useful in studying electrochemical interactions via analysis of transient states at the interfaces. By combining an active excitation mechanism by supplying external voltages to the AFM cantilever with stable hovering techniques, we can study both the time behavior of transient states as well as the interfacial properties. Brownian mapping of electrochemical interfaces can also help us to distinguish the active regions from non-active ones by measuring the fluctuations of the AFM cantilever from its equilibrium positions. It is expected that active regions will have (statistically) significantly larger fluctuations from equilibrium as compared to non-active regions. After transforming the recorded fluctuations to corresponding energy surfaces via Boltzmann statistics, we expect to find a good correlation between the measured energy depths and the electrochemical activity of surface.

The actual energy landscape measured by the tip is a function of both the magnitude of energies sampled as well as the time spent by the tip in each energy state. Increasing the cantilever's effective temperature via adding excitation increases its ability to sample large

energies while reducing the time spent in any state. A low metastable time would indicate that the cantilever was not effectively trapped by either the bound or the unbound states. As voltage increased towards the optimum of 4V, we were able to progressively sample the energy surface – primarily around the barrier region – while ensuring that the decrease in metastable time did not overshadow the range of sampled energy. At 4V, this combination was maximized and the tip was able to fully sample the energy landscape. Beyond 4V, the range of energy sampled remained the same while the metastable times decreased, leading to reconstructions with smaller energies.

Finally, our method was then validated with a model-based approach (Friddle-Noy-de Yoreo model) that relies on dynamic force spectroscopy results. The Brownian reconstruction method used here is not ideal at all excitations, however, it is clear that the salient features of the landscape's energy wells are best sampled at the excitation level at which the bound and unbound deflection distributions begin to overlap, or the point at which metastable binding is moderately present. Nonetheless, short-lived states within larger energy wells have been detected in deflection traces [30, 116, 187] and we demonstrated this capability with our system. Identifying the optimum excitation level for each energy well within a landscape will require a better understanding of the effect that cantilever spring constant, vibrational amplitude and approach velocity have on the metastable bond lifetimes and the final reconstructed energy landscape. This is the subject matter of Chapter 5. This method promises to be useful in the investigation of biological interactions, including ligand-receptor binding and the folding landscapes of proteins and nucleic acids, especially those with steep and/or deep energy wells. Detailed energy landscapes allow for the calculation of the kinetic rates [188] and landscape roughness

[189], and can be used to predict the structural stability of macromolecules, as well as their folding and binding pathways. With the advantage of using almost any probe to sample a wide variety of interactions, including those with stiff or "brittle" energy barriers, the approach demonstrated here extends AFM capabilities for accurately measuring energy landscapes.

CHAPTER 5

OPTIMAL EXCITATIONS FOR FULL ENERGY RECONSTRUCTION OF STEEP GRADIENT POTENTIALS BY SPRING PROBES

5.1 Introduction

Although statistical mechanics provide exact equations to calculate free energies, they are built on the assumption that all possible configurations of the system are sampled. The most pronounced limit to accurate free energy computations is therefore the imperfect sampling of a steep gradient potential field or high energy barrier, particularly in the case of interactions with small reaction coordinates. In the previous chapter, we had shown that increasing the stochastic fluctuations of a harmonic probe by active excitation results in increased sampling times of high gradient adhesive interactions and leads to accurate energy landscape reconstruction. We concluded that chapter by identifying a key limitation of the method, i.e. determination of the optimum excitation levels. This chapter is focused on addressing this limitation, through Brownian dynamics simulations and experiments. We use Brownian dynamics simulations of to test the impact of probe approach velocity, stiffness, and thermal energy to sample multiple wells of various depths and curvatures to understand the accuracy of energy surfaces reconstruction as a function of applied excitation. We show that through application of optimal stochastic excitations, we are able to obtain accurate energy landscape reconstruction for different probe and landscape parameters due to improved sampling of previously poorly probed interactions.

5.2. Background

One of the most complete quantitative description of intermolecular interactions is the free energy landscape. Free energy landscapes can be used to represent the energetics of a range of biological systems of interest, such as protein folding [188, 190], ligand receptor binding [191, 192], nucleic acid base flipping [193] and complex conformational changes in macromolecules [194]. Energy landscapes are also commonly used in computational studies of processes ranging from hydrophobic interactions [195] or organic reactions in water [196], to proton transfer [197] or ionic permeation through membrane channels [198], to peptide [199] and protein [200] equilibria. Energy landscapes therefore provide a valuable framework to describe the behavior of complicated systems in a straightforward and statistically rigorous manner. The energy landscape, $G(x)$, obtained from inverting the Boltzmann relation, is defined up to a constant C as

$$G(x) = -k_B T ln(P(x))) + C \qquad [5.1]$$

where $k_B T$ is the unit of thermal energy and $P(x)$ is the probability distribution with respect to a reaction coordinate of interest, x. The reaction coordinate [33, 201] represents a variable that can be used to follow the progress of an interaction, such as intermolecular distance or angle.

The experimental single molecule force measurements, for example with atomic force microscopy (AFM) [16, 157, 202, 203] or with optical tweezers [17, 66, 204] provides data for reconstruction of free energy landscapes. Free energy landscapes are reconstructed from experiments run under equilibrium conditions by binning the positional values of the chosen reaction coordinate into histograms to obtain an approximation of the

true probability distribution [205-207]. Similarly, energy landscapes can also be calculated from repeated non-equilibrium measurements by calculating the distribution of values of the mechanical work used to drive the system and transforming it into free energies [160, 208, 209].

A limitation of energy reconstructions of steep adhesive landscapes is that experiments may not generate sufficient data for a high quality reconstruction. This limitation stems from finite sampling time [205] due to sharp energy landscape barriers and probe dynamics which do not allow accurate tracking of energy gradients in equilibrium experiments [160]. In the equilibrium regime, the system is typically in a bistable state, driven by thermal fluctuations across the energy barrier between completely bound and fully unbound states [18]. For many realistic interactions, such as those with energy surfaces with high barriers, the transitions across the barrier may be so rare that it may not be currently possible to achieve sufficient equilibrium sampling at room temperature, in the time frame of an experiment. Researchers have used nonequilibrium force ramp experiments as a way to increase sampling in a given time frame and utilizing fluctuations theorems such as Jarzynski equality [208] to convert the nonequilibrium sampled work distributions to equilibrium free energies. However, the slow convergence of the Jarzynski equality with the increase in the number of samples [125] limits its applicability to near equilibrium fluctuation regimes only.

The cause of finite sampling in the case of steep adhesive energy landscapes with force gradients larger than probe stiffness can be attributed to limited thermal energy of the tip as well as its limited sampling range. The probe's thermal energy is insufficient to cross high energy barriers or escape deep energy wells and the tip's fluctuations are too small to

fully sample a steep adhesive landscape before it gets snapped onto the surface due the high interaction forces. The problem of the finite sampling in the case of the normal single molecule constant probe velocity equilibrium experiments can be overcome by supplying an external white noise based excitation [18] to the probe in order to increase its magnitude of fluctuations, and thereby its reaction coordinate sampling range at any given point in the coordinate. By combining this approach with the weighted harmonic analysis method (WHAM) [136, 138, 162, 166] for consistent transformation of fluctuations to energies for the entire reaction coordinate, it is possible to improve the reconstruction of the energy landscape. We have previously demonstrated this method in an AFM experiment in which we accurately measured the adhesive energy landscape of Si_3N_4-mica system with the help of white noise driven cantilevers. In this chapter, we perform a parametric sweep of energy barrier height, barrier slope, probe stiffness and probe velocity variables and use damped Brownian dynamics simulations to study their influence on sampling of the free energy landscape. Using the simulations, we are able to determine both the parametric trends and the optimal excitations required to best sample an interaction and minimize energy reconstruction errors. Finally, we demonstrate the applicability of our simulation results with AFM experiments conducted on a Si_3N_4-mica system at different probe velocities and validate that optimal probe velocities for best interaction sampling indeed follows the same trend as those predicted by the simulations. This technique may be used to analyze rough energy landscapes typical in many biophysically interesting systems without incorrect energy reconstruction estimations due to finite sampling errors.

5.3 Methods

5.3.1. Energy Landscape Model: The energy landscape $E(x)$ consists of two overlapping wells with a one dimensional Lorentzian profile, of the form

$$E(x) = -\left[\frac{A_1}{1+\frac{(x-\mu_1)}{\sigma_1^2}} + \frac{A_2}{1+\frac{(x-\mu_2)}{\sigma_2^2}}\right] \quad [5.2]$$

where A_1, A_2 correspond to well depths, μ_1 and μ_2 are the well location parameters and σ_1 and σ_2 are the well scaling parameters. We simplify the calculations by the making the landscape symmetric with the zero point of the reaction coordinate centrally placed between the two wells. A range of values μ and σ are employed in order to simulate different landscapes.

5.3.2. Brownian Dynamics Simulations: Overdamped Brownian dynamics (Langevin) simulations are used to model the behavior of a fluctuating cantilever tip under the influence of a potential landscape. At any given instant, the tip is subjected to fluctuating forces due to random impulses from neighboring fluid molecules as well as the forces due to the external potential field, while being constrained by the restoring force of the probe itself. Hence, the position x_i of the tip at time t_i during the *i*th step of the simulation can be given by the following equation [210-212]

$$x_i = x_{i-1} - \frac{k}{\eta}x_{i-1}\Delta t + \sqrt{2D\Delta t}w_i - \left[\frac{dE(x)}{dx}\right]_{i-1}\eta\Delta t \quad [5.3]$$

where η = 5×10^{-5} pN.s/nm is the friction coefficient, Δt = 5 ns is the time step of the simulation, k is the cantilever's spring constant, w_i is a Gaussian random number with a

mean value of 0 and a variance of 1 and D is the diffusion coefficient related to the the friction coefficient and thermal energy of the cantilever by Einstein relation $\eta D = k_B T$. 400 time steps are used between each recorded data point, which is obtained by dividing the data collection rate (Asylum Research MFP-3D Bio-AFM) of 50 kHz with the simulation time step of 5 ns. The cantilever spring, which superimposes a harmonic biasing potential to the underlying energy landscape, sweeps the reaction coordinate from -0.5 μm to 0.5 μm during the duration of the simulation at a constant velocity.

Fig. 5.1 shows a representative sample of the force curve generated by the simulation as the tip sweeps over the energy surface. As the tip traverses over the energy landscape (from bottom to top in Fig 5.1A), it experiences negligible interaction forces until -0.08 μm at which point the tip enters into the first well. Hence, on account of negligible tip forces, the tip and base of the cantilever on average move synchronously from -0.25 μm to -0.08 μm as evidenced by 45 degree line in Fig. 5.1B. From -0.08 μm until it reaches -0.030 μm, the tip experiences a steep potential gradient and hence the tip movement becomes larger than the Z-movement of the base, as seen as a sharp transition with force curve gradient greater than 45 degrees in the upper inset of Fig. 5.1B. Thereafter, tip moves to the bottom of the energy well and attains a minimum energy state whereupon it oscillates around a small range within the first well (with force curve gradient < 45 degrees) until it is forced to jump over the energy barrier into the second well by the constant movement of the base (bottom inset of Fig. 5.1B). The range of tip oscillations is governed by the thermal energy of the tip. Since the energy profile is symmetric, the force curve for the second well and subsequent energy profile is identical to the force curve

obtained before the jump. The bottom inset in Fig. 5.1B shows the region of interest in the force curve, which shows the neighboring events around the position when the cantilever jumps from one energy well to another. This region will be used for subsequent energy reconstructions.

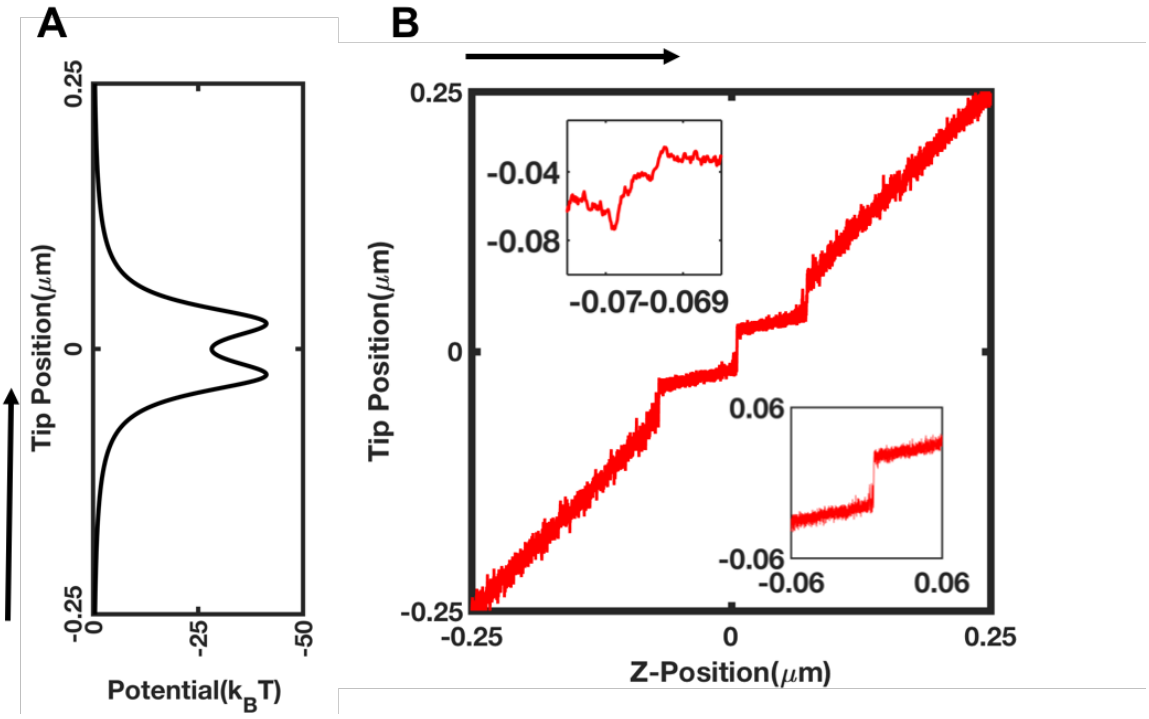

Figure 5.1A. A symmetric bimodal Lorentzian energy profile with overlapping wells. **B.** Force curve generated by an AFM probe tip while traversing over the energy landscape. Arrows show the direction of movement of the base of the probe as it approaches the surface. Inset on top shows a section of the force curve when the cantilever enters the energy well and inset on bottom shows another section of the force curve when the cantilever jumps between the wells typically observed in a binding/unbinding event

5.3.3. Energy Landscape Reconstruction and Error Computation: By recording the variations in fluctuations of the cantilever as it approaches and interacts with the substrate, the free energy landscape can be reconstructed. Energy landscape reconstruction is as

follows. The tip sample interaction potential was obtained from the overall tip sample distance data using a technique analogous to umbrella-sampling [134, 135], in which the cantilever's harmonic potential was used to constrain the tip movement within a small region to maximize local sampling. The umbrella sampling technique is used to determine how much data needs to collected at a given tip position, in order to accurately reconstruct its associated energy landscape. tip position data was parsed into multiple small windows and the tip positions from each window were binned into probability histograms, $P(x)$, in order to calculate the tip position probability density. The window sizes were chosen to ensure that data histograms from adjacent windows do not differ significantly from each other, such that maximum difference in average tip position between adjacent windows was 0.5 %. Directly measured histogram distributions are biased since they are dependent on both the cantilever harmonic potential as well as the interfacial potential. To remove the contribution of the probe spring, weighted histogram analysis methods (WHAM) [213, 214] were employed to iteratively solve for the interfacial potential distributions, $P_{\ interaction}(x)$. Finally, the inverse Boltzmann relation was used to convert the interfacial potential probability distributions into the overall energy landscape, $G(x) = -k_B T ln\left(P_{\ interaction}(x)\right)$. The reconstructions were carried out with 5000 point windows and 0.05 nm bin widths using custom routines written in MATLAB (MathWorks Inc., Natick, MA).

Due to imperfect sampling, two types of errors can be encountered in a reconstruction. (1) Either the reaction coordinate of the given energy landscape is not fully traversed (no reconstructed energy values for certain values of reaction coordinate) leading

to reconstruction errors when extrapolating the free energies to these under-sampled regions. [205]. Techniques such as series expansion or bootstrapping [215, 216] may not be effective to reconstruct free energies in these under-sampled regions because too much data is missing to enable a bootstrap to fill in the missing information [217]. (2) The probe is not sufficiently equilibrated when sampling the reaction coordinate, leading to errors when Boltzmann relation is used to transform these nonequilibrium fluctuations to free energies. The second type of error is handled by using a root mean square error (RMSE) measure to quantify the energy difference between the reconstructed energy and the underlying energy surface (numerator in Eq. 4.4). To account for the first type of error, we adjust the calculated RMSE by dividing it with a normalized range of reaction coordinate R that is being traversed by the reconstruction as shown in Eq. 4.4.

$$RMSE = \frac{\sqrt{\sum_i (G(x_i) - E(x_i))^2 / \sum i}}{R/R_{max.}} \quad [4.4]$$

where $R_{max.}$ is the maximum value of the sampled reaction coordinate R.

5.4 Results

Statistically, the mean and first moment can be used to describe a tip position probability distribution. However, such a description is not sufficient in regions of poor sampling and rare events are a major source of error [205]. Such cases of finite sampling exist when there is an energy barrier in the interaction energy landscape which cannot be sampled by the cantilever's thermal energy alone. Fig. 5.2 illustrates this concept through a schematic where a cantilever tip approaches a symmetric bimodal energy landscape from the left.

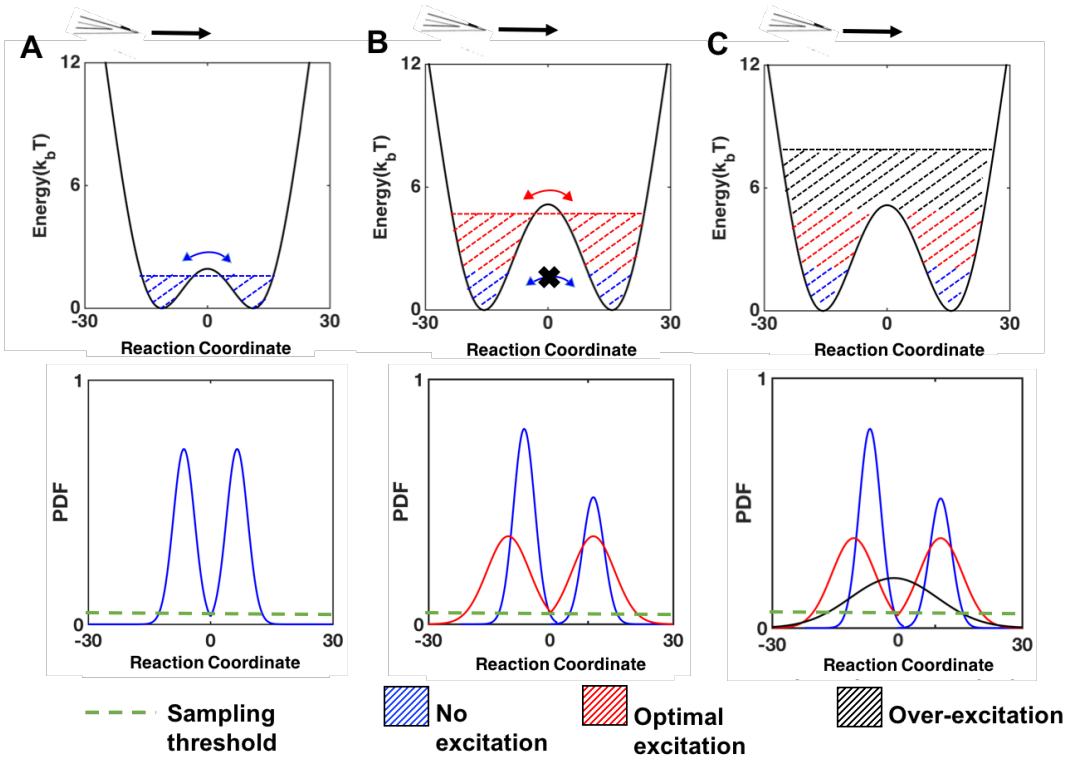

Figure 5.2: Schematic of an AFM tip approaching a symmetric bimodal energy landscape separated by a small barrier (**A**) and a large barrier (**B, C**) in the direction indicated by the arrow. The probability histograms of the detected positions of the tip are shown for no excitation case (in blue color), ideal excitation case (in red color) and overexcitation case (in black color). Green dotted line depicts the minimum number of detected tip positions needed to sample the reaction coordinate (sampling threshold).

In Fig. 5.2A (top), the energy barrier separating both the wells is nearly equal to the energy of cantilever's thermal fluctuations (shown as blue dotted lines) which allows the tip to spontaneously hop between both the wells multiple times without being trapped in either of the wells. As a result, the transition region is sufficiently sampled as indicated by the tip position histogram in Fig. 5.2A (bottom), which shows that the tip position sampling threshold (green dotted line) is crossed at all points in the reaction coordinate. The sampling

threshold is defined as the minimum number of times that the tip needs to sample a reaction coordinate in order to accurately reconstruct the underlying energy landscape. However, when we increased the energy well separation, thereby increasing the energy barrier height (Fig. 5.2B top), the cantilever tip's thermal energy becomes insufficient to cross the high barrier and therefore the tip oscillations between the two wells become rare. Hence, the tip spends more time in the first well than in the second well and the transition region sampling falls below the threshold (blue histogram in Fig. 5.2B bottom) resulting in a subsequent error in energy estimate. Amplifying the fluctuations increased the tip's energy to match that of the energy landscape barrier (red dotted lines in Fig. 5.2B top), thus restoring the spontaneous hopping behavior of the tip. The sampling threshold is crossed at all points of the reaction coordinate (red histograms in Fig. 5.2B bottom) including that of the transition region and an accurate reconstruction of the landscape is obtained. By further increasing the amplitude of fluctuations, the tip's energy became greater than the barrier height (black dotted lines in Fig. 5.2C top). In this condition, the tip oscillations were not constrained by the underlying energy landscape. Hence its position histogram reflected a unimodal Gaussian distribution (black curve in Fig. 5.2C bottom) with the ends of the histogram falling below the sampling threshold, making subsequent reconstructions prone to errors at these ends. Hence, it is essential that we need choose the correct tip energy, which is regulated via its effective temperature in order to optimize sampling and minimize reconstruction errors.

5.4.1. Effect of Energy Barrier Height:

$A_1 = A_2 = 0.15$ (pN), $\sigma_1 = \sigma_2 = 20$ (nm)

μ_1(nm)	-15	-19	-23	-27	-31	-33	-35
μ_2(nm)	15	19	23	27	31	33	35
$\Delta G(k_BT)$	1.9	6.3	10.9	15.2	18.4	19.8	21.1
T_{eff}(K)	300	500	700	900	1100	1400	1800

Table 5.1: Energy Landscape parameters used for the studying the effect of energy barrier height. The last two columns show the barrier height and the optimal tip effective temperatures required to accurately reconstruct the energy landscape

To study the effect of barrier height on energy reconstruction errors, we varied the barrier height by increasing the well separation. Table 5.1 shows the parameters used. All the parameters except the well positions were varied to simulate barrier heights from 1.9 k_BT to 21.1 k_BT , where *T*=300 K. Fig. 5.3A shows the force curves obtained through Langevin simulations of these 7 energy landscapes performed at room temperature (300 K), using a cantilever with a spring constant of 0.150 pN/nm which is sweeping the landscape from -60 nm to 60 nm with a constant velocity of 30 nm/s for 4 seconds. It can be seen that as the barrier height increases, sampling of the transition region becomes infrequent. To improve sampling at higher barrier heights, we increased the diffusion coefficient of the tip by raising its effective temperature by 100 K increments, thus increasing its sampling range at any given position. Fig. 5.3B. shows the force curves in a particular case where barrier height was 15.2 k_BT and the tip's effective temperature was raised from 300 K to 1100 K (200 K increments shown for ease of viewing). Then we reconstructed the energies from these force curves (red color) and superimposed them on the underlying free energy landscape (black color in Fig. 5.3C). As can be seen 300 K is insufficient to sample the energy landscape, and one needs to go as high as 900 K to

reconstruct them with minimal errors. Beyond 900 K, errors are reintroduced in the reconstructions due to the tip's dynamics not being constrained by the underlying energy landscape anymore. This is the optimal effective temperature for this particular barrier height (shown as enclosed in the green box) and has minimum RMSE with respect to the energy surface model. We quantified the energy reconstruction errors for all the temperatures at all barrier heights and recorded them in Fig. 5.3D. It shows that for each barrier height, RMSE for energy reconstructions decreases as the effective temperature is increased until an optimal temperature is reached at which the RMSE is minimized. Thereafter, the RMSE climbs back up with increasing temperature. Fig. 5.3E is used to record the values of optimal effective temperatures for each barrier height and can be used as a lookup to identify the range of effective temperatures needed to probe a given barrier height.

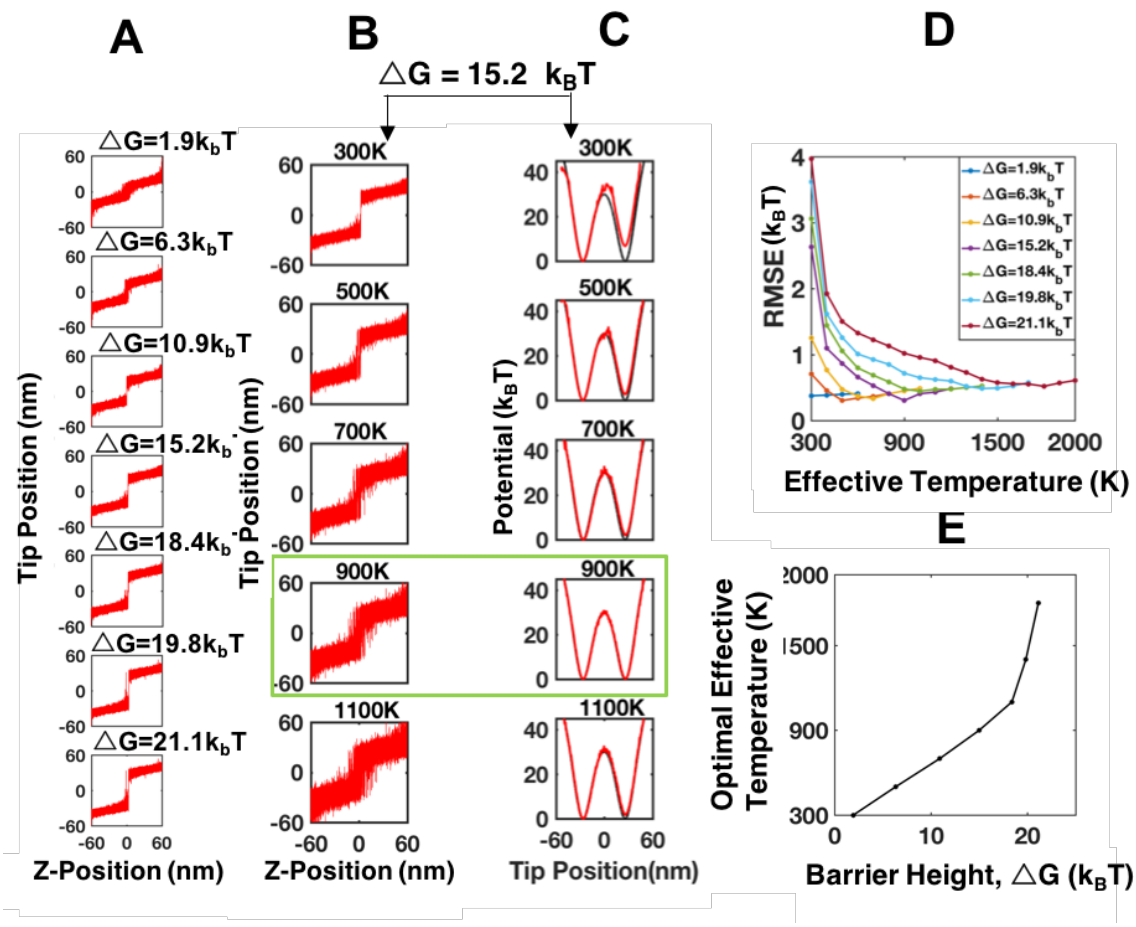

Figure 5.3A. Brownian dynamics simulated force curves at 300 K for 7 different energy barrier heights. **B.** Force curves simulated at different tip effective temperatures when the barrier height is 15.2 k_BT. **C.** Corresponding energy reconstructions (red color) and the underlying energy surface (black color) for each temperature. **D.** RMSE of energy reconstructions for different barrier heights plotted versus tip effective temperature. **E.** A plot of the optimal effective temperature versus the barrier height reflects the trend for temperatures needed to accurately reconstruct energy landscapes with different barrier heights

5.4.2. Effect of Energy Barrier Slope:

$A_1 = A_2 = 0.15$ (pN)

μ_1(nm)	-15	-12.75	-10.5	-8.25	-6.5	-4.875	-3.75
μ_2 (nm)	15	12.75	10.5	8.25	6.5	4.875	3.75
σ_1 (nm)	20	17	14	11	8	6.5	5
σ_2 (nm)	20	17	14	11	8	6.5	5
dE/dx(pN)	1.05	1.23	1.49	1.89	2.82	3.20	4.20
T_{eff} (K)	300	600	900	1100	1300	1500	1600

Table 5.2: Energy Landscape parameters used for the studying the effect of energy barrier slope. The last two columns show the barrier slope and the optimal tip effective temperatures required to accurately reconstruct the energy landscape

Here we varied the barrier slope by proportionately changing the two well locations and its scaling parameter values, but keeping the well depths fixed (Table 5.2). The simulated barrier curvatures *dE/dx* range from 1.05 to 4.20 pN. Fig. 5.4A shows the force curves recorded through Brownian simulations of these energy surfaces using a cantilever of stiffness of 0.150 pN/nm sweeping the landscape from -30 nm to 30 nm with a constant velocity of 30 nm/s for 4 seconds. Fig. 5.4B and 5.4C show the force curves and corresponding energy reconstructions, respectively for different tip effective temperatures when *dE/dx*=1.49 pN. Based on RMSE values with respect to the energy model, the optimal sampling temperature for this barrier slope is 900 K (highlighted in green box). Finally, RMSE values are computed for all barrier curvature at each effective temperature in 100K increments (Fig. 5.4D), which allows to obtain the optimal effective temperature for each barrier curvature (Fig. 5.4E).

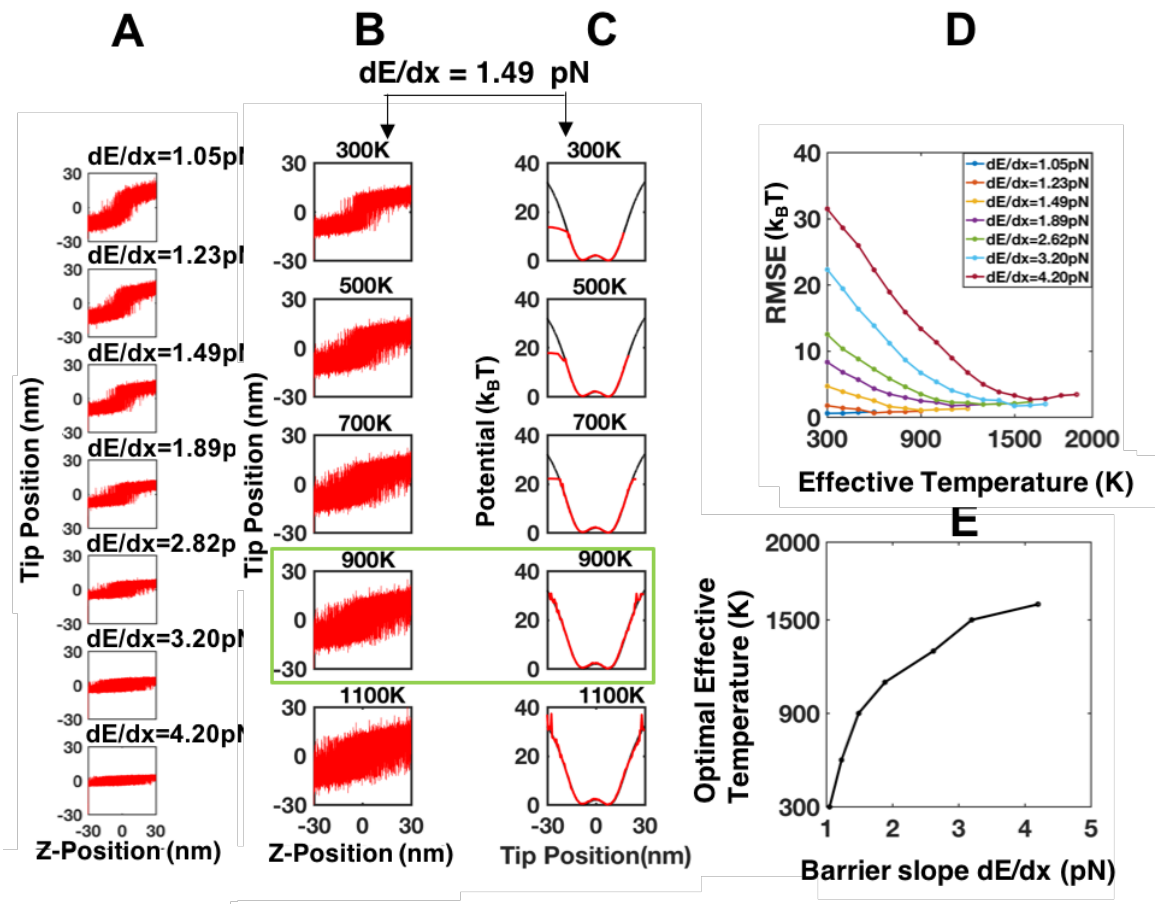

Figure 5.4A. Brownian dynamics simulated force curves at 300K for 7 different energy barrier slopes. **B.** Force curves simulated at different tip effective temperatures when the barrier slope, *dE/dx* is 1.49 pN **C.** Corresponding energy reconstructions (red color) and the underlying energy landscape (black color) for each temperature. **D.** RMSE of energy reconstructions for different barrier curvatures plotted versus tip effective temperature. **E.** A plot of the optimal effective temperature versus the barrier slope reflects the trend for temperatures needed to accurately reconstruct energy landscapes with different barrier slopes

5.4.3. Effect of Probe Stiffness:

$A_1 = A_2 = 0.15$ (pN), $\mu_1 = -\mu_2 = -15$ (nm), $\sigma_1 = \sigma_2 = 20$ (nm)

k (pN/nm)	0.025	0.050	0.075	0.100	0.125	0.150	0.175
T_{eff}(K)	1500	1100	800	600	400	300	300

Table 5.3: Energy Landscape parameters used for the studying the effect of probe stiffness. The last two columns show the probe stiffness and the optimal tip effective temperatures required to accurately reconstruct the energy landscape

Apart from complexities in the energy landscape, probe dynamics also affect the quality of sampling of the landscape. The range of tip fluctuations are limited by width of the biasing harmonic potential which in turn is governed by the probe stiffness. To study the effect of the cantilever probe stiffness, the energy landscape parameters are fixed and the probe stiffness is varied from k = 0.025 pN/nm to k = 0.175 pN/nm in 0.025 pN/nm increments (Table 5.3). Fig. 5.5A shows the force curves using different cantilever stiffnesses sweeping the landscape from -60 nm to 60 nm with a constant velocity of 30 nm/s for 4 seconds. Fig. 5.5B and 5.5C show the force curves and corresponding energy reconstructions, respectively for different tip effective temperatures when a cantilever with stiffness = 0.075 pN/nm is used. Based on RMSE values with respect to the energy model, the optimal sampling temperature for this probe is 800 K which is highlighted in the green box. The reconstruction errors are quantified for all probe stiffnesses at each effective temperature in 100 K increments (Fig. 5.5D) by computing their corresponding RMSE values. This allows us to obtain the optimal effective temperature for each probe stiffness (Fig. 5.5E). It should be noted that it might be tempting to use very stiff cantilevers to fully sample energy landscapes even at 300 K. However, choosing to employ very stiff cantilevers can result in low deflection sensitivity of the tip and the recorded fluctuations can fall below the noise level of the instrument, producing low signal to noise ratios.

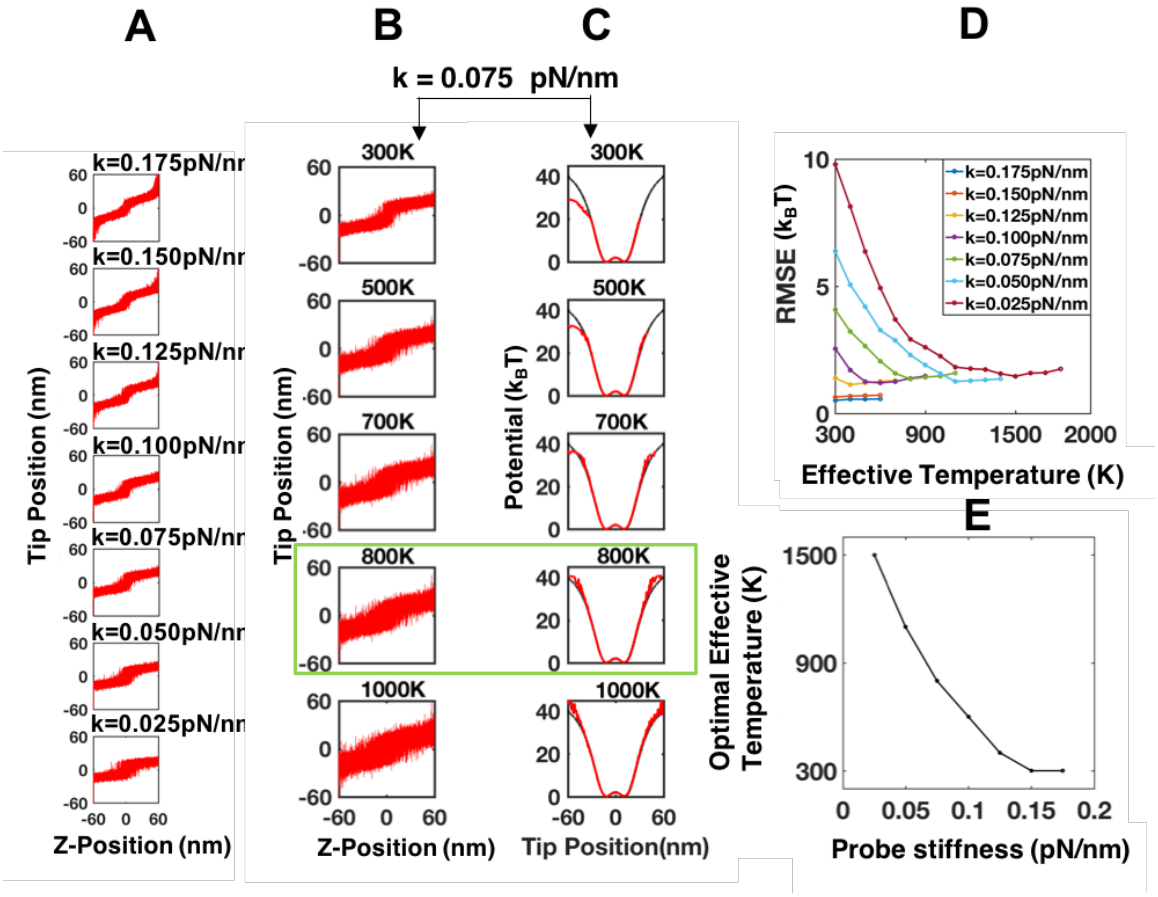

Figure 5.5A. Brownian dynamics simulated force curves at 300K for 7 different probe stiffnesses. **B.** Force curves simulated at different tip effective temperatures when the probe stiffness is 1.49 pN /nm **C.** Corresponding energy reconstructions (red color) and the underlying energy surface (black color) for each temperature. **D.** RMSE of energy reconstructions for different probe stiffness plotted versus tip effective temperature. **E.** A plot of the optimal effective temperature versus the probe stiffness reflects the trend for temperatures needed to accurately reconstruct energy landscapes with different probe stiffnesses

5.4.4. Effect of Probe Speed:

$A_1 = A_2 = 0.15$ (pN), $\mu_1 = -\mu_2 = -23$ (nm), $\sigma_1 = \sigma_2 = 20$ (nm)								
v (nm/s)	30	60	90	120	150	180	210	240
T_{eff}(K)	700	800	900	1000	1100	1200	1300	1400

Table 5.4: Energy Landscape parameters used for the studying the effect of probe approach speed. The last two columns show the probe approach speed and the optimal tip effective temperatures required to accurately reconstruct the energy landscape.

The speed of the biasing probe limits the number of samples obtained in a given time, and hence is a direct contributor to the energy landscape reconstruction error. The effect of probe speed on reconstruction is studied by keeping the energy landscape parameters fixed and varying the probe speeds in 30 nm/s increments from 30 nm/s to 240 nm/s (Table 5.4). The force curves are simulated using a cantilever of stiffness 0.150 pN/nm which sweeps the energy landscape from -60 nm to 60 nm (Fig. 5.6A). Fig. 5.6B and 5.6C show the force curves and corresponding energy reconstructions, respectively for different tip effective temperatures when the cantilever is moved across the energy surface at a speed of 120nm/s. Based on computed RMSE values with respect to the energy model, the optimal sampling temperature for this probe speed is 1000 K (highlighted in the green box). RMSE values are then computed for all probe speeds at each effective temperature in 100 K increments (Fig. 5.6D). This allowed us to obtain the optimal effective temperature for each probe speed (Fig. 5.6E).

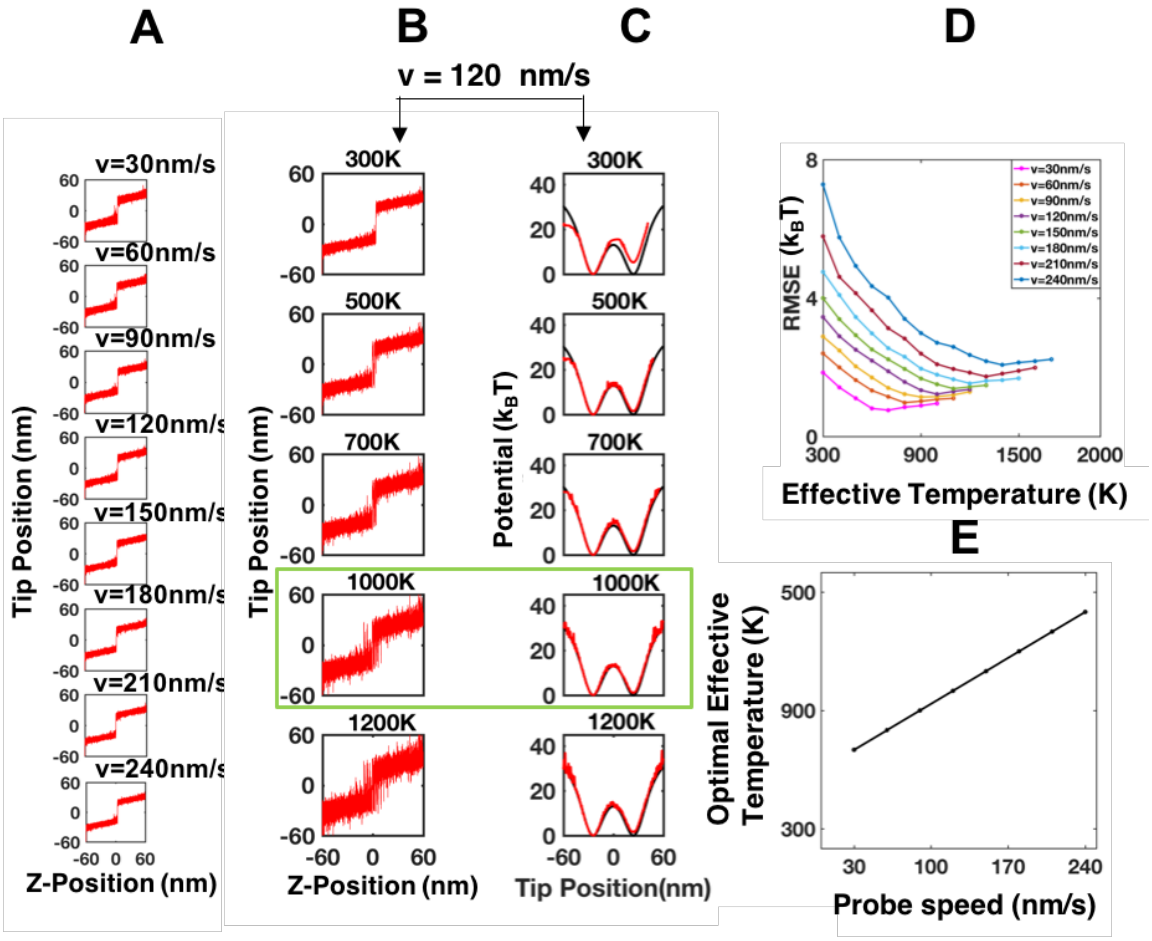

Figure 5.6A. Brownian dynamics simulated force curves at 300K for 8 different probe speeds. **B.** Force curves simulated at different tip effective temperatures when the probe speed is 120 nm/s **C.** Corresponding energy reconstructions (red color) and the underlying energy surface (black color) for each effective temperature. **D.** RMSE of energy reconstructions for different probe speeds plotted versus tip effective temperature. **E.** A plot of the optimal effective temperature versus the probe speeds reflects a linear trend of temperatures needed to accurately reconstruct energy landscapes with different probe speeds.

5.4.5. Global Choice of Parameters: Until now, by fixing all but one parameter, we studied the effect of variation of individual parameters on the accuracy of energy landscape

reconstructions. However, during an actual experiment when all the parameters are unknown, the experimentalist needs some guidance for selecting the initial values of these parameters, so that the energy landscape is sufficiently sampled. Fortunately, the conclusions drawn from simulations of individual parameters can be applied globally to determine the choice of probe parameters for a given energy landscape. To begin with, we should identify the noise level of the AFM or similar single molecule interaction measurement instrument. Then we should select the stiffest available cantilever as long as its deflection sensitivity exceeds the instrument noise level, thereby enabling us to resolve subtle changes in probe's deflections. Subsequently, we should move the probe towards the surface at the lowest sustainable speed. Typically, the approach speed is limited by the instrument drift and very slow approach speeds can place extraordinary demands on the instrument and the sample's stability. If we have knowledge of the underlying energy surface which is being sampled, such as its barrier height and curvature, it is possible to narrow down the choices for the probe parameters. For example, knowing the energy barrier curvature narrows down the choice of probe stiffnesses equal to or just greater than the double gradient of the barrier curvature. This ensures that the probe will not enter into an unstable regime where it could snap onto the surface. Once these initial probe parameters are chosen, we can begin the experiments knowing that we have maximized the sampling capability of the probe without any excitation. Further sampling enhancements can be achieved by supplying stochastic excitation to the probe according to the trends provided by the optimum effective temperature vs. the individual parameter plots, created using Brownian dynamics simulations.

5.4.6. Experimental Validation with AFM Measurements: The effect of probe speed on the quality of energy landscape sampling is verified in an AFM experiment where we measured the adhesive energy landscape of Si_3N_4-mica system with the help of white noise driven iDrive cantilevers. The white noise excitation is used to raise the cantilever tip's effective temperature $T_{effective}$ and its value is determined by the amplification of the tip's fluctuations as compared to those with no excitation at 300K (Eq. 5.5)

$$T_{effective} = \left(\frac{sd_{noise}}{sd_{300}}\right)^2 \times 300 \qquad [5.5]$$

where sd corresponds to standard deviation of the tip's fluctuations measured when it is far from the surface. The value of sd is governed by magnitude of voltage of the externally applied white noise signal.

We recorded slow approach force curves at 4 different voltages of 3, 4, 5 and 6 V choosing a range of probe approach speeds at each voltage, and used WHAM techniques to reconstruct their underlying tip-sample interaction energy landscapes. The corresponding effective temperatures at these voltages are 830 K, 1120 K, 1573 K and 2194 K. During the experiment, the speeds were varied continuously from 396 pm/s to 1196 pm/s. To discretize the approach speeds, we used a K-means clustering approach to partition the speed data into K=4 clusters and used the squared Euclidean distance measure to obtain the cluster centers [218, 219]. K-means was implemented using inbuilt MATLAB software functions (MathWorks Inc., Natick, MA). These cluster centers are located at 488.8, 629, 814.6 and 1155 pm/s and correspond to 4 discrete levels of approach speeds (Fig. 5.7).

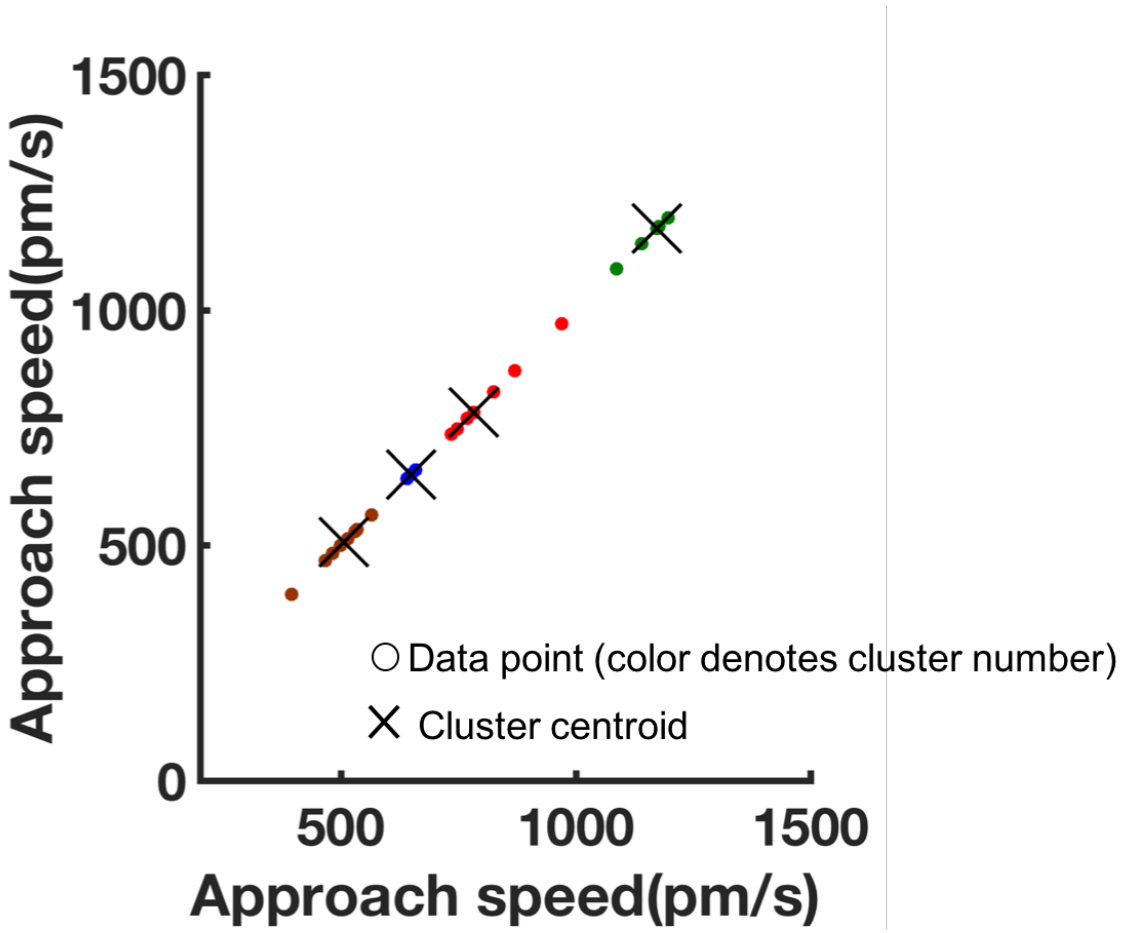

Figure 5.7. 2D graphical representation of the K-means approach used to partition the approach speed data set. The actual data points are denoted by the circle, and the color of the circle denotes belongingness of data points to a specific cluster. The location of the cluster centroid is denoted by X.

Fig. 5.8A shows representative approach force curves collected at each of the 4 voltages and 5.8B shows their energy reconstructions at an approach speed of 629 pm/s. To quantify the error in energy reconstruction estimations, the correct magnitude of average tip sample interaction energy (ΔG_{model}) needs to be estimated, which is done by fitting the retraction force data collected at no excitation to the Friddle-Noy-de Yoreo

model (Fig. 5.8C). ΔG_{model} is found to be 188.20 k_bT. Finally, error in energy reconstruction is estimated for each approach velocity by subtracting the peak value of reconstruction estimates from ΔG_{model} (Fig. 5.8D). From 5.8D, we see that low reconstruction errors correspond to slower approach speeds and one needs to increase the excitation level in order to reduce reconstruction error at high approach speeds. Fig. 5.8D also shows that there exists an optimal excitation level for each approach speed, at which it is best possible to sample the energy landscape. Fig. 5.8E plots these optimal tip effective temperatures as a function of the probe approach speeds and the near-linear trend agrees with those predicted by our simulations.

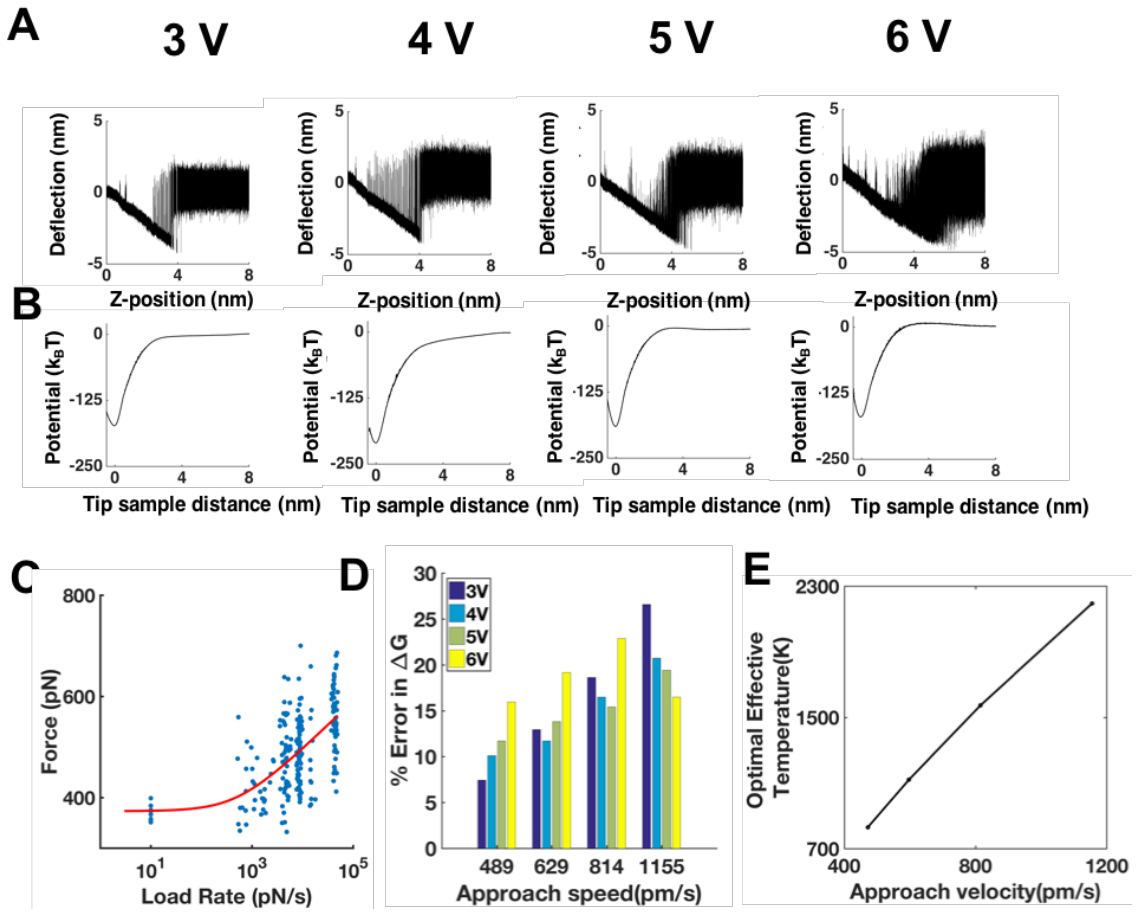

Figure 5.8A. Force curves of a Si_3N_4 AFM tip approaching a mica surface at a constant velocity of 629 pm/s at four different excitations levels of 3, 4, 5 and 6 V. **B.** Corresponding energy reconstructions of the force curves collected above. **C.** Friddle-Noy-deYoreo model used to estimate the tip sample interaction energy (ΔG_{model}) from retraction force versus load rate data. **D.** Comparison of the peak reconstructed energy value with that of ΔG_{model} is used to estimate errors in reconstructions for all voltages at different approach speeds. **E.** Plot of optimal effective temperature for each probe speed depicts a nearly linear trend, and is similar to what was observed in Langevin simulations.

5.5 Conclusions

We have used Brownian dynamics computer simulations to study the effect of different well barrier parameters and probe dynamics on the quality of sampling of energy surfaces by an AFM tip. The energy surface chosen for this study is a symmetric profile containing two overlapping Lorentzian wells. Even though some realistic energy landscapes may not be symmetric, the chosen symmetric energy profile can be used to simulate some conditions obtained in non-symmetric profiles. For e.g., many realistic bimodal energy landscapes have wells with unequal depths. However, it was found that the reconstruction of bimodal energy surfaces depends on the probe's ability to spontaneously hop between the wells, rather than the actual depth of the wells. Thus the important parameter is the height of the barrier separating the wells, which, for a symmetric energy landscape, can be varied by moving the location of the wells (controlled by parameter μ) in a symmetric energy profile. It should also be noted that the reconstruction accuracy strongly depends on the initial conditions, such as the direction of approach. Thus reconstructions for a non-symmetric energy surface from opposite directions would yield

different results. The effect of approach direction on energy landscape reconstruction would be an interesting subject of future studies important to understanding metastable binding states.

The sampling errors are quantified by calculating the errors in reconstructions of the underlying energy landscapes. Building upon our previous work, we have then proposed a method to improve the reconstructions by raising the AFM tip's effective temperature by driving it with an external white noise signal generator. The external noise can be interpreted as a thermal bath which is strongly coupled to the tip and not to the sample or the solvent medium. Raising the effective temperature increases the amplitude of cantilever's thermal fluctuations and increases its sampling range. We have proved that energy reconstructions are indeed improved by increasing the tip's effective temperatures, for each of the four different situations: high well barriers, steep barrier curvatures, and soft probes and fast approach speeds. Furthermore, we have also shown the existence of an optimal effective temperature for every reconstruction, at which point the RMSE is minimized. By computing the optimal effective temperatures for each of the four situations and providing corresponding trends, we have effectively computed a lookup table which can be used by the research community to accurately sample an energy landscape. Finally, we have demonstrated the applicability of our simulations for the case of varying approach speed, through AFM experiments on a Si_3N_4-mica system. We showed that by raising the tip's effective temperature which is achieved through driving the cantilever with white noise, it is possible to overcome the finite sampling limitations encountered in collecting fast approach force curves. We also confirmed the presence of optimal excitation levels for each probe speed as well as their nearly linear relationship with each other. The

understanding derived from this work will be very useful in the addressing the finite sampling issues typically encountered in biological interactions such as ligand-receptor binding and protein folding landscapes, especially those with steep and/or deep energy wells.

CHAPTER 6

CONCLUSIONS AND FUTURE WORK

6.1 Summary

Energy landscapes reconstructed from single molecule force spectroscopy have enjoyed notable success in explaining folding phenomena using the simple physical picture of diffusion over 1D profiles. A generic folding landscape of an interaction plots the free energy against a measure of the molecular configuration, typically called the reaction coordinate. An accurate energy landscape can predict the folding behavior of a molecule, such as the kinetic off rates. Knowledge of the energy landscape allows the discovery of information about the intermediate states, as well as the barrier locations and depths. Intermediate states are responsible for regulating the energy transfer between the bound and unbound states. The data needed for these reconstructions can be collected by a range of probing instruments, the most popular among them being Atomic Force Microscope and Optical Tweezers. Though full energy landscapes have been successfully reconstructed for folding phenomena, the same techniques have not been directly transferable to many adhesion phenomena which exhibit steep binding events, which includes many important ligand-receptor and interfacial systems. Steep binding events limits the amount of information obtained during the transition from bound to unbound states, which limits the accuracy of conventional Boltzmann weighted direct reconstruction methods. Other indirect techniques for estimating the energy landscapes in adhesion measurements, such as force integration or dynamic force spectroscopy measurements can only partially recreate the energy landscapes. In this thesis, we have fully reconstructed the energy

landscapes of these difficult-to-sample steep adhesive interactions, by developing an enhanced stochastic excitation technique and combining it with the Boltzmann transformation and the weighted histogram analysis method.

In this work, we have measured adhesion energy landscapes of both biological and interfacial interactions via direct equilibrium measurements using an atomic force microscope. Specifically, scientific contributions of this work are:

(i) Applied and validated a new weighted histogram analysis method (WHAM) which minimized errors of combining locally estimated Boltzmann energies to more accurately reconstruct energy landscapes of ligand receptor interactions across the entire reaction coordinate;

(ii) Demonstrated that an enhanced stochastic sampling technique can greatly improve the accuracy of reconstructions of steep adhesive energy landscapes; and

(iii) Investigated the entire parameter space of the factors affecting energy landscape sampling to identify the optimal values that maximize landscape reconstruction accuracy.

To sample interaction energy landscapes, we utilized the Brownian fluctuations of a microcantilever probe which is then brought into close proximity to the interaction potential of substrate surface. By recording the variations in fluctuations of the cantilever as it passes close to the substrate surface, the free energy landscape was reconstructed through a transformation of Boltzmann's equation. Adhesive energy landscapes contain

large energy barriers along the reaction coordinate, which prevented an accurate sampling of the interaction. When the cantilever tip encountered such large barriers, the cantilever spring's restoring force was unable to compensate for the high attractive force gradients of these barriers and it underwent a free fall movement unconstrained by the underlying energy landscape. As a result, the actual barrier itself was poorly sampled. To address this issue, we combined the Boltzmann technique with an umbrella sampling approach. In umbrella sampling, a biasing potential was superimposed on the interaction potential, which served to confine the movement of the cantilever tip within the funnel of the umbrella. This helped to achieve a more efficient sampling at the bottom of the funnel close to the cantilever's equilibrium position. The funnel protects the cantilever tip from jumping onto the surface even when it is close to a region of steep energy gradient, by restricting the natural unconstrained movement of the tip. This allows for very accurate sampling of regions very close to jump-ins, which would otherwise not have been possible. In the AFM, the biasing was naturally provided by the cantilever in the form of a harmonic potential. Because the sampling was confined to a small region within a single umbrella funnel, only a small piece of the free energy was accurately estimated. The z-piezo movement of the cantilever created many such equally spaced umbrellas across the entire reaction coordinate, through which multiple small pieces of free energy of the landscape were computed accurately. These small pieces of accurately estimated free energies were combined using weighted histogram (WHAM) techniques to obtain the entire free energy landscape.

Using the above mentioned methods, we reconstructed energy landscapes of ligand-receptor binding interactions (biotin-avidin system) using Brownian fluctuations of

an AFM microcantilever probe decorated with the ligand which approached a receptor molecules coated surface. Furthermore, we were able to experimentally determine an intermediate attractive energy well of biotin-avidin binding, which was only known previously through computational simulations. The energy landscape qualitatively resembled those obtained through computational simulation as biotin initially binds to an avidin loop followed by binding to beta-barrel residues. The specificity of binding was confirmed through higher pull off forces in retraction force experiments. The energy landscapes of biomolecules will be critical to the optimal design of biosensors such as by improving antibody specificity in recognition targeting, and will also provide a direct test to improve computational model potentials for biological interactions. However, even though our reconstructed energy landscapes were qualitatively accurate, the wells were shallower than published values. We hypothesized that insufficient sampling of the well limited our ability to fully reconstruct its depth. As such, slower approach rates or enhanced stochastic excitations will aid in probing more of the rare binding pathways that correspond to deeper potential wells of biotin-avidin interactions.

In the second part of the dissertation, we addressed the problems encountered in probing of energy landscapes with sharp transitions between states that leads to infrequent sampling of the transition state. A key limitation of reconstruction methods is their inability to map the complete interaction in the presence of attractive forces with gradients greater than the cantilever stiffness, which produces a rapid snap-in instability of the tip position. This is particularly a problem at small surface separations in which the attractive forces between tip and sample may exceed this value and cause the tip to snap to the surface or biomolecule. We proposed a method whereby it is possible to overcome limited transition

region sampling by increasing the sampling range of the cantilever vibrations through white noise excitation. Enhancing the vibrational noise of cantilevers increases the transient sampling of regions of large attractive interactions in which the cantilever is of a sufficient distance from the high gradient region such that the restoring force of the cantilever avoids jump to surface instabilities. We demonstrated this method via direct mapping of interfacial free-energies of Si_3N_4-mica interactions using enhanced thermal fluctuations and the Boltzmann sampling method. For this purpose, iDrive cantilevers were used which were driven with white noise signals of different voltages. Other methods such as piezoelectric [83], magnetic [220] or thermal actuation [221] techniques can also employed. Reconstructions were performed at voltages ranging from 0 through 7 V, and their accuracy compared with a Friddle-Noy-deYoreo model fit to the retraction force data collected at 0 V. Analysis of the energy landscape revealed that there exists an optimum excitation voltage (or optimum effective temperature) which corresponds to a maximum landscape reconstruction accuracy. This method holds great promise in the investigation of biological interactions such as ligand-receptor binding and protein folding landscapes, especially those with steep and/or deep energy wells.

In the third part of the dissertation, we built upon our work of improving energy reconstructions via enhanced stochastic excitations and explored the parameter space to optimize successful application of this method. In particular, we studied the influence of energy barrier height, barrier curvature, probe stiffness and probe speed on the energy reconstruction accuracy. We performed Brownian dynamics computer simulations on a Lorentzian bimodal energy landscape model, to study the effect of these parameters on the landscape sampling quality and quantified the errors in energy reconstructions using root

mean square errors. For each of the parameters, we also determined the optimal effective temperatures at which bias in reconstruction estimates are minimized. We also demonstrated the applicability of our simulations for the case of varying approach speed, through AFM experiments on a Si_3N_4-mica system. We showed that by raising the AFM cantilever tip's effective temperature which is achieved through driving the cantilever with white noise, it is possible to decrease the error in reconstruction estimates. We also confirmed the presence of optimal excitation levels for each probe speed.

5.4 Future Work

Other factors of AFM based energy reconstruction techniques not addressed in this study include the ability to covalently bind ligands to cantilever tips, cantilever drift limitations and finite sampling time at current data collection rates and possibly, complex tip sample interaction dynamics at the nanoscale levels. Even though addressing all these factors are very important in producing better measurements for energy reconstructions, we propose the following four as the logical next steps as the future directions for this research.

6.2.1. Full Energy Landscape Reconstructions of Biotin-Avidin Binding

Through application of Brownian fluctuation technique, we were able to sample the attractive energy landscape of biotin-avidin interactions. Even though our method was able to discriminate between the two attractive wells, we could not fully reconstruct the attractive binding wells due to limited sampling of the rare binding events. With the aid of subsequently developed enhanced stochastic excitation approach, we propose to revisit the biotin-avidin interaction with the aim of accurately reconstructing their binding energy landscapes both quantitatively and qualitatively.

6.2.2. Addressing the Sampling Time Limitations

The energy reconstruction method requires a substantial sampling (100,000+ samples) in proximity to the potential well, to reproduce the underlying energy surface. Therefore, methods analogous to force clamps, which will allow us to hover the cantilever at a fixed distance will substantially improve the recording of subtle variations of rare binding states. The tip-surface distance can be controlled by monitoring the cantilever quality factor (Q) in a closed feedback loop [222]. The determination of Q is done by fitting the thermal noise (Brownian fluctuations) of the tip to a Lorentzian function. In order for this technique to be applied in real time for strong tip surface interactions, Q determination and subsequent feedback signal to the tip needs to be extremely fast. Better signal processing techniques are great step in achieving this goal. Utilizing this method to hover the tip above a sample surface, we will be able to study slow protein folding-unfolding mechanisms, which exhibit slow conformational changes, over long periods of time.

6.2.3. Developing a Model for Determining Errors in Equilibrium Energy Measurements

Free energy reconstructions can obtain key information about an interaction, such as the reaction mechanisms or its rates. However, finite sampling errors are an intrinsic part of free energy measurement and can be an even more critical part of the analysis. In WHAM, free energies are computed by direct iteration of a set of coupled equations until self-consistency is achieved. In order to achieve self-consistency, substantial sampling of the landscape is required and failure to do so results in errors in WHAM free energy estimates. We proposed a method to reduce this error by increasing the landscape sampling via increase in cantilever tip's effective temperature, and used Brownian dynamics

simulations to show the existence of optimal effective temperature for different landscape and probe parameters. While simulations are a good tool to study the effect of a given parameter space on the optimal effective temperature, complicated energy landscapes can make it difficult to replicate experimental conditions owing to run time limitations. In this context, development of a theoretical model that explores the effect of these parameters would be ideal. The model will also be very useful to researchers who want to utilize the stochastic excitation method to sample an energy landscape, but are unsure as to what amount of excitation is ideal in their particular situation. Though computer simulations can provide the answer, they can be computationally expensive, depending the energetics that are being simulated.

6.2.4: **Application in Antibody Sampling:** Understanding the local minima in energy landscapes, both energy depth and extent along the reaction coordinate, will allow us to assess the multiple binding pathways that are available to the molecule to take before it binds to a complementary molecule or a substrate, resulting in better control over the rate of these binding processes [11]. As an example, these metastable states are known to play an important part in determining the specificity of antibodies in antigen recognition [12]. Since antibodies bind their specific antigen target with such high affinity (deep energy well), once locked into position they are effectively irreversible. However, finding this target requires reversible binding with many more non-target sites of binding. Identifying the conformational changes that may occur during induced fit can be a critical step in the molecular proofreading process, which can only be accurately quantified through an energy landscape [13, 14].

Addressing the first objective will enable us to complete our initial aim of full landscape reconstruction of ligand-receptor interactions. The following two objectives will complement the equilibrium energy reconstruction methods developed in this dissertation, and the final objective proposes an application which highlights the importance of accurate determination of energy landscapes.

Other than these immediate future directions, one can also look into other ways to increase the sampling of rare events leading to full energy landscape reconstructions. For example, the use of colored noise instead of white noise, or more complex drive mechanisms can be also used to bias the sampling in a useful manner. The advantage of using colored noise, which is characterized by non-uniform spectral power densities, is that they are better tuned for applications which operate within certain frequency limits or have spectrally dependent power requirements. On the other hand, complex drive mechanisms such as a multifrequency sweeping can be used to identify the ideal frequency to maximally excite the cantilever. In this context, band excitation method, developed by Jesse et al. [223] for broadband scanning probe microscopy imaging can be very useful. In band excitation, the probe is excited using a synthesized digital signal that spans a continuous band of frequencies, and the response is monitored within the same or a larger frequency band. The cantilever response is detected using high speed data acquisition hardware and then Fourier transformed. This Fourier transformed data is analyzed to extract relevant parameters of the cantilever behavior; in this case, the frequency ranges for maximum amplitude of oscillations. The tip can also be moved along the energy landscape, and corresponding frequencies of maximum excitation recorded for each tip position. Once the ideal frequency ranges are collected for the entire tip sample movement, the tip is then

vibrated at these chosen specific frequencies in order maximize the sampling range of the cantilever at each tip position. While this method promises to be quite useful for enhanced sampling, it requires signficant computational resources in order to perform real-time Fourier transformations and inverse Fourier transformations of the signal at each frequency at each tip sample distance.

The energy reconstruction techniques developed in this thesis promise to be very useful in the studying a wide variety of complicated energy landscapes with multiple barriers, be it biological phenomena such as ligand receptor binding or steep adhesive energy barriers seen in chemical interactions.

APPENDIX A: Brownian Reconstruction Routines

These routines have been written in MATLAB software (Mathworks Inc., Natick, MA)

```
% Main code
clear all;
T=300; % change to effective temperature
constraint_stiffness=90; %pN/nm (this is probe stiffness)
% change the following two values to the ranges of force curves that
are being studied
xmin=-2;
xmax=25;
txt_file_name_defl = 'defl_2_0V_pH3.txt'; % text data is in nm (change
to file name)
txt_file_name_pos = 'zpiezo_2_0V_pH3.txt'; % text data is in nm (change
to file name)

%% read text file data (can use flipud() to flip up to down)
master_afm_defl=table2array(readtable(txt_file_name_defl)); % nm
master_afm_pos=table2array(readtable(txt_file_name_pos)); % nm
afm_defl=master_afm_defl(1:end);
afm_pos=master_afm_pos(1:end);
% cut off data to the range desired
bool=afm_pos<xmax & afm_pos>xmin;
afm_pos=afm_pos(bool);
afm_defl=afm_defl(bool);
afm_tsd_raw=afm_defl+afm_pos;

%% Brownian parameters
windowSize=2000;
binWidth=0.01;%nm
numBins=floor(range(afm_tsd_raw)/binWidth);
numWindows=floor(length(afm_tsd_raw)/windowSize);

%% divide the data into windows
afm_defl=afm_defl(1:numWindows*windowSize);
afm_pos=afm_pos(1:numWindows*windowSize);
afm_tsd=afm_defl+afm_pos;

%% Generate matrices for WHAM analysis
for i=1:numWindows
    x_data(i,:)=afm_tsd((i-1)*windowSize+1:i*windowSize); % convert um
to nm for input to WHAM.m
    x_constraint(i)=mean(afm_pos((i-1)*windowSize+1:i*windowSize)); %
convert um to nm for input to WHAM.m
end

%% Call WHAM.m
[rp,sp,std_ts]=WHAM(x_data,x_constraint',constraint_stiffness,numBins,T
);
removed_energy=(rp==Inf);
sp(removed_energy)=[];
rp(removed_energy)=[];
rp=rp*T/300; % normalized to 300K if effective temperature was used
```

```
rp=rp-rp(end);

%% Plot the data
figure('units','normalized','outerposition',[0 0 1 1]);
fig1=figure(1); % plot potential data
plot(sp,rp,'red','LineWidth',2);
axis square;
xlim([xmin xmax]);
set(gca,'FontSize',50.4,'FontWeight','Bold','LineWidth',5);
ylabel('Potential(k_bT)','FontSize',50.4,'FontWeight','Bold');
xlabel('Tip sample distance(nm)','FontSize',50.4,'FontWeight','Bold');


% ----
% WHAM
% ----

% Parameters
% Xs:      a WxS matrix containing X coordinate values,
%          where W is the window and S is the step
% Bxs:     a Wx1 vector containing the location of the
%          umbrella window centers.
% ks:      probe stiffness in pN/nm
% num_bins:number of bins
% T       : effective temperature

% Outputs
% rU:      the PMF
% xspace:  a 1xB vector marking the edges of the bins along X,
%          where B is the number of bins
%
function [rU,xspace] = WHAM(Xs,Bxs,ks,num_bins,T)
KbT = 1.3806503E-2*T;     %%% energy unit, (pN nm)

%%% Default range for X
xspace = linspace(min(Xs(1:end)),max(Xs(1:end)),num_bins);
xsp = xspace(2)-xspace(1);


steps = size(Xs(1:end),2);  %%% total number of data points
numsims = size(Bxs,1);      %%% number of windows
numbins = size(xspace,2);   %%% number of bins

%%% Histograms of data
Hx_counts = histc(Xs',xspace);
Hx = histc(Xs',xspace)/steps;

%%% WHAM variables
Fx_old = zeros(1,numsims);   %%% Free energy constants Fx_i
Px = zeros(1,numbins);       %%% Probabilities from equation (8)

%%% Variables tracking the progress of change
Fprog = [];
iter = 0;
change = 0.05;
```

```
%%% WHAM iterations
while change > 0.001
    numPx = zeros(1,numbins);
    denPx = zeros(1,numbins);
    Px = zeros(1,numbins);
    Fx = zeros(1,numsims);

    %%% Calculate probabilities from free energies
    for sim = 1:numsims
        numPx = numPx + Hx(:,sim)';
        Ubias = 0.5*ks*((Bxs(sim)-(xspace+xsp/2)).^2);
        denPx = denPx + sum(Hx(:,sim))*exp((Fx_old(sim)-Ubias)/KbT);
    end
    Px = numPx./denPx;
    for sim = 1:numsims
        Ubias = 0.5*ks*((Bxs(sim)-(xspace+xsp/2)).^2);
        Fx(sim) = sum(Px.*exp(-Ubias/KbT));
    end
    Fx = -KbT*log(Fx);
    Fx(2:end) = Fx(2:end)-Fx(1);

    Fx_old = Fx;

    %%% Measure change in free energy constants
    Fprog = [Fprog; Fx];
    if iter > 2
        change = max(abs((Fprog(end-1,2:end)-Fprog(end,2:end))));
    end
    iter = iter + 1;
end

%%% Set minima to zero
rU = -log(Px);
rU = rU - min(rU(1:end));
end
```

References

[1] M. T. Woodside and S. M. Block, "Reconstructing folding energy landscapes by single-molecule force spectroscopy," *Annu Rev Biophys,* vol. 43, pp. 19-39, 2014.

[2] P. Hanggi, P. Talkner, and M. Borkovec, "Reaction-Rate Theory: Fifty Years After Kramers," *Rev. Mod. Phys.,* vol. 62, 1990.

[3] R. Merkel, P. Nassoy, A. Leung, K. Ritchie, and E. Evans, "Energy landscapes of receptor-ligand bonds explored with dynamic force spectroscopy," *Nature,* vol. 397, pp. 50-3, Jan 7 1999.

[4] K. A. Dill, S. B. Ozkan, M. S. Shell, and T. R. Weikl, "The protein folding problem," *Annu Rev Biophys,* vol. 37, pp. 289-316, 2008.

[5] J. N. Onuchic and P. G. Wolynes, "Theory of protein folding," *Curr Opin Struct Biol,* vol. 14, pp. 70-5, Feb 2004.

[6] D. Thirumalai and C. Hyeon, "RNA and protein folding: common themes and variations," *Biochemistry,* vol. 44, pp. 4957-70, Apr 5 2005.

[7] X. Chu and J. Wang, "Specificity and affinity quantification of flexible recognition from underlying energy landscape topography," *PLoS Comput Biol,* vol. 10, p. e1003782, Aug 2014.

[8] T. Jostock, M. Vanhove, E. Brepoels, R. Van Gool, M. Daukandt, A. Wehnert*, et al.*, "Rapid generation of functional human IgG antibodies derived from Fab-on-phage display libraries," *J Immunol Methods,* vol. 289, pp. 65-80, Jun 2004.

[9] W. Zheng, N. P. Schafer, A. Davtyan, G. A. Papoian, and P. G. Wolynes, "Predictive energy landscapes for protein-protein association," *Proc Natl Acad Sci U S A,* vol. 109, pp. 19244-9, Nov 20 2012.

[10] J. Simons, "Roles Played by Metastable States in Chemistry," in *ACS Symposium Series*, Washington DC, 1984.

[11] Y. Levy, S. S. Cho, J. N. Onuchic, and P. G. Wolynes, "A survey of flexible protein binding mechanisms and their transition states using native topology based energy landscapes," *J Mol Biol,* vol. 346, pp. 1121-45, Mar 4 2005.

[12] P. Kaur, Qiang-Fu, A. Fuhrmann, R. Ros, L. O. Kutner, L. A. Schneeweis*, et al.*, "Antibody-Unfolding and Metastable-State Binding in Force Spectroscopy and Recognition Imaging," *Biophysical Journal,* vol. 100, pp. 243-250, Jan 5 2011.

[13] D. D. Boehr, R. Nussinov, and P. E. Wright, "The role of dynamic conformational ensembles in biomolecular recognition," *Nat Chem Biol,* vol. 5, pp. 789-96, Nov 2009.

[14] L. C. James and D. S. Tawfik, "Conformational diversity and protein evolution--a 60-year-old hypothesis revisited," *Trends Biochem Sci,* vol. 28, pp. 361-8, Jul 2003.

[15] A. Bachmann and T. Kiefhaber, *Kinetic Mechanisms in Protein Folding, in Protein Folding Handbook* Weinheim, Germany: Wiley-VCH Verlag GmbH, 2008.

[16] A. Engel and D. J. Muller, "Observing single biomolecules at work with the atomic force microscope," *Nat Struct Biol,* vol. 7, pp. 715-8, Sep 2000.

[17] K. C. Neuman and S. M. Block, "Optical trapping," *Rev Sci Instrum,* vol. 75, pp. 2787-809, Sep 2004.

[18] U. Mayor, C. M. Johnson, V. Daggett, and A. R. Fersht, "Protein folding and unfolding in microseconds to nanoseconds by experiment and simulation," *Proc Natl Acad Sci U S A,* vol. 97, pp. 13518-22, Dec 5 2000.

[19] O. V. Galzitskaya and A. V. Finkelstein, "A theoretical search for folding/unfolding nuclei in three-dimensional protein structures," *Proc Natl Acad Sci U S A,* vol. 96, pp. 11299-304, Sep 28 1999.

[20] R. B. Best, B. Li, A. Steward, V. Daggett, and J. Clarke, "Can non-mechanical proteins withstand force? Stretching barnase by atomic force microscopy and molecular dynamics simulation," *Biophys J,* vol. 81, pp. 2344-56, Oct 2001.

[21] Y. Wei and R. A. Latour, "Determination of the adsorption free energy for peptide-surface interactions by SPR spectroscopy," *Langmuir,* vol. 24, pp. 6721-9, Jun 1 2008.

[22] E. Evans and K. Ritchie, "Dynamic strength of molecular adhesion bonds," *Biophys J,* vol. 72, pp. 1541-55, Apr 1997.

[23] G. I. Bell, "Models for the specific adhesion of cells to cells," *Science,* vol. 200, pp. 618-27, May 12 1978.

[24] F. Schwesinger, R. Ros, T. Strunz, D. Anselmetti, H. J. Guntherodt, A. Honegger*, et al.*, "Unbinding forces of single antibody-antigen complexes correlate with their thermal dissociation rates," *Proc Natl Acad Sci U S A,* vol. 97, pp. 9972-7, Aug 29 2000.

[25] J. Morfill, K. Blank, C. Zahnd, B. Luginbuhl, F. Kuhner, K. E. Gottschalk*, et al.*, "Affinity-matured recombinant antibody fragments analyzed by single-molecule force spectroscopy," *Biophys J,* vol. 93, pp. 3583-90, Nov 15 2007.

[26] T. A. Sulchek, R. W. Friddle, K. Langry, E. Y. Lau, H. Albrecht, T. V. Ratto*, et al.*, "Dynamic force spectroscopy of parallel individual Mucin1-antibody bonds," *Proc Natl Acad Sci U S A,* vol. 102, pp. 16638-43, Nov 15 2005.

[27] C. Ray, J. R. Brown, and B. B. Akhremitchev, "Rupture force analysis and the associated systematic errors in force spectroscopy by AFM," *Langmuir,* vol. 23, pp. 6076-83, May 22 2007.

[28] Z. N. Scholl and P. E. Marszalek, "Improving single molecule force spectroscopy through automated real-time data collection and quantification of experimental conditions," *Ultramicroscopy,* vol. 136, pp. 7-14, Jan 2014.

[29] H. A. Kramers, "Brownian Motion in a Field of Force and the Diffusion Model of Chemical Reactions," *Physica,* vol. 7, pp. 284-304, 1940.

[30] H. Yu, X. Liu, K. Neupane, A. N. Gupta, A. M. Brigley, A. Solanki*, et al.*, "Direct observation of multiple misfolding pathways in a single prion protein molecule," *Proc Natl Acad Sci U S A,* vol. 109, pp. 5283-8, Apr 3 2012.

[31] V. K. Shubin, P. J. , "Electrical Double Layer Structure Revisited via a Surface Force Apparatus: Mica Interfaces in Lithium Nitrate Solutions," *Colloid Interface Sci.,* vol. 155, pp. 108-123, 1993.

[32] D. O. H. Koralek, W.F.; Antonik, M.D.; Baik, A., "Probing deep interaction potentials with white-noise-driven atomic force microscope cantilevers," *App. Phys. Lett.,* vol. 76, pp. 2952-2954, 2000.

[33] H. Frauenfelder, S. G. Sligar, and P. G. Wolynes, "The energy landscapes and motions of proteins," *Science,* vol. 254, pp. 1598-603, Dec 13 1991.

[34] P. J. Steinbach, A. Ansari, J. Berendzen, D. Braunstein, K. Chu, B. R. Cowen*, et al.*, "Ligand binding to heme proteins: connection between dynamics and function," *Biochemistry,* vol. 30, pp. 3988-4001, Apr 23 1991.

[35] A. R. Fersht and E. I. Shakhnovich, "Protein folding: think globally, (inter)act locally," *Curr Biol,* vol. 8, pp. R478-9, Jul 2 1998.

[36] A. P. Ben-Zvi, J. Chatellier, A. R. Fersht, and P. Goloubinoff, "Minimal and optimal mechanisms for GroE-mediated protein folding," *Proc Natl Acad Sci U S A,* vol. 95, pp. 15275-80, Dec 22 1998.

[37] V. Munoz and W. A. Eaton, "A simple model for calculating the kinetics of protein folding from three-dimensional structures," *Proc Natl Acad Sci U S A,* vol. 96, pp. 11311-6, Sep 28 1999.

[38] P. G. Wolynes, J. N. Onuchic, and D. Thirumalai, "Navigating the folding routes," *Science,* vol. 267, pp. 1619-20, Mar 17 1995.

[39] J. Wang and P. Wolynes, "Intermittency of single molecule reaction dynamics in fluctuating environments," *Phys Rev Lett,* vol. 74, pp. 4317-4320, May 22 1995.

[40] K. A. Dill and H. S. Chan, "From Levinthal to pathways to funnels," *Nat Struct Biol,* vol. 4, pp. 10-9, Jan 1997.

[41] C. B. Anfinsen, E. Haber, M. Sela, and F. H. White, Jr., "The kinetics of formation of native ribonuclease during oxidation of the reduced polypeptide chain," *Proc Natl Acad Sci U S A,* vol. 47, pp. 1309-14, Sep 15 1961.

[42] C. B. Anfinsen, "Principles that govern the folding of protein chains," *Science,* vol. 181, pp. 223-30, Jul 20 1973.

[43] W. Kauzmann, "Some factors in the interpretation of protein denaturation," *Adv Protein Chem,* vol. 14, pp. 1-63, 1959.

[44] D. Poland and H. A. Scheraga, *Theory of Helix-Coil Transitions in Biopolymers; Statistical Mechanical Theory of Order-Disorder Transitions in Biological Macromolecules*. New York: Academic Press, 1970.

[45] G. Kikugawa, R. Apostolov, N. Kamiya, M. Taiji, R. Himeno, H. Nakamura*, et al.*, "Application of MDGRAPE-3, a special purpose board for molecular dynamics simulations, to periodic biomolecular systems," *J Comput Chem,* vol. 30, pp. 110-8, Jan 15 2009.

[46] M. Shirts and V. S. Pande, "COMPUTING: Screen Savers of the World Unite!," *Science,* vol. 290, pp. 1903-4, Dec 8 2000.

[47] K. Lindorff-Larsen, S. Piana, R. O. Dror, and D. E. Shaw, "How fast-folding proteins fold," *Science,* vol. 334, pp. 517-20, Oct 28 2011.

[48] M. Karplus and J. A. McCammon, "Molecular dynamics simulations of biomolecules," *Nat Struct Biol,* vol. 9, pp. 646-52, Sep 2002.

[49] E. Evans, D. Berk, and A. Leung, "Detachment of agglutinin-bonded red blood cells. I. Forces to rupture molecular-point attachments," *Biophys J,* vol. 59, pp. 838-48, Apr 1991.

[50] E. Evans, *Physical Actions in Biological Adhesion* vol. 1. Amsterdam: Elsevier, 1991.

[51] E. Evans, R. Merkel, K. Ritchie, S. Tha, and A. Zilker, "Picoforce Method to Probe Submicroscopic Actions in Biomembrane Adhesion," in *Studying Cell Adhesion*, ed Berlin: Springer Berlin Heidelberg, 1994, pp. 125-139.

[52] E. Evans, K. Ritchie, and R. Merkel, "Sensitive force technique to probe molecular adhesion and structural linkages at biological interfaces," *Biophys J,* vol. 68, pp. 2580-7, Jun 1995.

[53] J. D. Bryngelson and P. G. Wolynes, "Spin glasses and the statistical mechanics of protein folding," *Proc Natl Acad Sci U S A,* vol. 84, pp. 7524-8, Nov 1987.

[54] J. D. Bryngelson and P. Wolynes, "Intermediates and Barrier Crossing in a Random Energy Model (with Applications to Protein Folding)," *J. Phys. Chem.,* vol. 93, pp. 6902-6915, 1989.

[55] J. D. Bryngelson, J. N. Onuchic, N. D. Socci, and P. G. Wolynes, "Funnels, pathways, and the energy landscape of protein folding: a synthesis," *Proteins,* vol. 21, pp. 167-95, Mar 1995.

[56] K. A. Dill and J. L. MacCallum, "The protein-folding problem, 50 years on," *Science,* vol. 338, pp. 1042-6, Nov 23 2012.

[57] J. N. Onuchic, Z. Luthey-Schulten, and P. G. Wolynes, "Theory of protein folding: the energy landscape perspective," *Annu Rev Phys Chem,* vol. 48, pp. 545-600, 1997.

[58] R. L. Rich and D. G. Myszka, "Advances in surface plasmon resonance biosensor analysis," *Curr Opin Biotechnol,* vol. 11, pp. 54-61, Feb 2000.

[59] F. A. Tanious, B. Nguyen, and W. D. Wilson, "Biosensor-Surface Plasmon Resonance Methods for Quantitative Analysis of Biomolecular Interactions," in *Methods in Cell Biology*. vol. 84, ed: Elsevier, 2008.

[60] D. J. O'Shannessy, "Determination of kinetic rate and equilibrium binding constants for macromolecular interactions: a critique of the surface plasmon resonance literature," *Curr Opin Biotechnol,* vol. 5, pp. 65-71, Feb 1994.

[61] I. Jelesarov and H. R. Bosshard, "Isothermal titration calorimetry and differential scanning calorimetry as complementary tools to investigate the energetics of biomolecular recognition," *J Mol Recognit,* vol. 12, pp. 3-18, Jan-Feb 1999.

[62] M. W. Freyer and E. A. Lewis, "Isothermal titration calorimetry: experimental design, data analysis, and probing macromolecule/ligand binding and kinetic interactions," *Methods Cell Biol,* vol. 84, pp. 79-113, 2008.

[63] J. N. Israelachvili and D. Tabor, "The Measurement of Van Der Waals Dispersion Forces in the Range 1.5 to 130 nm," *Proc Royal Soc. A,* vol. 331, pp. 19-38, 1972.

[64] D. Tabor and R. H. Winterton, "Surface forces: direct measurement of normal and retarded van der Waals forces," *Nature,* vol. 219, pp. 1120-1, Sep 14 1968.

[65] E. Evans, "Probing the relation between force--lifetime--and chemistry in single molecular bonds," *Annu Rev Biophys Biomol Struct,* vol. 30, pp. 105-28, 2001.

[66] A. Ashkin and ebrary Inc. (2006). *Optical trapping and manipulation of neutral particles using lasers*.

[67] A. Noy, D. V. Vezenov, and C. M. Lieber, "Chemical Force Microscopy," *Annual Review of Materials Science,* vol. 27, pp. 381-421, 1997.

[68] P. Nassoy, "How Accurate Are Ultrasensitive Biophysical Force Probes?," *Biophys J,* vol. 93, pp. 361-362, 2007.

[69] K. Boye, "Development and Application of the Biomembrane Force Probe Technique," PhD, Dept. of Phys. and Chem., Univ. Southern Denmark, Denmark, 2007.

[70] A. N. Gupta, A. Vincent, K. Neupane, H. Yu, F. Wang, and M. T. Woodside, "Experimental validation of free-energy-landscape reconstruction from non-equilibrium single-molecule force spectroscopy measurements," *Nature Physics,* vol. 7, pp. 631-634, Aug 2011.

[71] M. Capitanio and F. S. Pavone, "Interrogating biology with force: single molecule high-resolution measurements with optical tweezers," *Biophys J,* vol. 105, pp. 1293-303, Sep 17 2013.

[72] V. T. Moy, E. L. Florin, and H. E. Gaub, "Intermolecular forces and energies between ligands and receptors," *Science,* vol. 266, pp. 257-9, Oct 14 1994.

[73] E. L. Florin, V. T. Moy, and H. E. Gaub, "Adhesion forces between individual ligand-receptor pairs," *Science,* vol. 264, pp. 415-7, Apr 15 1994.

[74] C. D. Frisbie, L. F. Rozsnyai, A. Noy, M. S. Wrighton, and C. M. Lieber, "Functional group imaging by chemical force microscopy," *Science,* vol. 265, pp. 2071-4, Sep 30 1994.

[75] P. D. Ashby, L. Chen, and C. M. Lieber, "Probing Intermolecular Forces and Potentials with Magnetic Feedback Chemical Force Microscopy," *J Am Chem Soc,* vol. 122, pp. 9467-9472, 2000.

[76] Y. Lyubchenko, L. Shlyakhtenko, R. Harrington, P. Oden, and S. Lindsay, "Atomic force microscopy of long DNA: imaging in air and under water," *Proc Natl Acad Sci U S A,* vol. 90, pp. 2137-40, Mar 15 1993.

[77] Y. L. Lyubchenko, P. I. Oden, D. Lampner, S. M. Lindsay, and K. A. Dunker, "Atomic force microscopy of DNA and bacteriophage in air, water and propanol: the role of adhesion forces," *Nucleic Acids Res,* vol. 21, pp. 1117-23, Mar 11 1993.

[78] H. Yamashita, A. Taoka, T. Uchihashi, T. Asano, T. Ando, and Y. Fukumori, "Single-Molecule Imaging on Living Bacterial Cell Surface by High-Speed AFM.," *J. Mol. Biol.,* vol. 422, pp. 300-309, 2012.

[79] G. Q. Binnig, C. F.; Gerber, C., ""Atomic-Force Microscope"," *Phys. Rev. Lett.,* vol. 56, pp. 930-933, 1986.

[80] P. D. Ashby and C. M. Lieber, "Brownian force profile reconstruction of interfacial 1-nonanol solvent structure," *J Am Chem Soc,* vol. 126, pp. 16973-80, Dec 29 2004.

[81] H. J. Butt, "Measuring electrostatic, van der Waals, and hydration forces in electrolyte solutions with an atomic force microscope," *Biophys J,* vol. 60, pp. 1438-44, Dec 1991.

[82] Y. Seo and W. Jhe, "Atomic Force Microscopy and Spectroscopy," *Rep. Prog. Phys.,* vol. 71, pp. 016101-016124, 2008.

[83] T. Sulchek, R. Hsieh, J. D. Adams, S. C. Minne, C. F. Quate, and D. M. Adderton, "High-speed atomic force microscopy in liquid," *Review of Scientific Instruments,* vol. 71, pp. 2097-2099, May 2000.

[84] M. L. Bloo, "Deformation and Wear of Pyramidal, Silicon-Nitride AFM Tips Scanning Micrometre-Size Features in Contact Mode," *Measurement,* vol. 25, pp. 203-211, 1999.

[85] H.-J. Butt, B. Cappella, and M. Kappl, "Force Measurements with the Atomic Force Microscope: Technique, Interpretation and Applications," *Surf. Sci. Rep.,* vol. 59, pp. 1-152, 2005.

[86] Y. F. Dufrene, "Atomic force microscopy, a powerful tool in microbiology," *Journal of Bacteriology,* vol. 184, pp. 5205-5213, Oct 2002.

[87] M. B. Viani, T. E. Schaffer, A. Chand, M. Rief, H. E. Gaub, and P. K. Hansma, "Small cantilevers for force spectroscopy of single molecules," *Journal of Applied Physics,* vol. 86, pp. 2258-2262, Aug 15 1999.

[88] A. Noy, S. Zepeda, C. A. Orme, Y. Yeh, and J. J. De Yoreo, "Entropic barriers in nanoscale adhesion studied by variable temperature chemical force microscopy," *J Am Chem Soc,* vol. 125, pp. 1356-62, Feb 5 2003.

[89] S. Zepeda, Y. Yeh, and A. Noy, "Determination of Energy Barriers for Intermolecular Interactions by Variable Temperature Dynamic Force Spectroscopy," *Langmuir,* vol. 19, pp. 1457-1461, 2003.

[90] M. Horton, G. Charras, and P. Lehenkari, "Analysis of ligand-receptor interactions in cells by atomic force microscopy," *J Recept Signal Transduct Res,* vol. 22, pp. 169-90, Feb-Nov 2002.

[91] B. Cappella and G. Dietler, "Force-Distance Curves by Atomic Force Microscopy," Lausanne, Switzerland1999.

[92] P. J. Cumpson, C. A. Clifford, J. F. Portoles, J. E. Johnstone, and M. Munz, "Cantilever Spring-Constant Calibration in Atomic Force Microscopy," *Applied Scanning Probe Methods Viii: Scanning Probe Microscopy Techniques,* pp. 289-314, 2008.

[93] J. E. Sader, J. A. Sanelli, B. D. Adamson, J. P. Monty, X. Z. Wei, S. A. Crawford*, et al.*, "Spring constant calibration of atomic force microscope cantilevers of arbitrary shape," *Review of Scientific Instruments,* vol. 83, Oct 2012.

[94] H.-J. Butt and M. Jaschke, "Calculation of thermal noise in atomic force microscopy," *Nanotechnology,* vol. 6, pp. 1-7, 1995.

[95] J. L. Hutter and J. Bechhoefer, "Calibration of Atomic-Force Microscope Tips (Vol 64, Pg 1868, 1993)," *Review of Scientific Instruments,* vol. 64, pp. 3342-3342, Nov 1993.

[96] W. Han and F. M. Serry. (2008, Force Spectroscopy with the Atomic Force Microscope: Application Note. *Agilent Technologies*.

[97] A. Noy and R. W. Friddle, "Practical single molecule force spectroscopy: How to determine fundamental thermodynamic parameters of intermolecular bonds with an atomic force microscope," *Methods,* vol. 60, pp. 142-150, Apr 1 2013.

[98] A. Ptak, M. Kappl, S. Moreno-Flores, H. Gojzewski, and H. J. Butt, "Quantitative characterization of nanoadhesion by dynamic force spectroscopy," *Langmuir,* vol. 25, pp. 256-61, Jan 6 2009.

[99] C. K. Lee, Y. M. Wang, L. S. Huang, and S. Lin, "Atomic force microscopy: determination of unbinding force, off rate and energy barrier for protein-ligand interaction," *Micron,* vol. 38, pp. 446-61, 2007.

[100] F. C. Collins and G. E. Kimball, "Diffusion-Controlled Reactions in Liquid Solutions," *Industrial and Engineering Chemistry,* vol. 41, pp. 2551-2553, 1949.

[101] N. G. van Kampen, *Stochastic Processes in Physics and Chemistry*. Amsterdam: North-Holland, 1992.

[102] T. Strunz, K. Oroszlan, R. Schafer, and H. J. Guntherodt, "Dynamic force spectroscopy of single DNA molecules," *Proc Natl Acad Sci U S A,* vol. 96, pp. 11277-82, Sep 28 1999.

[103] Z. Lv, R. Roychaudhuri, M. M. Condron, D. B. Teplow, and Y. L. Lyubchenko, "Mechanism of amyloid beta-protein dimerization determined using single-molecule AFM force spectroscopy," *Sci Rep,* vol. 3, p. 2880, 2013.

[104] R. Nevo, C. Stroh, F. Kienberger, D. Kaftan, V. Brumfeld, M. Elbaum*, et al.*, "A molecular switch between alternative conformational states in the complex of Ran and importin beta 1," *Nature Structural Biology,* vol. 10, pp. 553-557, Jul 2003.

[105] O. K. Dudko, G. Hummer, and A. Szabo, "Intrinsic rates and activation free energies from single-molecule pulling experiments," *Phys Rev Lett,* vol. 96, p. 108101, Mar 17 2006.

[106] O. K. Dudko, G. Hummer, and A. Szabo, "Theory, analysis, and interpretation of single-molecule force spectroscopy experiments," *Proc Natl Acad Sci U S A,* vol. 105, pp. 15755-60, Oct 14 2008.

[107] R. W. Friddle, A. Noy, and J. J. De Yoreo, "Interpreting the widespread nonlinear force spectra of intermolecular bonds," *Proc Natl Acad Sci U S A,* vol. 109, pp. 13573-8, Aug 21 2012.

[108] J. M. Teulon, Y. Delcuze, M. Odorico, S. W. Chen, P. Parot, and J. L. Pellequer, "Single and multiple bonds in (strept)avidin-biotin interactions," *J Mol Recognit,* vol. 24, pp. 490-502, May-Jun 2011.

[109] R. W. Friddle, "Unified model of dynamic forced barrier crossing in single molecules," *Phys Rev Lett,* vol. 100, p. 138302, Apr 4 2008.

[110] D. Alsteens, M. Pfreundschuh, C. Zhang, P. M. Spoerri, S. R. Coughlin, B. K. Kobilka*, et al.*, "Imaging G protein-coupled receptors while quantifying their ligand-binding free-energy landscape," *Nature Methods,* vol. 12, pp. 845-+, Sep 2015.

[111] W. J. Greenleaf, M. T. Woodside, and S. M. Block, "High-resolution, single-molecule measurements of biomolecular motion," *Annu Rev Biophys Biomol Struct,* vol. 36, pp. 171-90, 2007.

[112] M. T. Woodside, C. Garcia-Garcia, and S. M. Block, "Folding and unfolding single RNA molecules under tension," *Curr Opin Chem Biol,* vol. 12, pp. 640-6, Dec 2008.

[113] G. Zoldak and M. Rief, "Force as a single molecule probe of multidimensional protein energy landscapes," *Curr Opin Struct Biol,* vol. 23, pp. 48-57, Feb 2013.

[114] K. C. Neuman and A. Nagy, "Single-molecule force spectroscopy: optical tweezers, magnetic tweezers and atomic force microscopy," *Nat Methods,* vol. 5, pp. 491-505, Jun 2008.

[115] J. P. Cleveland, T. E. Schaffer, and P. K. Hansma, "Probing oscillatory hydration potentials using thermal-mechanical noise in an atomic-force microscope," *Phys Rev B Condens Matter,* vol. 52, pp. R8692-R8695, Sep 15 1995.

[116] M. T. Woodside, P. C. Anthony, W. M. Behnke-Parks, K. Larizadeh, D. Herschlag, and S. M. Block, "Direct measurement of the full, sequence-dependent folding landscape of a nucleic acid," *Science,* vol. 314, pp. 1001-4, Nov 10 2006.

[117] W. J. Greenleaf, M. T. Woodside, E. A. Abbondanzieri, and S. M. Block, "Passive all-optical force clamp for high-resolution laser trapping," *Phys Rev Lett,* vol. 95, p. 208102, Nov 11 2005.

[118] M. de Messieres, B. Brawn-Cinani, and A. La Porta, "Measuring the folding landscape of a harmonically constrained biopolymer," *Biophys J,* vol. 100, pp. 2736-44, Jun 8 2011.

[119] M. T. Woodside, W. M. Behnke-Parks, K. Larizadeh, K. Travers, D. Herschlag, and S. M. Block, "Nanomechanical measurements of the sequence-dependent folding landscapes of single nucleic acid hairpins," *Proc Natl Acad Sci U S A,* vol. 103, pp. 6190-5, Apr 18 2006.

[120] M. Schlierf, H. B. Li, and J. M. Fernandez, "The unfolding kinetics of ubiquitin captured with single-molecule force-clamp techniques," *Proceedings of the National Academy of Sciences of the United States of America,* vol. 101, pp. 7299-7304, May 11 2004.

[121] B. Jagannathan, P. J. Elms, C. Bustamante, and S. Marqusee, "Direct observation of a force-induced switch in the anisotropic mechanical unfolding pathway of a protein," *Proceedings of the National Academy of Sciences of the United States of America,* vol. 109, pp. 17820-17825, Oct 30 2012.

[122] H. Dietz and M. Rief, "Exploring the energy landscape of GFP by single-molecule mechanical experiments," *Proceedings of the National Academy of Sciences of the United States of America,* vol. 101, pp. 16192-16197, Nov 16 2004.

[123] K. Kawasaki and J. D. Gunton, "Theory of Nonlinear Transport Processes - Nonlinear Shear Viscosity and Normal Stress Effects," *Physical Review A,* vol. 8, pp. 2048-2064, 1973.

[124] G. N. Bochkov and Y. E. Kuzovlev, "Nonlinear Fluctuation-Dissipation Relations and Stochastic Models in Nonequilibrium Thermodynamics: I. Generalized Fluctuation-Dissipation Theorem," *Physica A: Statistical Mechanics and its Applications,* vol. 106, pp. 443-479, 1981.

[125] J. Gore, F. Ritort, and C. Bustamante, "Bias and error in estimates of equilibrium free-energy differences from nonequilibrium measurements," *Proceedings of the National Academy of Sciences of the United States of America,* vol. 100, pp. 12564-12569, Oct 28 2003.

[126] C. Bustamante, J. Liphardt, and F. Ritort, "The nonequilibrium thermodynamics of small systems," *Physics Today,* vol. 58, pp. 43-48, Jul 2005.

[127] Q. Zhang, J. Brujic, and E. Vanden-Eijnden, "Reconstructing Free Energy Profiles from Nonequilibrium Relaxation Trajectories," *Journal of Statistical Physics,* vol. 144, pp. 344-366, Jul 2011.

[128] R. B. Best and G. Hummer, "Coordinate-dependent diffusion in protein folding," *Proceedings of the National Academy of Sciences of the United States of America,* vol. 107, pp. 1088-1093, Jan 19 2010.

[129] C. B. Hyeon, G. Morrison, D. L. Pincus, and D. Thirumalai, "Refolding dynamics of stretched biopolymers upon force quench," *Proceedings of the National Academy of Sciences of the United States of America,* vol. 106, pp. 20288-20293, Dec 1 2009.

[130] M. D. H. Heinz W. F. ; Antonik, J. H. , "Reconstructing Local Interaction Potentials from Perturbations to the Thermally Driven Motion of an Atomic Force Microscope Cantilever," *J. Phys. Chem. B,* vol. 104, pp. 622-626, 2000.

[131] O. H. Willemsen, M. M. Snel, A. Cambi, J. Greve, B. G. De Grooth, and C. G. Figdor, "Biomolecular interactions measured by atomic force microscopy," *Biophys J,* vol. 79, pp. 3267-81, Dec 2000.

[132] O. H. K. L. V. d. W. Willemsen, K. O.; Grooth, B.G.; Greve, J, "Reconstruction of the Tip-Surface Interaction Potential by Analysis of the Brownian Motion of an Atomic Force Microscope Tip," *Langmuir,* vol. 16, pp. 4339-4347, 2000.

[133] P. D. Ashby, "Intermolecular and Interfacial Forces: Elucidating Molecular Mechanisms using Chemical Force Microscopy," Ph.D., Physical Chemistry, Harvard University, Cambridge, Massachusetts, 2003.

[134] G. M. Torrie and J. P. Valleau, "Monte-Carlo Study of a Phase-Separating Liquid-Mixture by Umbrella Sampling," *Journal of Chemical Physics,* vol. 66, pp. 1402-1408, 1977.

[135] G. M. Torrie and J. P. Valleau, "Non-Physical Sampling Distributions in Monte-Carlo Free-Energy Estimation - Umbrella Sampling," *Journal of Computational Physics,* vol. 23, pp. 187-199, 1977.

[136] S. Kumar, J. M. Rosenberg, D. Bouzida, R. H. Swendsen, and P. A. Kollman, "The weighted histogram analysis method for free-energy calculations on biomolecules. I. The method," *J. Comput. Chem.,* vol. 13, pp. 1011-1021, 1992.

[137] G. Ozer, S. Quirk, and R. Hernandez, "Adaptive steered molecular dynamics: validation of the selection criterion and benchmarking energetics in vacuum," *J Chem Phys,* vol. 136, p. 215104, Jun 7 2012.

[138] B. Roux, "The calculation of the potential of mean force using computer simulations," *Comp. Phys. Comm.,* vol. 91, pp. 275-282, 1995.

[139] D. H. Williams, E. Stephens, and M. Zhou, "Ligand binding energy and catalytic efficiency from improved packing within receptors and enzymes," *J Mol Biol,* vol. 329, pp. 389-99, May 30 2003.

[140] S. C. Kuo and D. A. Lauffenburger, "Relationship between receptor/ligand binding affinity and adhesion strength," *Biophys J,* vol. 65, pp. 2191-200, Nov 1993.

[141] M. H. Ultsch, C. Wiesmann, L. C. Simmons, J. Henrich, M. Yang, D. Reilly*, et al.*, "Crystal structures of the neurotrophin-binding domain of TrkA, TrkB and TrkC," *J Mol Biol,* vol. 290, pp. 149-59, Jul 2 1999.

[142] C. Wiesmann, M. H. Ultsch, S. H. Bass, and A. M. de Vos, "Crystal structure of nerve growth factor in complex with the ligand-binding domain of the TrkA receptor," *Nature,* vol. 401, pp. 184-8, Sep 9 1999.

[143] Y. Fang, "Ligand-receptor interaction platforms and their applications for drug discovery," *Expert Opin Drug Discov,* vol. 7, pp. 969-88, Oct 2012.

[144] G. Schreiber, "Kinetic studies of protein-protein interactions," *Curr Opin Struct Biol,* vol. 12, pp. 41-7, Feb 2002.

[145] A. C. Pan, D. W. Borhani, R. O. Dror, and D. E. Shaw, "Molecular determinants of drug-receptor binding kinetics," *Drug Discov Today,* vol. 18, pp. 667-73, Jul 2013.

[146] S. G. Patching, "Surface plasmon resonance spectroscopy for characterisation of membrane protein-ligand interactions and its potential for drug discovery," *Biochim Biophys Acta,* vol. 1838, pp. 43-55, Jan 2014.

[147] G. Siligardi, R. Hussain, S. G. Patching, and M. K. Phillips-Jones, "Ligand- and drug-binding studies of membrane proteins revealed through circular dichroism spectroscopy," *Biochim Biophys Acta,* vol. 1838, pp. 34-42, Jan 2014.

[148] J. J. Maguire, R. E. Kuc, and A. P. Davenport, "Radioligand binding assays and their analysis," *Methods Mol Biol,* vol. 897, pp. 31-77, 2012.

[149] P. Estep, F. Reid, C. Nauman, Y. Liu, T. Sun, J. Sun*, et al.*, "High throughput solution-based measurement of antibody-antigen affinity and epitope binning," *MAbs,* vol. 5, pp. 270-8, Mar-Apr 2013.

[150] T. Sun, F. Reid, Y. Liu, Y. Cao, P. Estep, C. Nauman*, et al.*, "High throughput detection of antibody self-interaction by bio-layer interferometry," *MAbs,* vol. 5, pp. 838-41, Nov-Dec 2013.

[151] S. Peuker, A. Cukkemane, M. Held, F. Noe, U. B. Kaupp, and R. Seifert, "Kinetics of ligand-receptor interaction reveals an induced-fit mode of binding in a cyclic nucleotide-activated protein," *Biophys J,* vol. 104, pp. 63-74, Jan 8 2013.

[152] E. Meneses and A. Mittermaier, "Electrostatic interactions in the binding pathway of a transient protein complex studied by NMR and isothermal titration calorimetry," *J Biol Chem,* vol. 289, pp. 27911-23, Oct 3 2014.

[153] A. P. Turnbull and P. Emsley, "Studying protein-ligand interactions using X-ray crystallography," *Methods Mol Biol,* vol. 1008, pp. 457-77, 2013.

[154] T. A. Aweda and C. F. Meares, "Combination of isothermal titration calorimetry and time-resolved luminescence for high affinity antibody-ligand interaction thermodynamics and kinetics," *Methods,* vol. 56, pp. 145-53, Feb 2012.

[155] E. L. R. Florin, M.; Lehmann, H.; Ludwig, M.; Dornmair, C.; Moy, V.T.; Gaub, H.E, "Sensing specific molecular interactions with the atomic force microscope," *Biosensors and Bioelectronics,* vol. 10, pp. 895-892, Jan 1 1995 1995.

[156] C. Y. Lee, J. Lou, K. K. Wen, M. McKane, S. G. Eskin, S. Ono*, et al.*, "Actin depolymerization under force is governed by lysine 113:glutamic acid 195-mediated catch-slip bonds," *Proc Natl Acad Sci U S A,* vol. 110, pp. 5022-7, Mar 26 2013.

[157] M. Rief, M. Gautel, F. Oesterhelt, J. M. Fernandez, and H. E. Gaub, "Reversible unfolding of individual titin immunoglobulin domains by AFM," *Science,* vol. 276, pp. 1109-12, May 16 1997.

[158] P. W. Fok and T. Chou, "Reconstruction of potential energy profiles from multiple rupture time distributions," *Proceedings of the Royal Society a-Mathematical Physical and Engineering Sciences,* vol. 466, pp. 3479-3499, Dec 8 2010.

[159] G. Hummer and A. Szabo, "Free energy reconstruction from nonequilibrium single-molecule pulling experiments," *Proc Natl Acad Sci U S A,* vol. 98, pp. 3658-61, Mar 27 2001.

[160] N. C. Harris, Y. Song, and C. H. Kiang, "Experimental free energy surface reconstruction from single-molecule force spectroscopy using Jarzynski's equality," *Phys Rev Lett,* vol. 99, p. 068101, Aug 10 2007.

[161] A. Ebner, L. Wildling, A. S. Kamruzzahan, C. Rankl, J. Wruss, C. D. Hahn*, et al.*, "A new, simple method for linking of antibodies to atomic force microscopy tips," *Bioconjug Chem,* vol. 18, pp. 1176-84, Jul-Aug 2007.

[162] F. Zhu and G. Hummer, "Convergence and error estimation in free energy calculations using the weighted histogram analysis method," *J Comput Chem,* vol. 33, pp. 453-65, Feb 5 2012.

[163] I. J. General, R. Dragomirova, and H. Meirovitch, "Absolute Free Energy of Binding of Avidin/Biotin, Revisited," *Journal of Physical Chemistry B,* vol. 116, pp. 6628-6636, Jun 14 2012.

[164] I. J. General, R. Dragomirova, and H. Meirovitch, "New Method for Calculating the Absolute Free Energy of Binding: The Effect of a Mobile Loop on the

Avidin/Biotin Complex," *Journal of Physical Chemistry B,* vol. 115, pp. 168-175, Jan 13 2011.

[165] T. Lazaridis, A. Masunov, and F. Gandolfo, "Contributions to the binding free energy of ligands to avidin and streptavidin," *Proteins-Structure Function and Genetics,* vol. 47, pp. 194-208, May 1 2002.

[166] M. Souaille and B. Roux, "Extension to the weighted histogram analysis method: combining umbrella sampling with free energy calculations," *Comp. Phys. Comm.,* vol. 135, pp. 40-57, 2001.

[167] S. Manne, Gaub, H. E., "Force microscopy: Measurement of local interfacial forces and surface stresses," *Curr. Opin. Colloid Interface Sci.,* vol. 2, pp. 145-152, 1997.

[168] I. Tinoco, Jr. and C. Bustamante, "The effect of force on thermodynamics and kinetics of single molecule reactions," *Biophys Chem,* vol. 101-102, pp. 513-33, Dec 10 2002.

[169] S. P. Jarvis, H. Yamada, S. I. Yamamoto, H. Tokumoto, and J. B. Pethica, "Direct Mechanical Measurement of Interatomic Potentials," *Nature Lett.,* vol. 384, pp. 247-249, 1996.

[170] N. A. Burnham and R. J. Colton, "Measuring the Nanomechanical Properties and Surface Forces of Materials Using an Atomic Force Microscope," *Journal of Vacuum Science & Technology A-Vacuum Surfaces and Films,* vol. 7, pp. 2906-2913, Jul-Aug 1989.

[171] S. A. Joyce and J. E. Houston, "A New Force Sensor incorporating Force-Feedback Control for Interfacial Force Microscopy," *Rev Sci Instrum,* vol. 62, 1991.

[172] R. W. Stark, T. Drobek, and W. M. Heckl, "Thermomechanical noise of a free v-shaped cantilever for atomic-force microscopy," *Ultramicroscopy,* vol. 86, pp. 207-15, Jan 2001.

[173] T. Stecher, N. Bernstein, and G. Csanyi, "Free Energy Surface Reconstruction from Umbrella Samples Using Gaussian Process Regression," *J Chem Theory Comput,* vol. 10, pp. 4079-97, Sep 9 2014.

[174] L. S. Dorobantu, S. Bhattacharjee, J. M. Foght, and M. R. Gray, "Analysis of force interactions between AFM tips and hydrophobic bacteria using DLVO theory," *Langmuir,* vol. 25, pp. 6968-76, Jun 16 2009.

[175] J. A. Brant and A. E. Childress, "Membrane-colloid interactions: Comparison of extended DLVO predictions with AFM force measurements," *Environmental Engineering Science,* vol. 19, pp. 413-427, Nov-Dec 2002.

[176] B. W. Ninham, "On progress in forces since the DLVO theory," *Advances in Colloid and Interface Science,* vol. 83, pp. 1-17, Dec 1 1999.

[177] R. H. Tredgold, "An Introduction to Ultrathin Organic Films - from Langmuir-Blodgett to Self-Assembly - Ulman,A," *Nature,* vol. 354, pp. 120-120, Nov 14 1991.

[178] K. L. Johnson, K. Kendall, and A. D. Roberts, "Surface Energy and Contact of Elastic Solids," *Proceedings of the Royal Society of London Series a-Mathematical and Physical Sciences,* vol. 324, pp. 301-313, 1971.

[179] K. H. Chung, Y. H. Lee, and D. E. Kim, "Characteristics of fracture during the approach process and wear mechanism of a silicon AFM tip," *Ultramicroscopy,* vol. 102, pp. 161-171, Jan 2005.

[180] B. Xue, Y. D. Yan, Z. J. Hu, and X. S. Zhao, "Study on Effects of Scan Parameters on the Image Quality and Tip Wear in AFM Tapping Mode," *Scanning,* vol. 36, pp. 263-269, Mar 2014.

[181] H. J. Butt, B. Cappella, and M. Kappl, "Force measurements with the atomic force microscope: Technique, interpretation and applications," *Surface Science Reports,* vol. 59, pp. 1-152, Oct 2005.

[182] C. Rotsch and M. Radmacher, "Mapping local electrostatic forces with the atomic force microscope," *Langmuir,* vol. 13, pp. 2825-2832, May 14 1997.

[183] N. N. Gosvami, E. Parsons, C. Marcovich, M. L. Berkowitz, B. W. Hoogenboom, and S. Perkin, "Resolving the structure of a model hydrophobic surface: DODAB monolayers on mica," *Rsc Advances,* vol. 2, pp. 4181-4188, 2012.

[184] D. J. Riley and R. G. Carbonell, "Mechanisms of Particle Deposition from Ultrapure Chemicals onto Semiconductor Wafers - Deposition from Bulk Liquid during Wafer Submersion," *Journal of Colloid and Interface Science,* vol. 158, pp. 259-273, Jul 1993.

[185] S. Nishimura, H. Tateyama, K. Tsunematsu, and K. Jinnai, "Zeta-Potential Measurement of Muscovite Mica Basal-Plane Aqueous-Solution Interface by Means of Plane Interface Technique," *Journal of Colloid and Interface Science,* vol. 152, pp. 359-367, Sep 1992.

[186] S. Assemi, J. Nalaskowski, J. D. Miller, and W. P. Johnson, "Isoelectric point of fluorite by direct force measurements using atomic force microscopy," *Langmuir,* vol. 22, pp. 1403-5, Feb 14 2006.

[187] K. Neupane, A. Solanki, I. Sosova, M. Belov, and M. T. Woodside, "Diverse metastable structures formed by small oligomers of alpha-synuclein probed by force spectroscopy," *PLoS One,* vol. 9, p. e86495, 2014.

[188] A. P. Manuel, J. Lambert, and M. T. Woodside, "Reconstructing folding energy landscapes from splitting probability analysis of single-molecule trajectories," *Proc Natl Acad Sci U S A,* vol. 112, pp. 7183-8, Jun 9 2015.

[189] C. Hyeon and D. Thirumalai, "Can energy landscape roughness of proteins and RNA be measured by using mechanical unfolding experiments?," *Proc Natl Acad Sci U S A,* vol. 100, pp. 10249-53, Sep 2 2003.

[190] J. E. Shea and C. L. Brooks, 3rd, "From folding theories to folding proteins: a review and assessment of simulation studies of protein folding and unfolding," *Annu Rev Phys Chem,* vol. 52, pp. 499-535, 2001.

[191] H. J. Woo and B. Roux, "Calculation of absolute protein-ligand binding free energy from computer simulations," *Proc Natl Acad Sci U S A,* vol. 102, pp. 6825-30, May 10 2005.

[192] T. Steinbrecher and A. Labahn, "Towards accurate free energy calculations in ligand protein-binding studies," *Curr Med Chem,* vol. 17, pp. 767-85, 2010.

[193] N. Huang, N. K. Banavali, and A. D. MacKerell, Jr., "Protein-facilitated base flipping in DNA by cytosine-5-methyltransferase," *Proc Natl Acad Sci U S A,* vol. 100, pp. 68-73, Jan 7 2003.

[194] J. Wereszczynski and I. Andricioaei, "On structural transitions, thermodynamic equilibrium, and the phase diagram of DNA and RNA duplexes under torque and tension," *Proc Natl Acad Sci U S A,* vol. 103, pp. 16200-5, Oct 31 2006.

[195] N. Perunov and J. L. England, "Quantitative theory of hydrophobic effect as a driving force of protein structure," *Protein Sci,* vol. 23, pp. 387-99, Apr 2014.

[196] J. L. Gao, "A Priori Computation of a Solvent-Enhanced SN2 Reaction Profile in Water - The Menshutkin Reaction," *J Am Chem Soc,* vol. 113, pp. 7796-7797, 1991.

[197] K. Hinsen and B. Roux, "Potential of Mean Force and Reaction Rates for Proton Transfer in Acetylacetone," *J. Chem. Phys.,* vol. 105, pp. 3567-3577, 1997.

[198] T. W. Allen, O. Andersen, and B. Roux, "Energetics of Ion Conduction through the Gramicidin Channel," *Proc Natl Acad Sci U S A,* vol. 86, pp. 117-122, 2004.

[199] M. Karplus and B. M. Pettitt, "The Potential of Mean Force Surface for the Alanine Dipeptide in Aqueous Solution," *Chem. Phys. Lett.,* vol. 121, pp. 194-201, 1985.

[200] Z. Guo, E. M. Boczko, and C. L. Brooks, "Exploring the Folding Free-energy Surface of a Three-Helix Bundle Protein," *Proc Natl Acad Sci U S A,* vol. 94, pp. 10161–10166, 1997.

[201] K. Fukui, "Formulation of the Reaction Coordinate," *J. Phys. Chem.,* vol. 74, pp. 4161-4163, 1970.

[202] C. Bustamante, J. C. Macosko, and G. J. Wuite, "Grabbing the cat by the tail: manipulating molecules one by one," *Nat Rev Mol Cell Biol,* vol. 1, pp. 130-6, Nov 2000.

[203] T. E. Fisher, P. E. Marszalek, and J. M. Fernandez, "Stretching single molecules into novel conformations using the atomic force microscope," *Nat Struct Biol,* vol. 7, pp. 719-24, Sep 2000.

[204] H. Clausen-Schaumann, M. Seitz, R. Krautbauer, and H. E. Gaub, "Force spectroscopy with single bio-molecules," *Curr Opin Chem Biol,* vol. 4, pp. 524-30, Oct 2000.

[205] R. H. Wood, W. C. F. MuhlBauer, and P. Thompson, "Systematic Errors in Free Energy Perturbation Calculations Due to a Finite Sample of Configuration Space," *J. Phys. Chem.,* vol. 95, pp. 6670-6675, 1991.

[206] A. Pohorille, C. Jarzynski, and C. Chipot, "Good practices in free-energy calculations," *J Phys Chem B,* vol. 114, pp. 10235-53, Aug 19 2010.

[207] P. Liu, F. Dehez, W. Cai, and C. Chipot, "A Toolkit for the Analysis of Free-Energy Perturbation Calculations," *J Chem Theory Comput,* vol. 8, pp. 2606-16, Aug 14 2012.

[208] C. Jarzynski, "Nonequilibrium Inequality for Free Energy Differences," *Phys Rev Lett,* vol. 78, pp. 2690-2693, 1997.

[209] J. Preiner, H. Janovjak, C. Rankl, H. Knaus, D. A. Cisneros, A. Kedrov*, et al.*, "Free energy of membrane protein unfolding derived from single-molecule force measurements," *Biophys J,* vol. 93, pp. 930-7, Aug 1 2007.

[210] G. Volpe and G. Volpe, "Simulation of a Brownian particle in an optical trap," *American Journal of Physics,* vol. 81, pp. 224-230, Mar 2013.

[211] B. G. de Grooth, "A simple model for Brownian motion leading to the Langevin equation," *American Journal of Physics,* vol. 67, pp. 1248-1252, Dec 1999.

[212] A. La Porta, N. A. Denesyuk, and M. de Messieres, "Optimal reconstruction of the folding landscape using differential energy surface analysis," *Physical Review E,* vol. 87, Mar 20 2013.

[213] S. Kumar, D. Bouzida, R. H. Swendsen, P. A. Kollman, and J. M. Rosenberg, "The Weighted Histogram Analysis Method for Free-Energy Calculations on Biomolecules .1. The Method," *Journal of Computational Chemistry,* vol. 13, pp. 1011-1021, Oct 1992.

[214] B. Roux, "The Calculation of the Potential of Mean Force Using Computer-Simulations," *Computer Physics Communications,* vol. 91, pp. 275-282, Sep 1995.

[215] D. A. Kofke and P. T. Cummings, "Quantitative Comparison and Optimization of Methods for Evaluating the Chemical Potential by Molecular Simulation," *Mol. Phys.,* vol. 92, pp. 973-996, 1997.

[216] D. A. Kofke and P. T. Cummings, "Precision and Accuracy of Staged Free-Energy Perturbation Methods for Computing the Chemical Potential by Molecular Simulation," *Fluid Phase Equilibria,* vol. 150, pp. 41-49, 1998.

[217] N. Lu, D. A. Kofke, and T. B. Woolf, "Improving the efficiency and reliability of free energy perturbation calculations using overlap sampling methods," *J Comput Chem,* vol. 25, pp. 28-39, Jan 15 2004.

[218] D. Steinley, "K-means clustering: a half-century synthesis," *Br J Math Stat Psychol,* vol. 59, pp. 1-34, May 2006.

[219] T. Hastie, R. Tibshirani, and J. Friedman, *The Elements of Statistical Learning*. New York: NY Springer, 2001.

[220] G. R. Jayanth, Y. Jeong, and C. H. Menq, "Direct tip-position control using magnetic actuation for achieving fast scanning in tapping mode atomic force microscopy," *Review of Scientific Instruments,* vol. 77, pp. (053704)1-7, May 2006.

[221] R. Pedrak, T. Ivanov, K. Ivanova, T. Gotszalk, N. Abedinov, I. W. Rangelow*, et al.*, "Micromachined atomic force microscopy sensor with integrated piezoresistive, sensor and thermal bimorph actuator for high-speed tapping-mode atomic force microscopy phase-imaging in higher eigenmodes," *Journal of Vacuum Science & Technology B,* vol. 21, pp. 3102-3107, Nov-Dec 2003.

[222] L. Fan, D. Potter, and T. Sulchek, "Constant tip-surface distance with atomic force microscopy via quality factor feedback," *Rev Sci Instrum,* vol. 83, p. 023706, Feb 2012.

[223] S. Jesse, R. K. Vasudevan, L. Collins, E. Strelcov, M. B. Okatan, A. Belianinov*, et al.*, "Band Excitation in Scanning Probe Microscopy: Recognition and Functional Imaging," *Annual Review of Physical Chemistry, Vol 65,* vol. 65, pp. 519-536, 2014.